HORIZONTAL SHEAR TRANSFER BETWEEN ULTRA HIGH PERFORMANCE CONCRETE AND LIGHTWEIGHT CONCRETE

by

Timothy E. Banta

Thesis submitted to the faculty of the
Virginia Polytechnic Institute and State University
in partial fulfillment of the requirements for the degree of

MASTERS OF SCIENCE
IN
CIVIL ENGINEERING

APPROVED:

Carin Roberts-Wollmann, Chairperson

W. Samuel Easterling

Thomas Cousins

February 2005
Blacksburg, Virginia

Keywords: Ductal, Lightweight, Horizontal Shear Transfer

HORIZONTAL SHEAR TRANSFER BETWEEN ULTRA HIGH PERFORMANCE CONCRETE AND LIGHTWEIGHT CONCRETE

by

Timothy E. Banta

ABSTRACT

Ultra high performance concrete, specifically Ductal® concrete, has begun to revolutionize the bridge design industry. This extremely high strength material has given smaller composite sections the ability to carry larger loads. As the forces being transferred through composite members are increasing in magnitude, it is vital that the equations being used for design are applicable for use with the new materials. Of particular importance is the design of the horizontal shear reinforcement connecting the bridge deck to the top flange of the beams. Without adequate shear transfer, the flexural and shearing capacities will be greatly diminished. The current design equations from ACI and AASHTO were not developed for use in designing sections composed of Ductal® and Lightweight concrete.

Twenty-four push-off tests were performed to determine if the current horizontal shear design equations could accurately predict the horizontal shear strength of composite Ductal® and Lightweight concrete sections. Effects from various surface treatments, reinforcement ratios, and aspect ratios, were determined. The results predicted by the current design equations were compared to the actual results found during testing. The current design equations were all found to be conservative. For its ability to incorporate various cohesion and friction factors, it is recommended that the equation from AASHTO LRFD Specification (2004) be used for design.

ACKNOWLEDGEMENTS

I would like to thank Dr. Carin Roberts-Wollmann for all of her guidance and help throughout the years. Having her as a professor in my undergraduate studies inspired me to come back to Virginia Tech to obtain my Masters Degree. The concern she has for her students should be a model for all of her peers. It truly was a pleasure working with Dr. Wollmann for the past four years. I would also like to thank Dr. Sam Easterling and Dr. Thomas Cousins for their guidance throughout my graduate and undergraduate studies.

None of my research could have been possible without the help of Brett Farmer and Dennis Huffman. Their help in the lab on all of my assorted research projects has been greatly appreciated. I also want to thank my fellow graduate students who assisted me out in the lab. I would specifically like to thank Dave, Kyle, Onur, and Steve for all of their help.

Lastly, I would like to thank my family for giving me support in all of my endeavors. I want to thank you for being there for me throughout the years. Without your guidance and counsel; I could not have achieved all that I have done.

TABLE OF CONTENTS

LIST OF FIGURES

Page

LIST OF TABLES

CHAPTER 1: INTRODUCTION

1.1 Horizontal Shear Transfer

For years, precast prestressed concrete beams have been used in the construction of bridges throughout the world. A variety of standard shapes have gained wide use amongst the bridge design community. One of the standard cross-sectional designs becoming more commonly used is the bulb-tee. This design incorporates broad flanges that allow for more material away from the center of gravity of the section. This not only makes the design much more efficient, but it helps to reduce the amount of bridge deck formwork. The size and overall shape of the beam allows for a lighter cross-section with increased maximum span lengths.

Along with the optimization of the beam's cross-section, the materials used for construction have become both stronger and more durable. By using materials that have increased strength, modern bridge designs have been able to use increasing amounts of prestressing strands in smaller cross-sections. The combinations of these factors are allowing engineers to span greater lengths with less material.

Common design practice is for the bridge beam and deck to act as a composite system for live loads and superimposed dead loads. The forces developing in these composite systems have increased as the span lengths have become longer. It is important that horizontal shear forces being carried in both the deck and beam can readily cross the interface zone between these two members. Figure 1.1 shows an illustration of the horizontal shear forces. The transfer of these shearing forces is commonly known as interface shear transfer or shear friction.

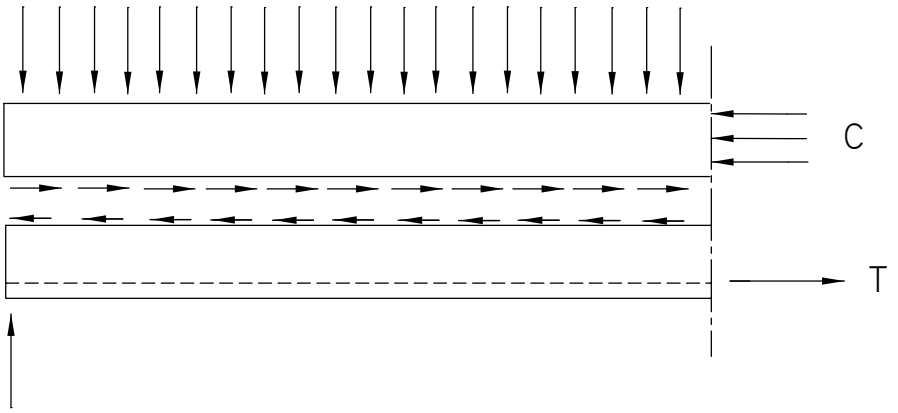

Figure 1.1 Horizontal Shear Forces

To aid engineers in the design of this horizontal shear transfer, various equations to determine nominal shear resistance have been developed. The design equations account for both mechanical and frictional shear transfer in determining the nominal shear resistance of an interface zone. As opposing horizontal forces develop in the bridge deck and the beam, there is some relative slip between the surfaces. This can occur due to micro cracking along the interface. As the relative slip occurs, reinforcing steel protruding from the beam into the deck develops tensile forces, and subsequently causes compressive forces along the interface zone. These forces act normal to the horizontal shearing forces. Horizontal shearing forces are transferred across the interface by friction due to the compressive forces, dowel action of the reinforcing steel and by aggregate interlock along the micro cracks. Figure 1.2 diagrams the forces developed along the interface due to the relative slip of the two surfaces (based on MacGregor 1997). Later sections of this report detail the design equations used in determining the horizontal nominal shear resistance of interface zones.

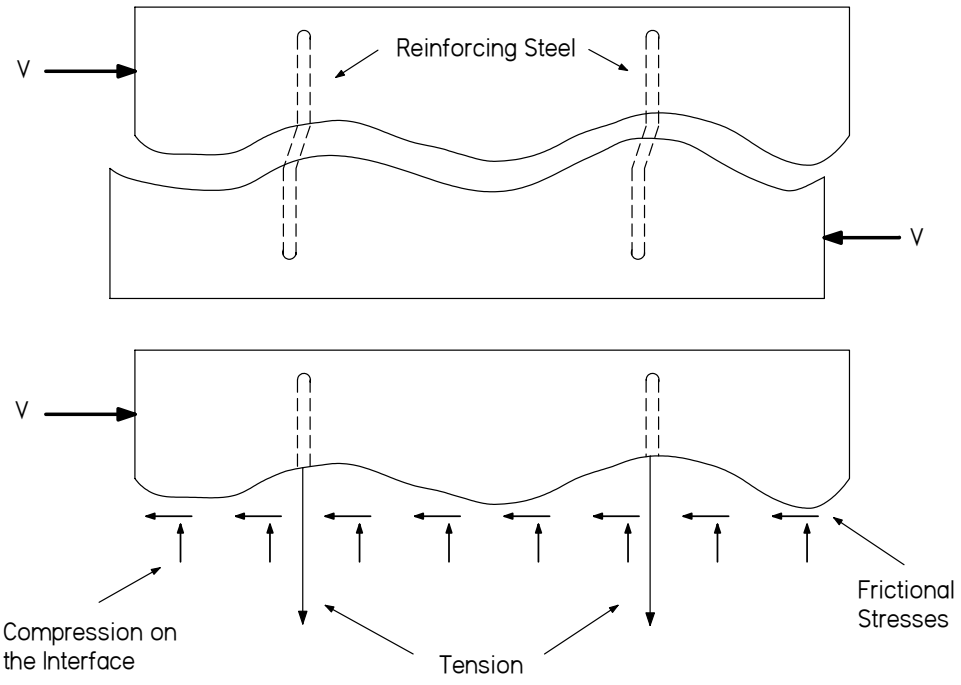

Figure 1.2 Interface Forces

As mentioned earlier, accompanying the introduction of new high strength materials, has been the optimization of the cross-sections of beams. Ultra-High Performance Concrete (UHPC) is gaining acceptance as a viable product for use in bridge construction. UHPC can be self-consolidating, have ultra low permeability, high ductility, ultra high compressive strength and a multitude of other advantageous design characteristics. This report will focus on the aspects and behavior of UHPC concrete, more specifically the horizontal shear transfer between lightweight concrete and Ductal® concrete blocks.

Ductal® concrete has a fluid nature that is unlike normal concrete. After placement, it has a tendency to self-level, and would result in the top flange of a Ductal® beam being very smooth. Any deformations in the fluid Ductal® concrete will not be permanent. It is important to determine the cohesion between this smooth Ductal® concrete surface and deck concrete cast directly on it.

1.2 Project Objectives and Work Plan

The Virginia Department of Transportation (VDOT) is designing a new bridge using UHPC concrete. The long span bridge will have prestressed precast Ductal® concrete bulb-tee girders as the beams, with a lightweight concrete cast-in-place deck. The design calls for the beams and deck to act compositely. To achieve this, mild steel stirrups will be used as shear connectors. VDOT has requested that this research project analyze and model the horizontal shear transfer across the deck to beam interface. The goal of this project is to determine if the present equations used to determine the horizontal shear transfer in bridge design are applicable for use with Ductal® concrete, and to make recommendations to VDOT as to any needed modifications to those equations. The equations in question come from the ACI 318 (2002), AASHTO Standard Specifications (2002), and AASHTO LRFD (2004) design codes.

To analyze the horizontal shear transfer across the Ductal® to lightweight concrete interface, 24 push-off tests were performed. Twelve shear connector details were tested with two repetitions of each detail. The specimens varied in size, reinforcement ratio and surface conditions. For each size specimen, a specific dead weight block provided a normal force across the interface area. Upon loading each specimen to failure, the load and slip were measured and recorded. Strain in the shear connectors was also measured and recorded where applicable. Figure 1.3 shows a typical test specimen.

It is expected that tests will show that the size of a specimen, its reinforcement ratio and the surface conditions all play a role in the nominal shear resistance of the Ductal® to lightweight concrete interface. From the shear connector strain data, the applicability of using the yield stress (f_y) in the design equations is investigated. It is possible that full yielding of the reinforcing steel across the interface zone is not achieved at the time cohesion between the two surfaces is lost.

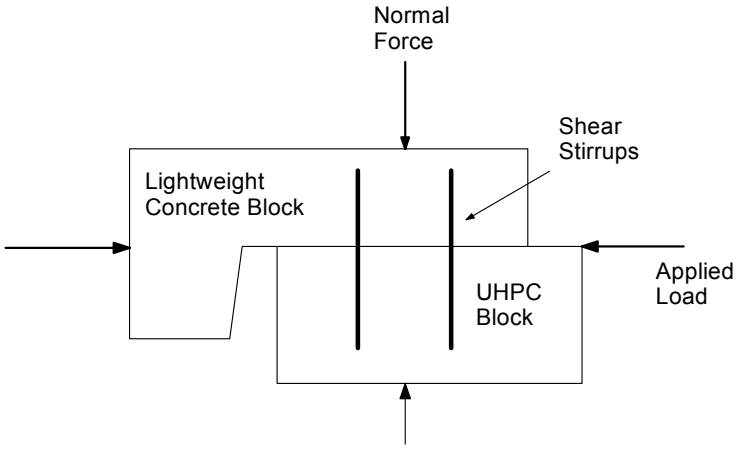

Figure 1.3 Typical Test Specimen

1.3 Thesis Organization

Chapter 2 of this thesis contains a review of the previous research performed on horizontal shear transfer and the development of the nominal shear resistance equations. This chapter also contains background information on the material properties of UHPC, specifically Ductal® concrete. Chapter 3 focuses on the specifics of the test setup and all background information relevant to each setup. Chapter 4 discusses the results obtained from the 24 push-off tests and those predicted using strut-and-tie modeling. This chapter also examines how the test results compare to calculated strengths obtained using present design equations. The final chapter, Chapter 5, discusses all relevant conclusions obtained from the test results. This chapter presents modifications, where applicable, to the present design equations for determining nominal shear resistance.

CHAPTER 2: LITERATURE REVIEW

2.1 Ultra High Performance Concrete

The use of concrete in bridge elements has been common place for many years. Although common, concrete's use as a structural material has one major downfall: the strength to weight ratio has caused beam elements in particular to be relatively inefficient. This inefficiency becomes apparent in long span structures. One way to increase the efficiency of concrete beams is to increase the overall compressive strength of the concrete used for construction.

Extensive research at both the professional and institutional level has resulted in the development of Ultra High Performance Concrete (UHPC). UHPC has many unique physical properties that allow for an increased efficiency in design. UHPC can be self consolidating, have ultra low permeability, high ductility, increased tensile strengths, abrasion resistance, and ultra high compressive strength. One such UHPC, known as Ductal® concrete, has made its way to the commercial market in North America. Table 2.1 shows an example of the material characteristics for Ductal® concrete (Perry 2003).

Table 2.1 Material Characteristics for Ductal® Concrete

Material Characteristics for Ductal® Concrete	
Compressive Strength	23 -33 ksi
Youngs Modulus (E)	8 – 8.5 x 10^6 psi
Total Fracture Energy	1,300 – 2,000 lb (F)- ft/ft^2
Elastic Fracture Energy	1.3 – 2.0 lb (F)- ft/ft^2
Chloride Ion Diffusion (CI)	0.02 x 10^{-11} ft^2/s
Carbonation Penetration Depth	<0.02 in
Freeze/thaw (after 300 cycles)	100%
Salt-scaling (loss of residue)	<0.0025 lb/ft^2
Abrasion (relative volume loss index)	1.2

2.2 Ductal® Concrete

Ductal® concrete was developed by Bouygues SA and is being marketed by Lafarge, Inc. It has been available in North America since 2001. The primary constituents of this material are portland cement, silica fume, quartz flour, fine silica sand, high-range water reducer, water and steel or organic fibers (Perry 2003). The use of steel fibers not only makes the material highly ductile, but virtually eliminates the need for secondary reinforcement. This is primarily due to the ability of Ductal® concrete to deform and support both flexural and tensile loads, even after initial cracking.

2.2.1 Properties of Ductal® Concrete

Ductal® concrete can be characterized as having a viscous nature prior to cure. This allows the concrete to flow during placement, and virtually eliminates any need for vibration. Tests have shown that the distribution of fibers throughout the concrete can be greatly effected by a number of placement processes. Any flow of the concrete tends to align the fibers in the direction of the flow, fibers close to formwork and walls naturally align themselves parallel to the walls, and settlement of the fibers in the viscous phase of the concrete prior to cure, can have a distinct impact on the tensile capacity of the Ductal® concrete. It is very important to take note of placement methods and fiber orientation, when considering the incorporation of increased tensile capacities in design.

Two factors contribute to the increased tensile capacity and ductility of this material, as compared with normal concrete. First, the initial elastic tensile capacity of the concrete matrix is greatly increased in Ductal® concrete. Tests have shown that the 28-day direct tensile strength of the matrix can be as much as 1,200 psi (Hajar et al 2003). This allows the matrix to withstand higher tensile stresses prior to initial cracking. Secondly, once the matrix has cracked, the densely compacted and interwoven steel fiber lattice continues to carry load.

The concrete matrix and steel lattice in Ductal® concrete are very tightly compacted. This allows for extremely low porosity, and very low permeability. These two factors combine to allow for a high resistance to corrosion and increase in durability over conventional concrete. Due to the compactness of the concrete matrix and the absence of coarse aggregate, Ductal® concrete has been shown to have almost no shrinkage or creep after cure, making it very suitable for pre-stressed applications (Perry 2003).

Various methods used to cure Ductal® concrete have been found to have significant effects on the material properties, particularly the ultimate compressive strength and shrinkage due to hydration. Graybeal and Hartmann (2003) showed that ultimate compressive strengths can vary as much as 35% between ambient air and steam cured specimens. The ambient air cured specimens were shown to only have 65% of the compressive strength of their steam cured counterparts. Similar results were found in the limited shrinkage study performed by Graybeal and Hartmann (2003).

Initial measurements of 1 in. by 1 in. by 11 in. Ductal® bars were taken immediately after the stripping of the molds. Each specimen was cured using steam, tempered steam, delayed steam or ambient air methods. Upon the completion of the curing process final measurements were taken and compared with the initial measurements. The results showed that steam cured specimens shrank approximately half as much as ambient air cured specimens. The high shrinkage values can be attributed to high cement content, and the lack of coarse aggregate (Graybeal and Hartmann 2003). Although initial shrinkage values are high, with its impermeability to water and closed pore structure, Ductal® concrete has been shown to resist delayed hydration. This in turn causes any subsequent shrinkage values to be very minimal.

2.3 Shear friction

The development of new and stronger materials has allowed bridge spans to increase, and the corresponding beam sections to decrease in overall size. As this trend continues, the forces carried by composite sections will inevitably

continue to increase. In order for beam and deck sections to act compositely, horizontal shearing forces must be transferred across their interface. Throughout the years, many equations have been developed to determine both the horizontal shearing force in a composite section, and the horizontal shearing capacity of a particular section. The horizontal shearing forces developed in a fully composite section are illustrated in Figure 2.1.

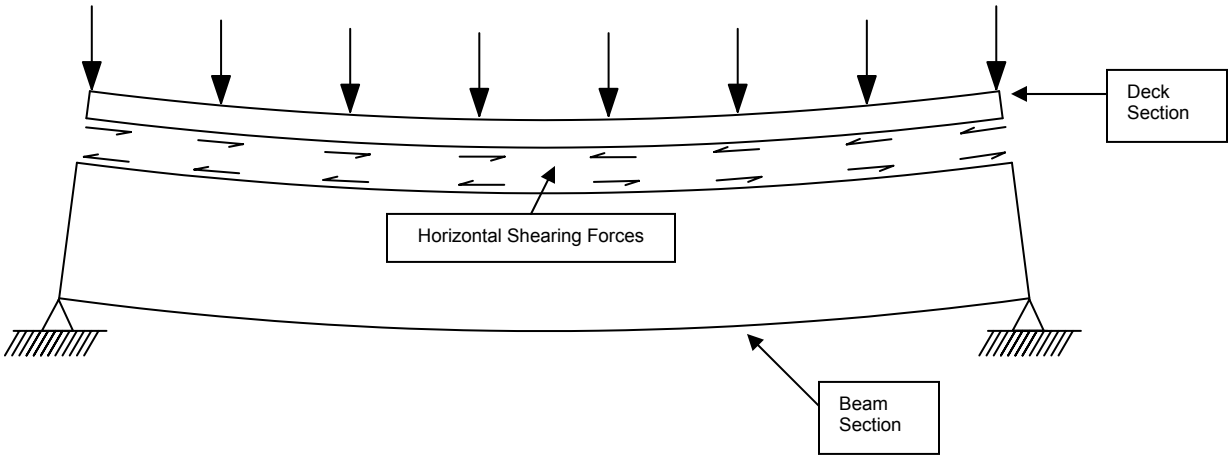

Figure 2.1 Horizontal Shearing Forces in a fully composite section

2.3.1 Horizontal Shearing Stresses

There are multiple equations that can be used to determine the horizontal shearing stress at any point on the cross-section of a beam. Perhaps the most well known and fundamental equation comes from elastic beam theory. Provided the concrete beam and deck are 1) uncracked, 2) fully composite, and 3) remain in the elastic stress range, one can use the following equation to determine the horizontal shearing stress at the interface.

$$v_h = \frac{VQ}{It} \tag{2.1}$$

where:

v_h = horizontal shearing stress.

V = the vertical shear in a given cross section.

Q = the first moment of area of the section above the interface, with respect to the elastic neutral axis of the entire cross section.

I = the uncracked moment of inertia for the entire composite section.

t = the width of the interface.

Tests have shown that equation 2.1 is valid for cracked sections as long as both Q and I are found using the cracked section properties (Loov and Patnaik 1994).

ACI Code 318 (2002) allows designers to compute the horizontal shearing stress at the interface of composite sections using two methods. ACI Code 318, Sec. 17.5.2, states that the horizontal forces in the composite section must adhere to the following limit state:

$$V_u \leq \phi V_{nh} \tag{2.2}$$

where:

V_u = the ultimate shear force on a given section.

ϕV_{nh} = the design horizontal shear strength at a given cross section.

The horizontal shear stress can be determined with the following equation:

$$v_h = \frac{V_u}{b_v d} \tag{2.3}$$

where:

v_h = horizontal shearing stress.

V_u = the factored vertical shear in a given cross section.

b_v = width of the interface.

d = distance from extreme compression fiber to centroid of tension reinforcement for entire composite section.

ACI Code 318, Sec. 17.5.3, provides an alternative method to solve for the horizontal shearing stresses in a composite section, using equilibrium conditions. Sec. 17.5.3 allows horizontal shear to be computed in a composite section from

the change in compressive or tensile force in the slab in any segment of its length (MacGregor 1997). This can be expressed as the following:

$$v_h = \frac{C}{b_v l_v} \tag{2.4}$$

where:

v_h = horizontal shearing stress.

C = Change in the compressive force in the flange.

b_v = width of the interface.

l_v = length over which the horizontal shear is to be transferred.

To better understand this concept, one can look at a simply supported beam where the maximum compressive force in the deck occurs at midspan. At the end of the beam, this compressive force has dropped to zero. The horizontal force that must be transferred across the interface from midspan to the end of the beam is equal to the compressive force in the deck at midspan. This value divided by the interface area will give the average horizontal shearing stress for the composite section.

The three previous equations appear to be unrelated, but each shares a common trait. Each equation has the shear per unit length, or shear flow, in the flange as part of its makeup. VQ/I is the shear flow in the flange in equation 2.1, V/d in equation 2.3 is a non-conservative simplification of VQ/I, and C/l_v is the average change of force per unit length in the flange in equation 2.4. Each equation must be used in the proper design situation. For example, equation 2.4 may be unsafe for design of sections with uniform loading, due to varying shear (Loov and Patnaik 1994).

2.3.2 Horizontal Shear Strength Equations

Throughout the years, there have been many proposed equations for determining the horizontal shear strength of the interface zone in composite sections. These proposed equations range in both complexity and accuracy in

predicting shear strengths. This thesis discusses some of the horizontal shear equations proposed throughout the years. For all of the proposed equations, the term $\rho_v f_y$ refers to the clamping stress, and v_n refers to the horizontal shear strength.

2.3.2.1 Mast Equation

A linear shear-friction equation was introduced by Mast (1968), and was later revised by Anderson (1960). The equation is as follows:

$$v_n = \rho_v f_y \mu \tag{2.5}$$

The coefficient of friction at the interface is represented by μ. According to Loov and Patnaik (1994), this equation is very conservative for low clamping stresses, and unsafe for sections with high clamping stresses.

2.3.2.2 Hanson Research

Research performed by Hanson (1960) determined that the maximum horizontal shear strength between precast beams and cast-in-place slabs was approximately 300 psi for smooth surfaces, and 500 psi for rough bonded surfaces. Hanson also found that the horizontal shear strength of a joint could be increased by approximately 175 psi for each percent of reinforcing steel crossing the interface between the two surfaces. For Hanson's research, he considered that the maximum horizontal shear strength was reached when a slip of 0.005 in. had occurred. Subsequent research by Saemann and Washa (1964) incorporated this slip limit into its results.

2.3.2.3 Saemann and Washa Equation

Tests performed by Saemann and Washa (1964) on full size beams yielded an equation for determining the horizontal shear strength of a composite section. This equation takes into account the percent of steel crossing the interface, the span length, and the effective depth of the section. The effects of surface conditions were not included in the equation. This was intentionally left out since it was found that contributions from surface conditions were diminished

as the amount of reinforcement crossing the interface increased. Saemann and Washa's proposed equation is as follows:

$$Y = \frac{2700}{X+5} + 300P\left(\frac{33-X}{X^2+6X+5}\right) \text{(psi)} \qquad (2.6)$$

where:

Y = ultimate shear strength

P = percent steel crossing the interface

X = effective depth

The first portion of the equation represents the strength curve if no reinforcing steel is crossing the interface. If reinforcing steel is used, any added strength due to clamping forces is shown in the second portion of the equation.

2.3.2.4 Birkeland Equation

One of the first researchers to propose a parabolic function for the horizontal shear strength was Birkeland and Birkeland (1966). Birkeland's equation only incorporated a factor times the clamping stress as shown below:

$$v_n = 33.5\sqrt{\rho_v f_y} \text{ (psi)} \qquad (2.7)$$

Nothing in Birkeland's equation accounted for varying surface treatments or concrete strengths.

2.3.2.5 Walraven Equation

Walraven et al (1987) performed numerous push-off tests in order to develop equations that would accurately represent the horizontal shear strength of a given specimen. An extensive statistical analysis of the 88 push-off specimens yielded the following equation:

$$v_n = C_3\left(0.0007\rho_v f_y\right)^{C_4} \text{ (psi)} \qquad (2.8)$$

For the following equations, f'$_c$ is equal to 0.85 times the compressive strength found using 150 mm cubes. The equations for the C factors are as follows:

$$C_3 = 16.8 f'_c{}^{0.406} \qquad \text{and} \qquad C_4 = 0.0371 f'_c{}^{0.303}$$

2.3.2.6 Mattock Equation's

Throughout the years, Mattock (1974) has presented multiple equations to determine horizontal shear strengths. One equation was a modification to Walraven's equations, in order to account for the effects of concrete strength. This equation eliminated the C factors from Walraven's original equation. It is as follows:

$$v_n = 4.5 f'_c{}^{0.545} + 0.8\left(\rho_v f_y + \sigma_n\right) \text{ (psi)} \qquad (2.9)$$

$$\text{and } v_n \le 0.3 f'_c$$

Mattock et al (1975) later proposed the following linear equation to determine the horizontal shear strength of an initially cracked interface:

$$v_n = 400 + 0.8\rho f_y \text{ (psi)} \qquad (2.10)$$

where:

$$v_n \le 0.3 f'_c \text{ (psi)}$$

Mattock et al (1976) performed research on the horizontal shear strength of lightweight concrete. From this research, Mattock et al determined that the shear strength of lightweight concrete is less than that of normal weight concrete of the same compressive strength. It was found that ACI 318 (2002) equations used to calculate shear transfer strengths were valid provided a lightweight concrete multiplier was used to modify the coefficients of friction used in Section 11.7.4.3. Mattock proposed that the coefficient of friction variable (μ) should be multiplied by a factor λ. For all lightweight concrete with a unit weight not less than 92 lbs/ft^3, λ should be 0.75. For sand lightweight concrete with a unit weight not less

than 105 lbs/ft^3 λ should be 0.85. In the same research, Mattock proposed the following equation for horizontal shear strength of lightweight concrete.

For sand lightweight concrete with a unit weight not less than 105 lb/ft^3:

$$v_n = 0.8\rho f_y + 250 \text{ psi} \quad (2.11)$$

where:

$$v_n \le 0.2 f'_c$$

$$v_n \le 1000 \text{ psi}$$

$$\rho f_y \ge 200 \text{ psi}$$

For all lightweight concrete with a unit weight not less than 92 lb/ft^3:

$$v_n = 0.8\rho f_y + 200 \text{ psi} \quad (2.11)$$

where:

$$v_n \le 0.2 f'_c$$

$$v_n \le 800 \text{ psi}$$

$$\rho f_y \ge 200 \text{ psi}$$

2.3.2.7 Loov Equation

Loov (1978) was one of the first researchers to incorporate the influence of concrete strength directly into the horizontal shear equation. The proposed equation is shown below:

$$v_n = k\sqrt{\rho_v f_y f'_c} \quad (2.12)$$

where:

$$k = \text{constant}$$

For an initially uncracked surface, Loov suggested using a k factor of 0.5. Hsu et al (1987) proposed, in a similar equation, using a k factor of 0.66 for both initially cracked and uncracked interfaces. According to Loov and Patnaik (1994), one advantage of this equation is that any consistent system of units can be used with out changing the equation.

2.3.2.8 Shaikh Equation

Shaikh (1978) proposed an equation for horizontal shear strength that was used by PCI as the basis for their design equations. The equation is as follows:

$$v_n = \phi \rho_v f_y \mu_e \tag{2.13}$$

where:

Φ = 0.85 for shear

$$\mu_e = \frac{1000\lambda^2}{v_n} \text{ (psi)}$$

λ = 1.0 for normal weight concrete

λ = 0.85 for sand-lightweight concrete

λ = 0.75 for all-lightweight concrete

The simplified form of this equation used by PCI is shown below:

$$v_n = \lambda\sqrt{1000\phi\rho_v f_y} \le 0.25 f'_c \lambda^2 \text{ and } 1000\lambda^2 \text{ (psi)}$$

2.3.2.9 Loov and Patnaik Equation

In 1994, Loov and Patnaik (1994) introduced an equation that combined equation 2.12 with an equation for the horizontal shear strength of composite beams without shear connectors. From that combination, a continuous curve equation for horizontal shear strength was developed. This equation, shown below, is applicable for both high and low clamping stresses.

$$v_n = k\lambda\sqrt{\left(15 + \rho_v f_y\right) f'_c} \le 0.25 f'_c \text{ (psi)} \tag{2.14}$$

where:

k = 0.6 as a lower bound for this range of concrete strength

λ = the lightweight concrete factors used in equation 2.13

Patnaik (2001) proposed a linear variation on his previous horizontal shear equations. This equation is presented below.

$$v_n = 87 + \rho_v f_y \leq 0.2 f'_c \text{ and } 800 \text{ psi} \qquad (2.15)$$

$$v_n = 0 \text{ for } \rho_v f_y < 50 \text{ psi}$$

Patnaik states that it is possible to obtain some nominal shear strength from a smooth interface with no reinforcing, but for design this is not recommended.

2.3.2.10 Kumar and Ramirez Research

Kumar and Ramirez (1996) performed research which showed that shear connectors in a beam were not strained prior to an initial slip of the interface. It was found that the strain in the shear connectors remained close to zero until an initial slip was observed. After the initial slip, the strain increased up to the yield capacity which led to the subsequent failure of the specimen. These tests revealed that Hanson's limiting slip parameter of 0.005 in. could significantly effect the horizontal shear capacity of an interface. If the specimen is not allowed to slip, the reinforcing steel provides very little contribution to the strength of the interface.

2.3.3 ACI Code 318/318R – 02

The ACI 318 Building Code and Commentary (2002) sets forth a series of linear design equations that can be used to determine the nominal horizontal shear strength of a particular composite design. These four design equations are to be used according to the guidelines set forth the ACI 318 code and are shown below. The factored shear force to be used for design can be considered to be V_u. This is shown in equation 2.2.

$$V_u \leq \phi V_{nh} \qquad (2.2)$$

An alternative method to determining the factored shear force is to determine the change in force along any segment of the beam. Once the shear force to be designed for is found, the nominal horizontal shear strength will need to be determined. This can be done using one of the four equations shown below.

If:

$$V_u > \phi(500 b_v d) \text{ (lbs)}$$

Then:

$$V_{nh} = A_{vf} f_y \mu \le \min(0.2 f'_c A_c \text{ or } 800 A_c) \text{ (lbs)}$$

where:

$\phi = 0.75$

$b_v =$ the width of the interface

$d =$ distance from extreme compression fiber to centroid of tension reinforcement for entire composite section

$A_{vf} =$ area of reinforcement crossing the interface

$f_y =$ yield stress of shear reinforcement

$A_c =$ the area of concrete section resisting shear transfer

$f'_c =$ concrete strength

$\mu = 1.4\lambda$ for concrete placed monolithically

$\mu = 1.0\lambda$ for concrete placed against hardened concrete with surface intentionally roughened

$\mu = 0.6\lambda$ for concrete placed against hardened concrete with surface not intentionally roughened

$\mu = 0.7\lambda$ for concrete placed anchored to as rolled structural steel by headed studs or by reinforcing bars

$\lambda = 1.0$ for normal weight concrete

$\lambda = 0.85$ for sand-lightweight concrete

$\lambda = 0.75$ for all lightweight concrete

If:

$$V_u \le \phi(500 b_v d) \text{ (lbs)}$$

Then:

$V_{nh} = 80 b_v d$ (lbs) when contact surfaces are clean, free of laitance, intentionally roughened, and have no shear reinforcement

$V_{nh} = 80 b_v d$ (lbs) when contact surfaces are clean, free of laitance, not intentionally roughened and the minimum ties are provided

$$A_{v\min} = 0.75\sqrt{f'_c}\frac{b_v s}{f_y} \ge \frac{50 b_v s}{f_y}$$

$s =$ spacing of shear reinforcing

$V_{nh} = (260 + 0.6\rho_v f_y)\lambda b_v d \le 500 b_v d$ (lbs) when contact surfaces are clean, free of laitance, intentionally roughened to a full amplitude of approximately ¼ in. and no less than the minimum ties are provided

According to the commentary in section 11.7.3, the above equations are conservative for design. The provisions in the ACI 318 design manual allow for other relationships to be used in order to give a closer estimate of the shear transfer strength.

2.3.4 AASHTO Standard Specifications

Another method used by designers for determining the horizontal shear strength of a composite section is in the AASHTO *Standard Specifications* (2002). The method for design laid out by the AASHTO *Standard Specifications* is very similar to the ACI Method. The design methodology is shown below.

As with ACI 318, equation 2.2 is used to determine what the nominal horizontal shear capacity of a composite section must be.

$$V_u \leq \phi V_{nh} \tag{2.2}$$

where:

V_u = factored vertical shear force acting at the section

V_{nh} = nominal horizontal shear strength

ϕ = 0.90

When the interface is intentionally roughened:

$V_{nh} = 80 b_v d$ when no reinforcement is provided

$V_{nh} = 350 b_v d$ when minimum vertical ties are provided

$V_{nh} = 330 b_v d + 0.40 A_{vh} f_y d / s$ when required area of ties exceeds the minimum area

where:

$A_{vh} = 50 \dfrac{b_v s}{f_y}$ (minimum area of ties)

$b_v =$ width of the interface

$d =$ distance from extreme compression fiber to centroid of the prestressing force, $d \geq 0.80h$

$s =$ maximum spacing not to exceed 4 times the least-web width of support element nor 24 in.

$f_y =$ yield stress of the reinforcing steel crossing the interface

2.3.5 AASHTO LRFD Specifications

The final design guide of importance for this thesis, is the AASHTO LRFD Specification (2004). This guide uses a linear equation to determine the horizontal shear strength of a composite section. The design guide does not provide guidance for finding the ultimate horizontal shear at a section, but equation 2.3 can be used.

$$v_{uh} = \frac{V_u}{b_v d_v} \tag{2.3}$$

where:

$v_{uh} =$ horizontal factored shear force per unit area of interface

$V_u =$ factored vertical shear force at specified section

$d_v =$ the distance between resultants of tensile and compressive forces

$b_v =$ width of the interface

Equation 2.3 can be can be used in the following equation for design purposes.

$$v_{uh} A_{cv} \leq \phi V_n$$

where:

$\phi =$ 0.90

The nominal shear resistance of the interface plane shall be taken as:

$$V_n = cA_{cv} + \mu\left(A_{vf} f_y + P_c\right)$$

where:

$V_n \leq 0.2 f'_c \, A_{cv}$

$V_n \leq 0.8 A_{cv}$

$A_{cv} =$ interface area

$A_{vf} =$ area of horizontal shear reinforcement

$f_y =$ yield strength of reinforcement

$c =$ cohesion factor

$\mu =$ friction factor

$P_c =$ permanent compressive normal force.

If normal force is tensile, $P_c = 0.0$

$f'_c =$ concrete compressive strength

For concrete placed monolithically:

$c = 0.150$ ksi

$\mu = 1.4\lambda$

For concrete placed against clean, hardened concrete with surface intentionally roughened to an amplitude of 0.25 inches:

$c = 0.100$ ksi

$\mu = 1.0\lambda$

For concrete placed against hardened concrete clean and free of laitance, but not intentionally roughened:

$c = 0.075$ ksi

$\mu = 0.6\lambda$

For concrete anchored to as-rolled structural steel by headed studs or by reinforcing bars where all steel in contact with concrete is clean and free of paint:

$c = 0.025$ ksi

$\mu = 0.7\lambda$

$\lambda = 1.00$ for normal weight concrete

$\lambda = 0.85$ for sand-lightweight concrete

$\lambda = 0.75$ for lightweight concrete

According to the PCI Design Handbook (1992), the minimum required reinforcement must be provided regardless of the stress levels at the interface. Designers may choose to limit this requirement for economic purposes where applicable. Designers may choose to forgo shear connectors in cases where v_{uh}/Φ is not greater than 0.10 ksi.

2.4 Summary of Literature Review

This review of the development of the horizontal shear transfer equations throughout the years illustrates the many available methods to design composite sections. The previous research and equations do not provide information on designing for lightweight concrete placed on Ductal® beams. The following research presented in Chapter 3 was performed to test the validity of using the aforementioned equations to design the shear connections for a lightweight concrete bridge deck placed on hardened precast Ductal® bridge beams.

CHAPTER 3: SPECIMEN DETAILS AND TEST SETUP

3.1 Typical Specimen and Dead Weight Block Details

To analyze the horizontal shear transfer, Twenty-four push-off tests were performed. Push-off tests are commonly used for testing shear resistance. They allow for the application of direct shear along an interface. Each specimen contained one Ductal® concrete block cast at PSI pre-cast plant in Lexington, Kentucky. At Virginia Tech's structural engineering research laboratory, a lightweight concrete slab was placed directly on top of each Ductal® block. In doing so, an L-shaped slab was formed. The shape of the slabs allowed for load to be placed directly in line with the interface between the lightweight slab and the Ductal® block. Figure 3.1 shows a typical 18 in. test specimen. Also included in the study were 12 in. and 24 in. long specimens.

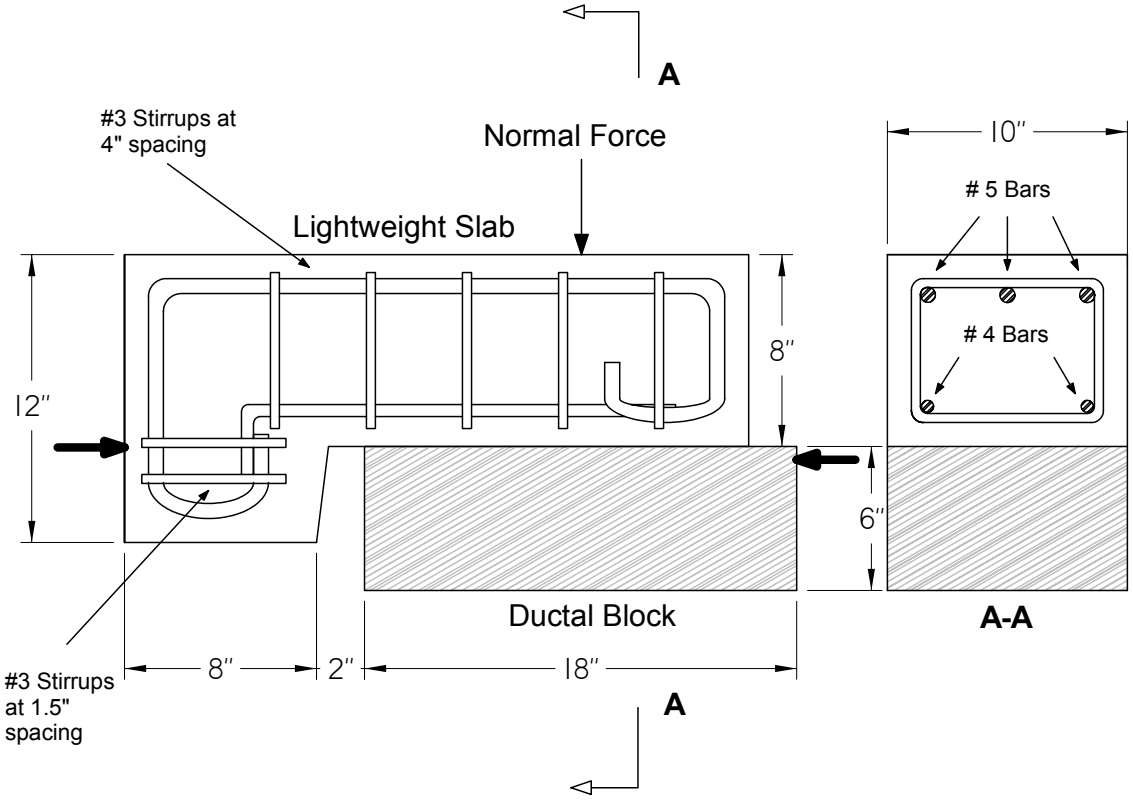

Figure 3.1 Typical 18 in. push-off test specimen

To simulate the dead load exerted by the bridge deck on the full size beams, a normal force was applied to each specimen during testing. The full size beams would have approximately 1.6 psi of dead load exerted on the top flange of the bulb-tee beam. The normal force was determined by assuming that the dead load from an 8 in. thick bridge deck would be distributed along the full 3 ft. 11 in. width of the top flange of the beams spaced 10 ft. on center. To provide this normal force, a dead weight block was placed on the lightweight concrete slab. Three dead load blocks were fabricated, one for each of the specimen lengths tested. Each dead weight block only exerted load along the interface zone. Figure 3.2 shows a plan and cross-section view of a typical dead weight block.

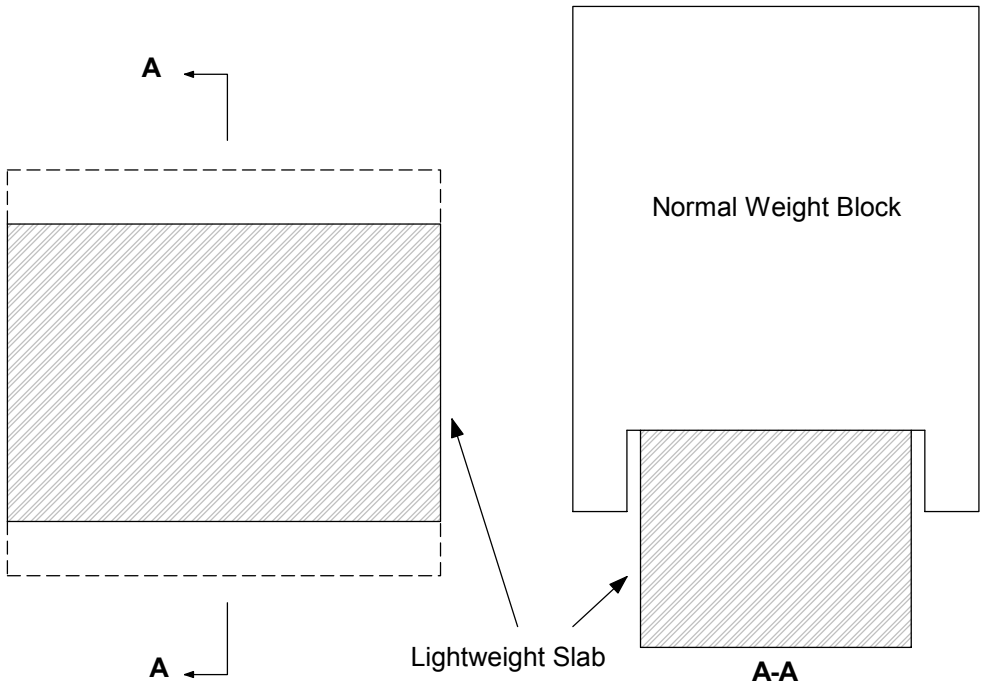

Figure 3.2 Typical Dead Weight Block

3.2 Ductal® Block Fabrication

As mentioned earlier, each specimen consisted of both Ductal® and lightweight concrete. The Ductal® blocks represented the top flange of the pre-cast Ductal® concrete bulb tee beams that are to be utilized in the construction of the actual bridge in Virginia. The Ductal® portions of the specimens were formed and cast at the PSI pre-cast plant in Lexington, Kentucky. Each specimen had a height of 6 in. and a width of 10 in. The lengths of the specimens were 12 in., 18 in., and 24 in. The intermediate length specimens of 18 in. were formed with a variety of interface surface treatments, both smooth and roughened.

Two of each of the following surface treatments were cast and subsequently tested for their ability to increase the horizontal interface shear transfer. These surface treatments consisted of:

- shear keys
- ½ in. deformations at 2 in. on center
- chipped surfaces

The shear keys were formed using 2 x 4's with angled cuts running lengthwise along each side. The shear keys were 10 in. in length by 1.5 in. in height. The average width of each shear key was approximately 3 in. Due to the viscoelastic nature of the Ductal® concrete prior to cure, the 2 x 4's were secured in place at the top of the Ductal® block forms and were not removed until the form work for the blocks was removed. Figure 3.3 illustrates a Ductal® block with a keyed surface.

A similar method of formwork was used to mimic the raking deformations commonly used on normal concrete pre-cast beams. Once again due to the viscoelastic nature of the Ductal® concrete, any deformations caused by raking the surface of the block prior to cure would not be permanent. To mimic the raking of the surface, ½ in. quarter-round was tacked to a sheet of plywood, 2 in. on center along the length of the board. Each piece of quarter-round was 10 in. in length. Immediately after the Ductal® concrete was poured, the plywood was set on top of the block, and left in place until the Ductal® block form work was removed. Figure 3.4 illustrates a Ductal® block with a deformed surface.

Figure 3.3 Keyed Surface Treatment

Figure 3.4 Deformed Surface Treatment

The final surface treatment was a chipped surface. This type of treatment not only caused an increase in the surface deformations, but it also exposed the steel fibers present throughout the Ductal® block. This allowed for both a chemical and mechanical bond to be present between the slab and beam concrete. After the Ductal® blocks reached a compressive strength around 30 ksi, a jackhammer was used to chip the surface. The jackhammer was only used enough to randomly remove small portions of the top layer of the Ductal® block concrete. Figure 3.5 illustrates a Ductal® block with a chipped surface.

Figure 3.5 Chipped Surface Treatment

To best examine the horizontal shear transfer across a smooth surface, control specimens were cast, which had surfaces representative of the actual top flange of the pre-cast beam. These “smooth” blocks had no formed surface deformations, and the Ductal® concrete in each block was allowed to self level. Two of these specimens were cast in each representative size block to allow for size effects to be determined. To prevent early age drying cracking, plastic

sheets were placed and smoothed onto the surface of each block. The final surfaces were slightly deformed and glassy. Figure 3.6 illustrates a Ductal® block with a smooth surface.

Figure 3.6 Smooth Surface Treatment

To determine the effects that reinforcement ratios had on the interface shear transfer, No. 3 mild steel reinforcing stirrups were used as shear reinforcing. The amount of horizontal shear reinforcing varied from a single leg No. 3 bar to six legs of No. 3 reinforcing. Two of each of the 12 in., 18 in., and 24 in. specimens were formed with 4 legs of No. 3 reinforcing steel. This allowed for the analysis of the relationship between the amount of steel crossing the interface zone and the ratio of steel to interface area. Two of each of the 18 in. specimens were formed having single leg, double legs and six legs of No. 3 bars crossing the interface zone. The surface treatment on all of the reinforced specimens was a smooth surface. Figures 3.7 to 3.10 illustrate the specimens with various amounts of reinforcing steel.

Figure 3.7 1 Leg of No. 3

Figure 3.8 2 Legs of No. 3

Figure 3.9 4 Legs of No. 3

F*igure 3.10 6 Legs of No. 3*

For this research project, twelve types of specimens with two of each type were tested. The specimens had variable interface areas, surface treatments, and amount of reinforcement crossing the interface. The various types and details of each of the 24 specimens are shown in Table 3.1.

Table 3.1 Specimen Details

Specimen	Ductal® Block Size	Interface Area	Legs of #3 Shear Stirrups	Area of Steel	Surface
	in	in^2		in^2	-
12S-0L-0-A	6x10x12	100	0	-	Smooth
12S-0L-0-B	6x10x12	100	0	-	Smooth
12S-2L-2-A	6x10x12	100	4	0.44	Smooth
12S-2L-2-B	6x10x12	100	4	0.44	Smooth
18S-1L-1-A	6x10x18	160	1	0.11	Smooth
18S-1L-1-B	6x10x18	160	1	0.11	Smooth
18S-2L-1-A	6x10x18	160	2	0.22	Smooth
18S-2L-1-B	6x10x18	160	2	0.22	Smooth
18S-2L-2-A	6x10x18	160	4	0.44	Smooth
18S-2L-2-B	6x10x18	160	4	0.44	Smooth
18S-2L-3-A	6x10x18	160	6	0.66	Smooth
18S-2L-3-B	6x10x18	160	6	0.66	Smooth
18S-0L-0-A	6x10x18	160	0	-	Smooth
18S-0L-0-B	6x10x18	160	0	-	Smooth
18D-0L-0-A	6x10x18	160	0	-	Deformed
18D-0L-0-B	6x10x18	160	0	-	Deformed
18K-0L-0-A	6x10x18	160	0	-	Keyed
18K-0L-0-B	6x10x18	160	0	-	Keyed
18C-0L-0-A	6x10x18	160	0	-	Chipped
18C-0L-0-B	6x10x18	160	0	-	Chipped
24S-0L-0-A	6x10x24	220	0	-	Smooth
24S-0L-0-B	6x10x24	220	0	-	Smooth
24S-2L-2-A	6x10x24	220	4	0.44	Smooth
24S-2L-2-B	6x10x24	220	4	0.44	Smooth

Specimen name key: (24S-2L-2-B) The first number, in this case the 24, is the length of the Ductal® concrete block in inches. The letter just after this number, S in this case, is the surface treatment. The next set of numbers and letters, in this case the 2L, designates the number of legs of reinforcing in each stirrup. The final number, 2 for this specimen, is the number of stirrups used. The final letter, A or B, tells which of the two specimens is being tested.

3.3 Light Weight Slab Fabrication

As previously mentioned, each Ductal® concrete block had a lightweight concrete slab placed directly on top of it. The lightweight concrete slab, used to represent the lightweight concrete bridge deck, was designed for a maximum applied load of 100 kips. The design was performed using strut and tie modeling assuming an f'_c value of 4000 psi for the deck concrete, and an f_y value of 60 ksi for the tension ties. From this modeling, it was determined that 3 each No. 5 bars placed in the top portion of the deck would adequately withstand the tensile forces induced in each specimen during testing. Two No. 4 bars near the bottom face of the deck, and multiple No. 3 stirrups were used as both confining reinforcing and to aid in the placement of the No. 5 tension ties. Figure 3.1 illustrates the configuration of the reinforcing steel in the lightweight concrete slab. Figure 3.11 shows a typical 12 in. specimen. The number and spacing of the No. 3 stirrups varied depending on specimen length. Figure 3.12 shows the blocks immediately prior to casting.

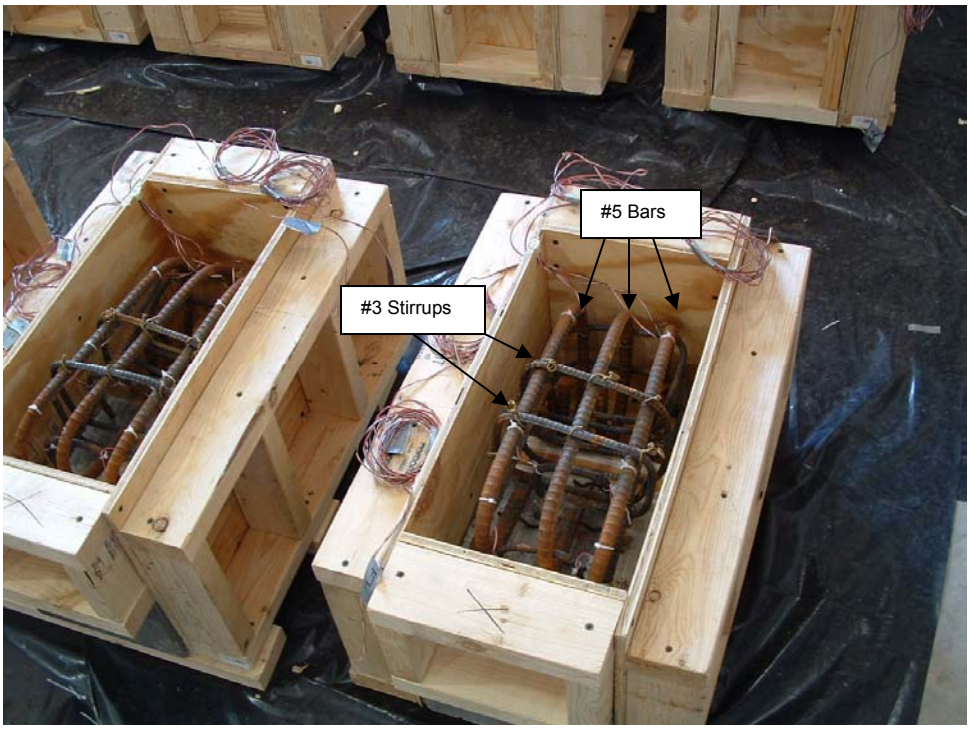

Figure 3.11 Typical formwork and reinforcing cage

Figure 3.12 Lightweight concrete formwork

3.4 Test Setup

After the lightweight concrete achieved adequate compressive strength, all formwork was removed, and the specimens were prepared for testing. Each specimen was banded along the interface zone; the banding wire helped to limit the forces on the interface zone during the movement of the specimens into the testing frame. After placement into the testing frame, the banding was removed and the blocks were tested to failure.

The testing frame consisted of one W-section and one T-section bolted to a reaction floor beam. To account for the varying specimen lengths, the W-section could be moved and reattached at various locations when needed. The W-section was used to restrain any horizontal displacement of the Ductal® block under loading. Attached to the T-section was a 200 kip hydraulic actuator, and attached to the piston on the actuator was a thick steel loading plate. A 150 kip load cell was placed between the 200 kip actuator and the loaded face of the test specimen. This load cell allowed for an accurate measurement of the

horizontal shearing force being applied to the specimen throughout each test. Figure 3.13 shows the testing frame and a typical test setup.

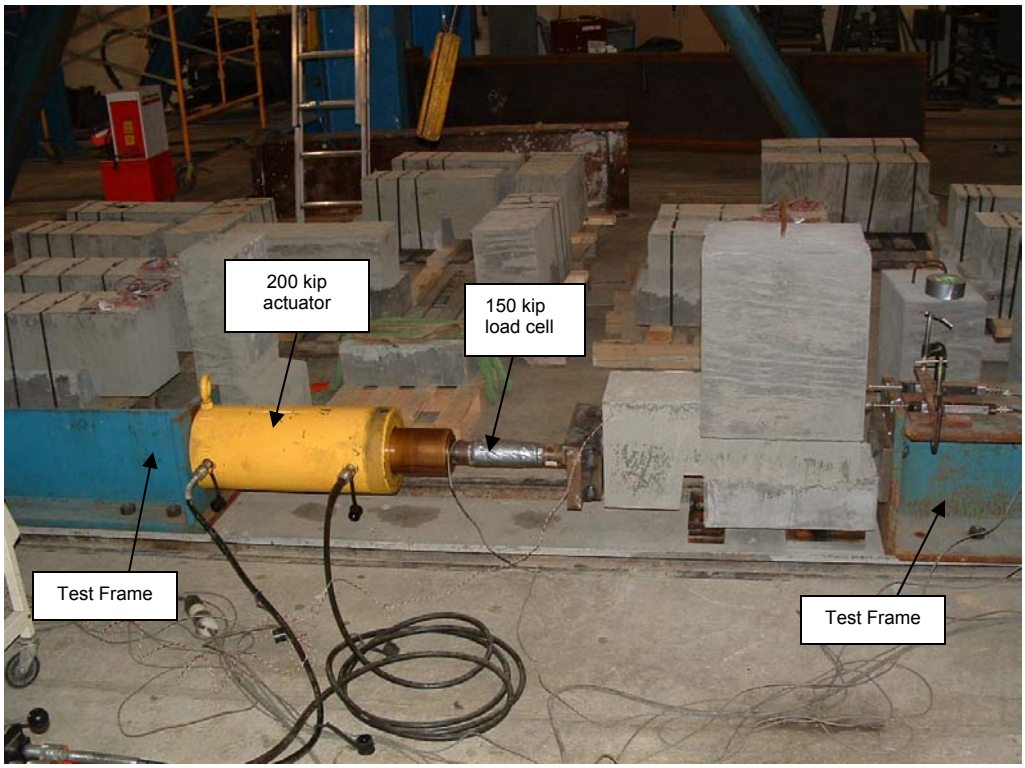

Figure 3.13 Test Frame, Load Cell and Actuator

3.4.1 Specimen Preparation and Instrumentation

One of the variables used in the design equations for horizontal shear transfer is the f_y value for the shear stirrups. It was intended as part of this research to test the validity of using the full value of f_y in the equations. To do this, electrical resistance strain gages were attached to each leg of reinforcing steel crossing the interface zone. This was performed prior to the lightweight concrete being placed. These strain gages were attached as close to the interface zone as possible. In doing so it was possible to accurately determine the strain in the reinforcing steel as each specimen was loaded. Of particular importance, strain at the moment of slip along the interface was measured. Each strain gage was bonded to the reinforcing steel using epoxy, and adequately protected from moisture that would be encountered during the

concrete placement. Figure 3.14 illustrates the strain gage configuration for a typical 6 legged reinforced specimen.

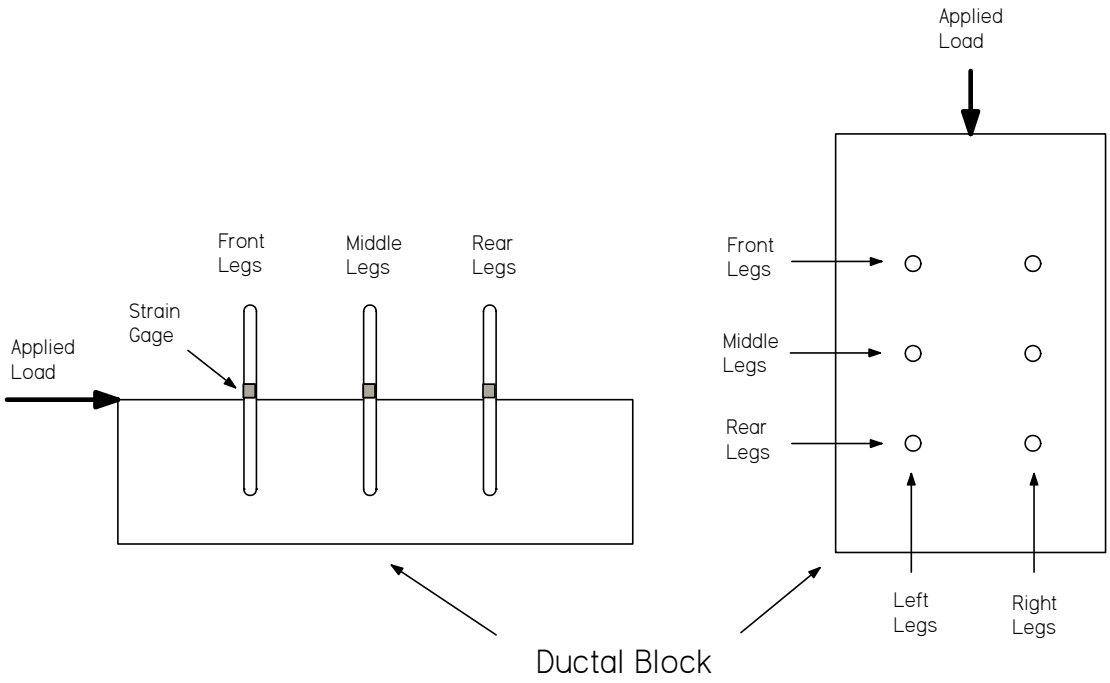

Figure 3.14 Reinforcement and Strain Gage Configuration

In order to accurately measure the slip along the interface zone, two spring loaded plunger type potentiometers were used. These devices were fixed to the testing frame and allowed to rest against the test specimen. Since the Ductal® concrete block rested against the rear portion of the testing frame it remained stationary throughout the test. By fixing the potentiometers to the test frame and allowing them to rest against the lightweight concrete portion of the specimen, the relative displacement of the lightweight concrete portion to the Ductal® block, under loading could be accurately measured. This was done by allowing the plunger to be depressed by the moving lightweight concrete block. Figure 3.15 illustrates the test setup and instrumentation. Figure 3.16 illustrates the location of the displacement potentiometers in relation to the lightweight concrete slabs.

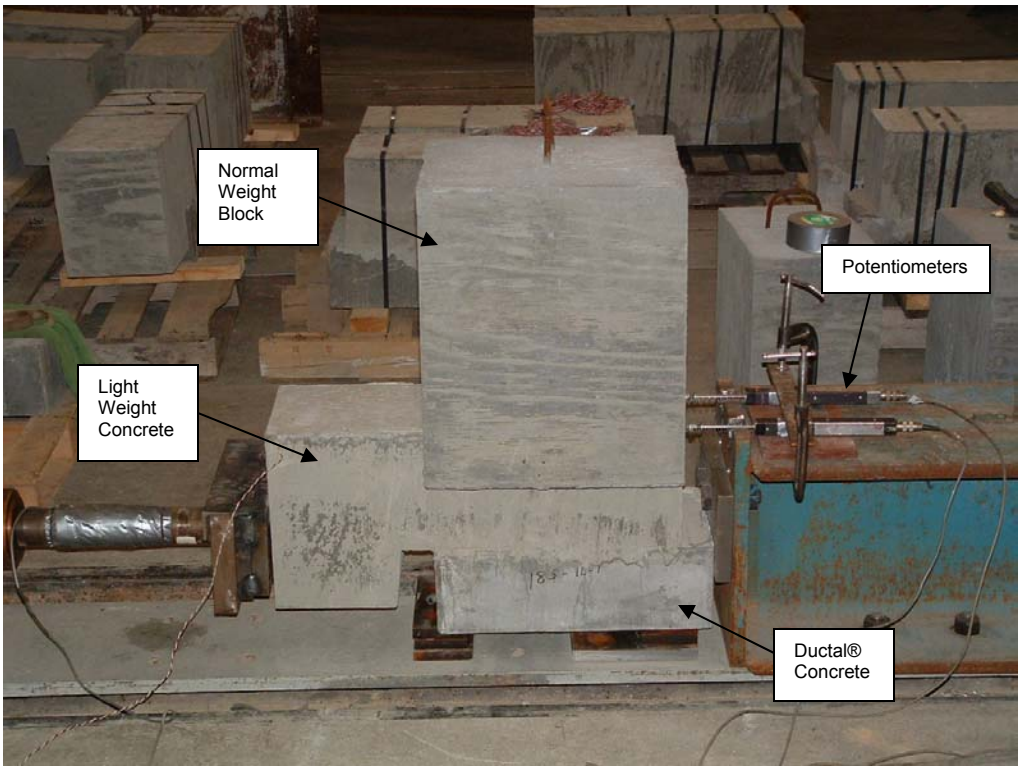

Figure 3.15 Typical test setup and Instrumentation

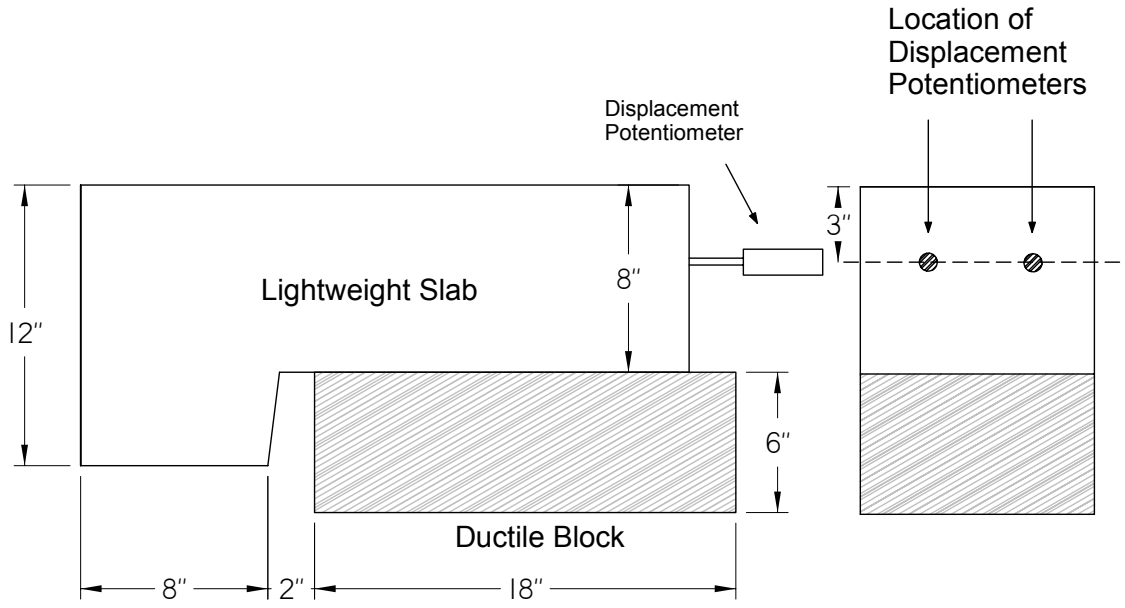

Figure 3.16 Location of the Displacement Potentiometers

All of the applied load, strain in the reinforcing steel and displacement measured by each respective instrument was recorded at half second intervals throughout the test. The data was recorded using a Measurements Group, Strain Smart System 5000 data acquisition system. The data from each test was reduced from the computer into spreadsheet format and subsequently analyzed.

3.4.2 Testing Procedure

Each specimen was placed into position using the overhead crane, and placed in such a manner that the rear face of the Ductal® block was resting against the test frame. The contact area between the Ductal® block and testing frame was only one inch below the interface area along the full width of the Ductal® block. This allowed for all of the horizontal shearing loads being applied to the specimen to be resisted by the test frame as close to the interface zone as possible. By having a small contact area between the Ductal® block and the test frame, the forces acting on the specimen were almost directly in line with the interface between the lightweight slab and the Ductal® block. The compressive stresses experienced by the Ductal® concrete block during maximum loading, due to the restraining forces at the contact area, were well below the design f'_c value of 30 ksi. By minimizing the contact area, the moment acting to overturn the test specimen at maximum loading was also greatly reduced and considered to be negligible.

Once the specimen was centered in the testing frame, the banding wires were cut, and the normal weight block was placed on the block along the interface zone. The normal weight block provided enough force on the specimen to simulate the normal forces that would be experienced by the top flange of the actual Ductal® concrete beam due to the lightweight concrete bridge deck. By having the normal weight block resting freely on the specimen the normal force would not change under testing. If the specimen “jumps” upward when the interface between the lightweight and Ductal® concrete slips under loading, the normal force will remain constant and act independently of the movement of the lightweight block.

Subsequent to the placement of the normal weight block, the potentiometers were attached to the test frame and allowed to touch the rear face of the lightweight concrete portion of the specimen. Before each test, the calibration of the potentiometers was checked using various size metal plates, with known values for each. If the potentiometer needed recalibration, it was removed, recalibrated using a dial gage, and reattached to the test frame.

The final portion of the test setup was the attaching of the loading plate to the actuator. In order to account for any irregularities in the geometry of the loaded face of the specimen, a neoprene pad was attached between the loading plate and the lightweight concrete. This plate was attached to the actuator and allowed for the horizontal shearing load to be applied in line with the interface zone between the lightweight and Ductal® concrete. The plate extended 3 in. above and below the interface zone, and the full width of the specimen. The maximum compressive stress in the loaded face of the lightweight concrete due to the loading was below the design f'_c value of 4 ksi.

With the specimen instrumented, the instruments zeroed and calibrated, and the specimen properly placed in the testing frame, the testing could commence. As previously mentioned, the data acquisition system recorded readings from all of the instruments at ½ second intervals throughout the testing process. Upon beginning the recording process, the loading of the test specimen began. The initial loading, or the touch load, placed upon the specimen caused the loading plates, specimen, and frame to settle into a stationary position. The data recorded by the instruments during this initial loading phase, particularly the displacements, were recorded and included in the charts in the appendix, but was not used for analysis. This will be discussed in greater detail in Chapter 4 of this thesis.

Throughout the test, the specimen was loaded in a monotonically increasing fashion. The loading was increased by using a hand pump to increase the hydraulic fluid pressure in the 200 kip actuator. The loading was increased until an initial slip or crack formed in the specimen along the interface zone. For unreinforced specimens, the loading dropped almost immediately to a

negligible value, and the test was completed. For reinforced specimens, the initial slip across the interface caused the load to drop, but each specimen continued to hold load. The load was continually increased until either all of the reinforcing steel across this interface ruptured, or the displacement of the lightweight concrete block relative to the Ductal® block approached 2 in. After each test, the lightweight and Ductal® concrete blocks were examined for localized crushing of the concrete around the ruptured reinforcing steel.

CHAPTER 4: PRESENTATION OF RESULTS AND ANALYSIS

4.1 Typical Test Behavior

Each of the 24 push-off tests followed a similar pattern once the testing procedure commenced. Each specimen was able to hold an increasing amount of horizontal load up to an initial cracking load. It was at this load that the initial bond between the concrete at the interface released. For the specimens with no horizontal shear reinforcement, this was the ultimate load. After the initial release, the load carrying capacity of the interface became negligible. For the reinforced specimens, the initial cracking at the interface was not the ultimate horizontal load applied during each test. Upon cracking, the shear reinforcement began to pick up load and subsequently apply a clamping force to the interface. This allowed an increasing amount of load to be applied to the specimen until the ultimate rupture of the reinforcing steel. One trait common to nearly all of the reinforced specimens was the minimal amount of strain in the horizontal shear connectors prior to the initial separation of the interface. After the initial separation, the strain in the reinforcing steel increased significantly. The load versus strain diagrams, presented later in this chapter, clearly show this trend.

For all of the tests performed, any initial load on the specimens in the beginning of each test was considered to be the “touch” load. This settled the blocks into place in the testing frame. Displacement readings were taken throughout the testing process, with the initial zero displacement being taken prior to initial loading. Once the specimens were completely settled into the testing frame, the load versus slip plots increased linearly until the initial separation of the interface. From the linear portion of the load versus slip plot for each specimen, interpolation was used to determine the differential displacement at the initial slip load, and at the maximum load. This process can be seen in the load versus slip plots incorporated into this chapter, and in the subsequent appendix.

4.1.1 Tests with No Shear Connectors and a Smooth Surface

Each of the specimens tested that had no horizontal shear connectors and a smooth surface exhibited very similar failure modes. The load on each specimen increased until the bond between the concrete at the interface released. At the moment of initial slip, the load dropped to almost zero. Any subsequent horizontal shearing capacity was considered negligible.

The overall smoothness of each specimen appeared to have a significant effect on the ultimate shearing strength of the interface. Although the Ductal® concrete was self leveling, prior to steam curing, plastic was placed by hand on top of each specimen while the concrete was still fluid. Due to the tendency of initially placed Ductal® concrete to crack when exposed to ambient air, it was very important that no air spaces remained between the plastic and the concrete. How carefully the plastic was placed on the specimen, determined the smoothness of the Ductal® block. The hand placed plastic had the tendency to cause small ripples on the top of the Ductal® blocks. These minor, yet irregular surface deformations had a significant effect on the ultimate horizontal shearing capacity of the various unreinforced smooth surface specimens. For example, the surface of specimen 18S-0L-0-A was slightly rougher than specimen 18S-0L-0-B. Specimen A held an ultimate load that was nearly 30% higher than specimen B. A similar trend was apparent in the 12 in. unreinforced smooth surface specimens. Specimen 12S-0L-0-A was slightly smoother than specimen 12S-0L-0-B, and had an ultimate shearing capacity that was nearly 80% lower than specimen B. The maximum shearing stress across the interface for the smooth surface specimens ranged from 102 psi to 227 psi. Figure 4.1 illustrates the typical behavior of the unreinforced smooth surface specimens in a load versus slip plot. Figure 4.2 shows a smooth surface specimen after testing. Tables 4.1 and 4.2 show the test results for typical 18 in. and 12 in. smooth surface specimens.

Table 4.1 Test Results for a Typical 18 in. Smooth Surface Specimen

Reinforcing	none
Area of Reinforcing, A_{vh}	-
Yield Stress of reinforcing	-
Normal force, P_n	256 lbs
Width of interface, b_v	10 in
Length of interface, s	16 in
f'c, lightweight concrete	5862 psi
Surface type	Smooth
f'c, ductile concrete	32.3 ksi
Slip Load	16.38 kips
Ultimate Load	16.38 kips
Displacement at Slip Load	0.034 in
Displacement at Ultimate Load	0.034 in

Table 4.2 Test Results for a Typical 12 in. Smooth Surface Specimen

Reinforcing	none
Area of Reinforcing, A_{vh}	-
Yield Stress of reinforcing	-
Normal force, P_n	160 lbs
Width of interface, b_v	10 in
Length of interface, s	10 in
f'c, lightweight concrete	5862 psi
Surface type	Smooth
f'c, ductile concrete	32.3 ksi
Slip Load	19.03 kips
Ultimate Load	19.03 kips
Displacement at Slip Load	0.023 in
Displacement at Ultimate Load	0.023 in

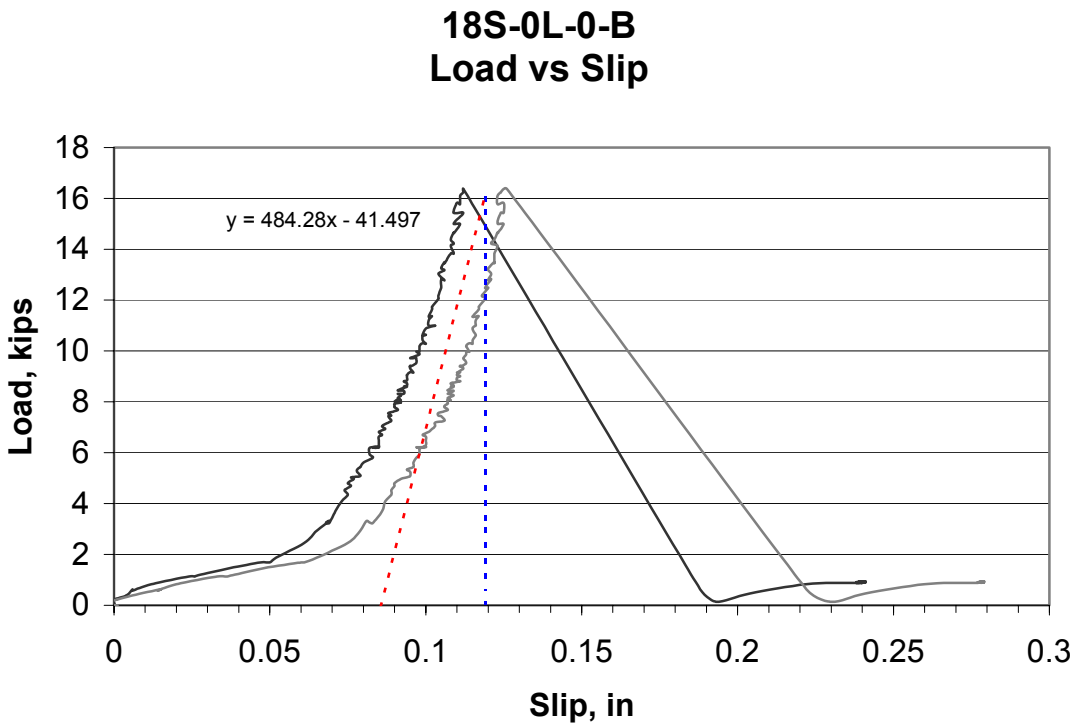

Figure 4.1 Typical Load versus Slip Plot for the Unreinforced Smooth Surface Specimens

In Figure 4.1, the differential displacement was found by averaging the measurements taken by the displacement potentiometers and comparing that against the best fit line found using linear interpolation. For this example, the differential displacement was found to be 0.034 in., and the maximum horizontal load was 16.38 kips.

Figure 4.2 Ductal® Side of Smooth Surface Specimen (After Testing)

4.1.2 Tests with No Shear Connectors and Deformed Surfaces

The failure modes of the tests specimens with no shear connectors and deformed surfaces were very similar to the specimens with no shear connectors and smooth surfaces. The deformed surface specimens exhibited higher horizontal shearing capacities than the smooth surface specimens of similar geometry. The surface treatments were either keyed, deformed, or chipped. Six tests, two of each surface treatment, were performed. All of the specimens with deformed surfaces were 18 in. in length. Once again, the load on each specimen increased until the bond between the concrete at the interface released. At the moment of initial slip, the load dropped to almost zero. For all of the specimens, any subsequent horizontal shearing capacity was considered negligible.

The chipped surface specimens were able to hold much higher horizontal shearing loads than the unreinforced smooth surface specimens. The chipped surface specimens appeared to experience both a chemical and mechanical

bond at the interface. This can be attributed to the exposure of fibers when the surface was chipped. These fibers bonded with the lightweight concrete, and may be analogous to small reinforcing ties distributed across the interface. Although the horizontal shearing capacity of the chipped surface specimens was increased by a factor of almost three when compared to smooth surface specimens with the same interface area, the failure was still brittle, and the displacement at slip was not significantly increased. Figure 4.3 illustrates the typical behavior of the unreinforced chipped surface specimens in a load versus slip plot. Figure 4.4 shows a typical chipped surface specimen after testing. Table 4.3 shows the test results for a typical 18 in. chipped surface specimen.

Table 4.3 Test Results for a Typical 18 in. Chipped Surface Specimen

Reinforcing	none
Area of Reinforcing, A_{vh}	-
Yield Stress of reinforcing	-
Normal force, P_n	256 lbs
Width of interface, b_v	10 in
Length of interface, s	16 in
f'c, lightweight concrete	5862 psi
Surface type	Chipped
f'c, ductile concrete	32.3 ksi
Slip Load	64.09 kips
Ultimate Load	64.09 kips
Displacement at Slip Load	0.046 in
Displacement at Ultimate Load	0.046 in

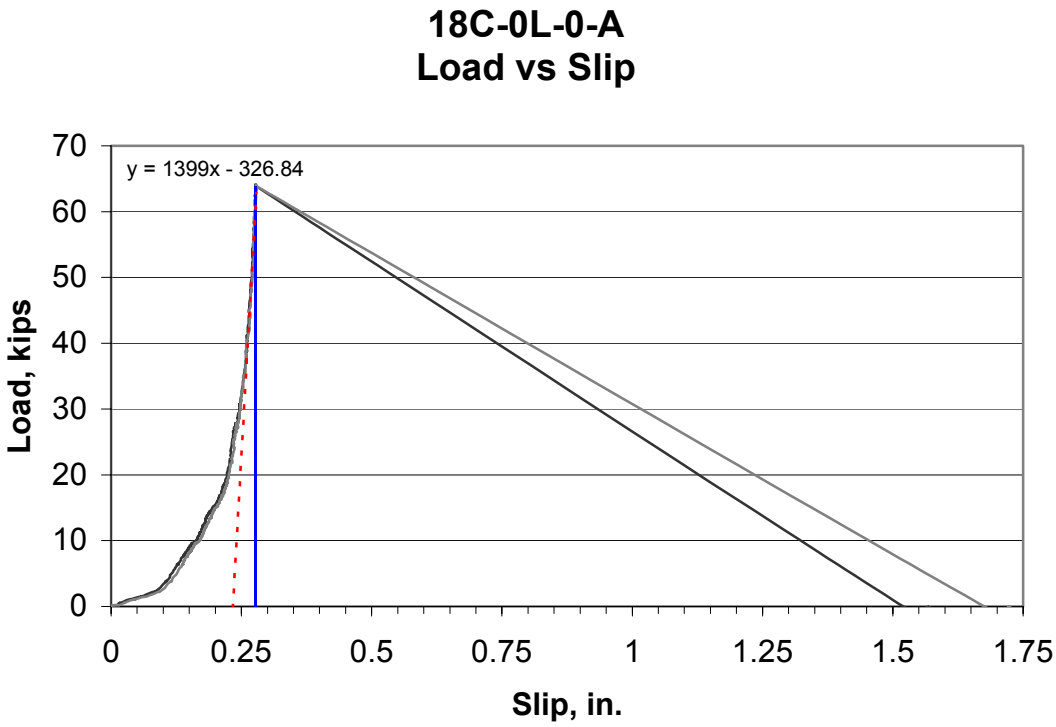

Figure 4.3 Typical Load versus Slip Plot for the Chipped Surface Specimens

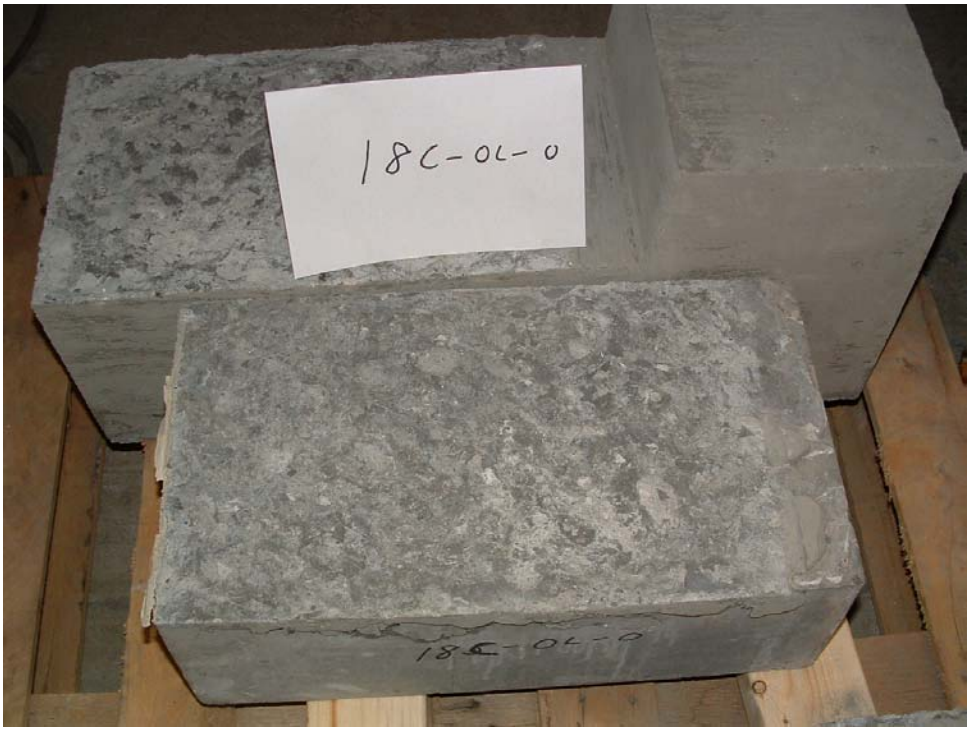

Figure 4.4 Ductal® Side of Chipped Surface Specimen (After Testing)

Both of the keyed specimens experienced a higher horizontal shearing capacity than comparable smooth surface specimens. The average ultimate load experienced by these two specimens was approximately 2.5 times that of the smooth surface specimens. As was seen with the chipped surface specimens, the keyed specimens experienced a higher shearing capacity, with very minimal increase in the displacement of the specimen at slip. The higher shearing capacity of these two specimens can be attributed to the shear failure plane passing through the cross-section of each of the shear keys. Figure 4.5 illustrates the typical behavior of the unreinforced keyed surface specimens in a load versus slip plot. Figure 4.6 shows a typical keyed surface specimen after testing. Table 4.4 shows the test results for a typical 18 in. keyed surface specimen.

Table 4.4 Test Results for a Typical 18 in. Keyed Surface Specimen

Reinforcing	none
Area of Reinforcing, A_{vh}	-
Yield Stress of reinforcing	-
Normal force, P_n	256 lbs
Width of interface, b_v	10 in
Length of interface, s	16 in
f'c, lightweight concrete	5862 psi
Surface type	Keyed
f'c, ductile concrete	32.3 ksi
Slip Load	50.09 kips
Ultimate Load	50.09 kips
Displacement at Slip Load	0.035 in
Displacement at Ultimate Load	0.035 in

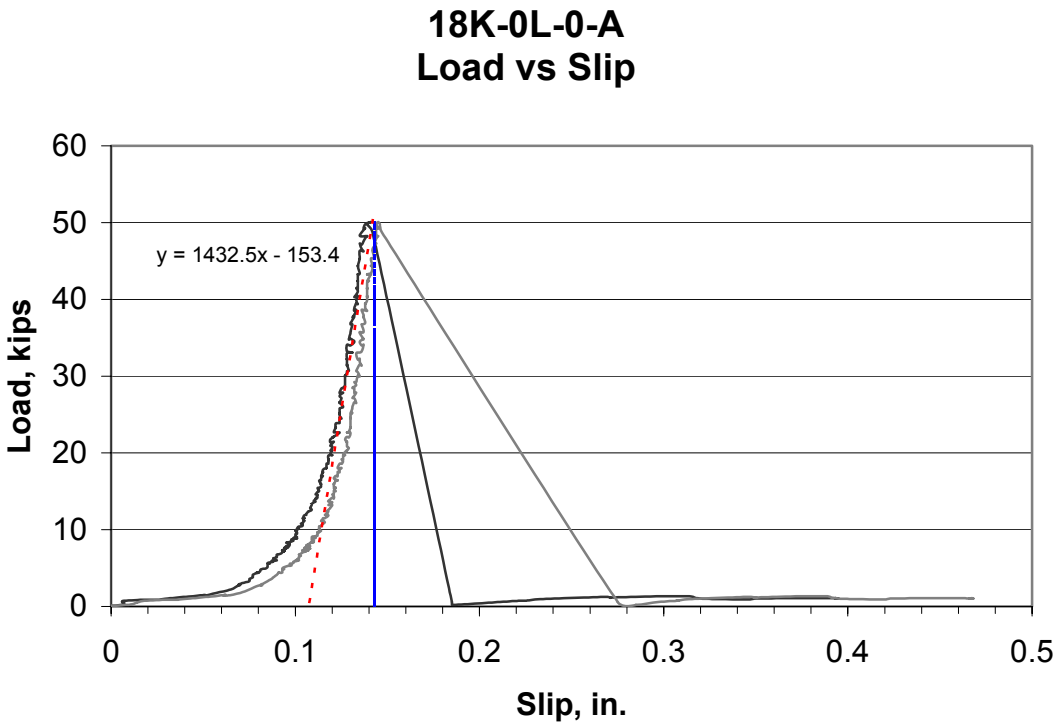

Figure 4.5 Typical Load versus Slip Plot for the Keyed Specimens

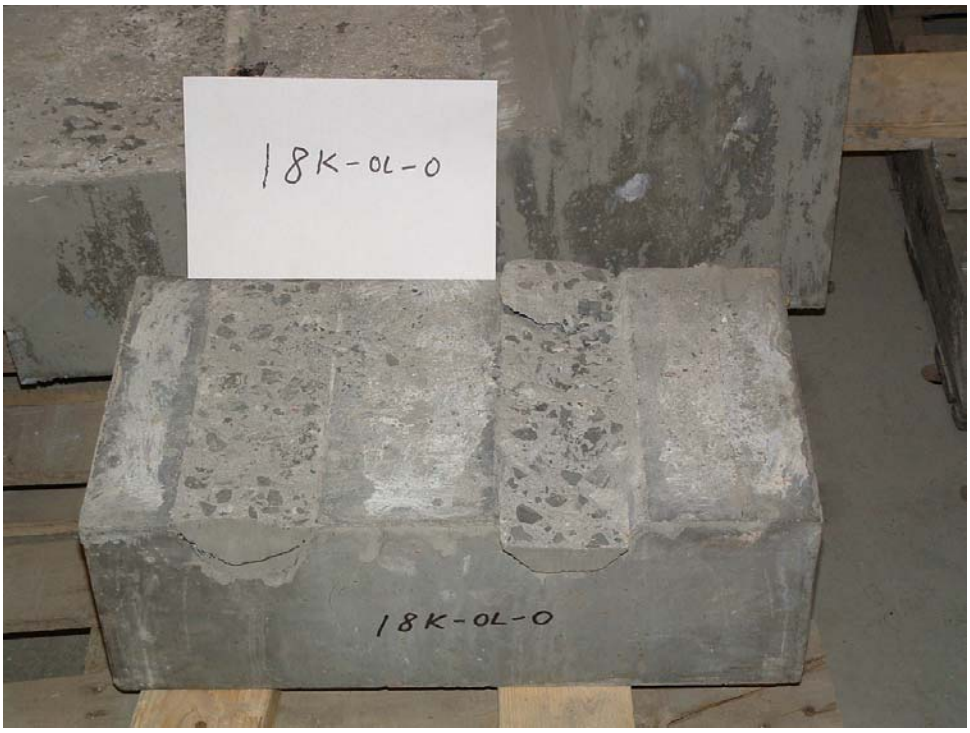

Figure 4.6 Ductal® Side of Keyed Surface Specimen (After Testing)

All of the deformed surface specimens experienced an increase in the horizontal shearing capacity, but the least effective was the “deformed” specimens. The average increase in the shearing capacity versus comparable smooth surface specimens was only a factor of 1.5, and the average displacement at slip was lower than the smooth surface specimens. The failure mode of the deformed specimens was not like the keyed specimens. The failure plane followed the deformations, and caused the lightweight concrete to cleanly separate from the Ductal® concrete. Figure 4.7 illustrates the typical behavior of the deformed surface specimens in a load versus slip plot. Figures 4.8 shows a typical deformed surface specimen after testing. Table 4.5 shows the test results for a typical 18 in. deformed surface specimen.

Table 4.5 Test Results for a Typical 18 in. Deformed Surface Specimen

Reinforcing	none
Area of Reinforcing, A_{vh}	-
Yield Stress of reinforcing	-
Normal force, P_n	256 lbs
Width of interface, b_v	10 in
Length of interface, s	16 in
f'c, lightweight concrete	5862 psi
Surface type	Deformed
f'c, ductile concrete	32.3 ksi
Slip Load	27.06 kips
Ultimate Load	27.06 kips
Displacement at Slip Load	0.018 in
Displacement at Ultimate Load	0.018 in

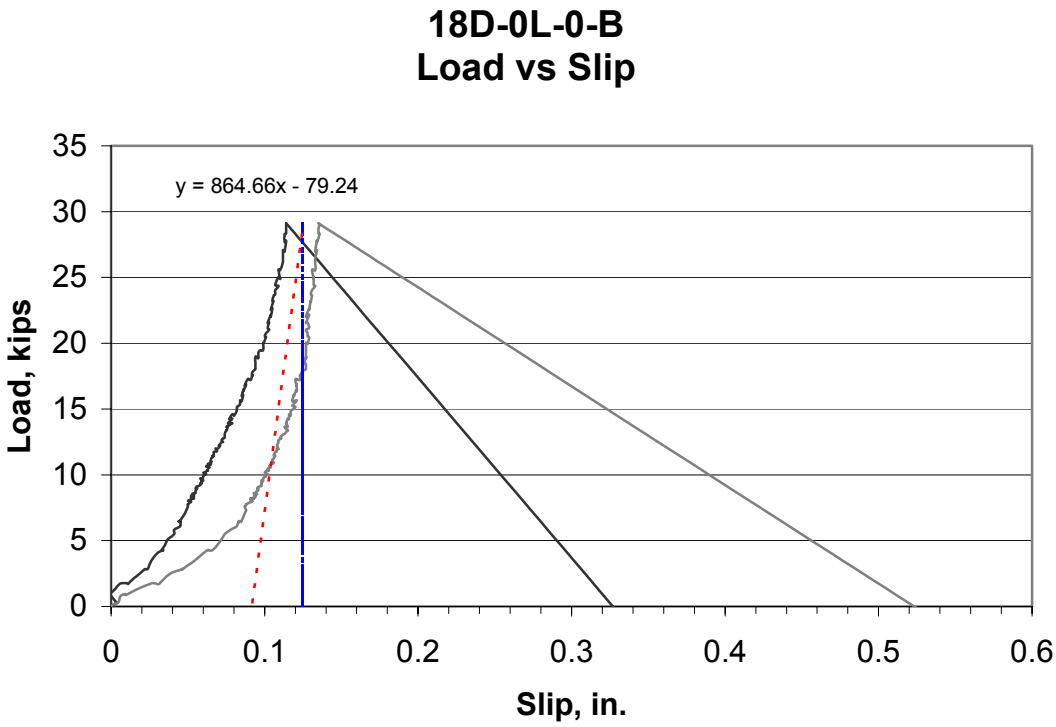

Figure 4.7 Typical Load versus Slip Plot for the Deformed Surface Specimens

Figure 4.8 Deformed Surface Specimen (After Testing)

4.1.3 Tests with Shear Connectors and Smooth Surfaces

All of the specimens with reinforcing steel crossing the interface had smooth surfaces. These specimens exhibited very different failures depending on the ratio of reinforcing steel to the interface area. Each leg of reinforcing steel crossing the interface had a strain gage attached as close to the interface as possible. These gages were used to monitor the stress in the reinforcing steel throughout the test. This provided valuable information about the forces acting on the interface prior to and after the initial slip.

Tests specimens with one or two legs of reinforcing steel exhibited very similar failure modes. For these specimens with low reinforcement ratios, the horizontal load was increased until an initial slip occurred. Prior to this initial slip, the reinforcing steel was virtually unstressed. After the initial slip, the load was resisted by the reinforcing steel. It was at this point that the strain gage readings showed a significant jump in the strain in the reinforcing steel. Subsequent to the initial slip, the applied load was increased as the reinforcing steel experienced strain hardening. For both the single and double leg specimens, the load was increased until ultimate rupture of the reinforcing steel occurred. All of the legs of reinforcing steel ruptured simultaneously. Figures 4.9 through 4.12 show the load versus slip plots and the load versus strain plots for the single and double leg specimens. Tables 4.6 and 4.7 show the test results for typical 18 in. smooth surface specimens with single and double legs of reinforcing steel crossing the interface.

Table 4.6 Test Results for a Typical 18 in. Single Leg Specimen

Reinforcing	1 leg of No. 3 bar
Area of Reinforcing, A_{vh}	0.11 in^2
Yield Stress of reinforcing	72 ksi
Normal force, P_n	256 lbs
Width of interface, b_v	10 in
Length of interface, s	16 in
f'c, lightweight concrete	5862 psi
Surface type	Smooth
f'c, ductile concrete	32.3 ksi
Slip Load	29.60 kips
Ultimate Load	13.61 kips
Displacement at Slip Load	0.024 in
Displacement at Ultimate Load	0.613 in

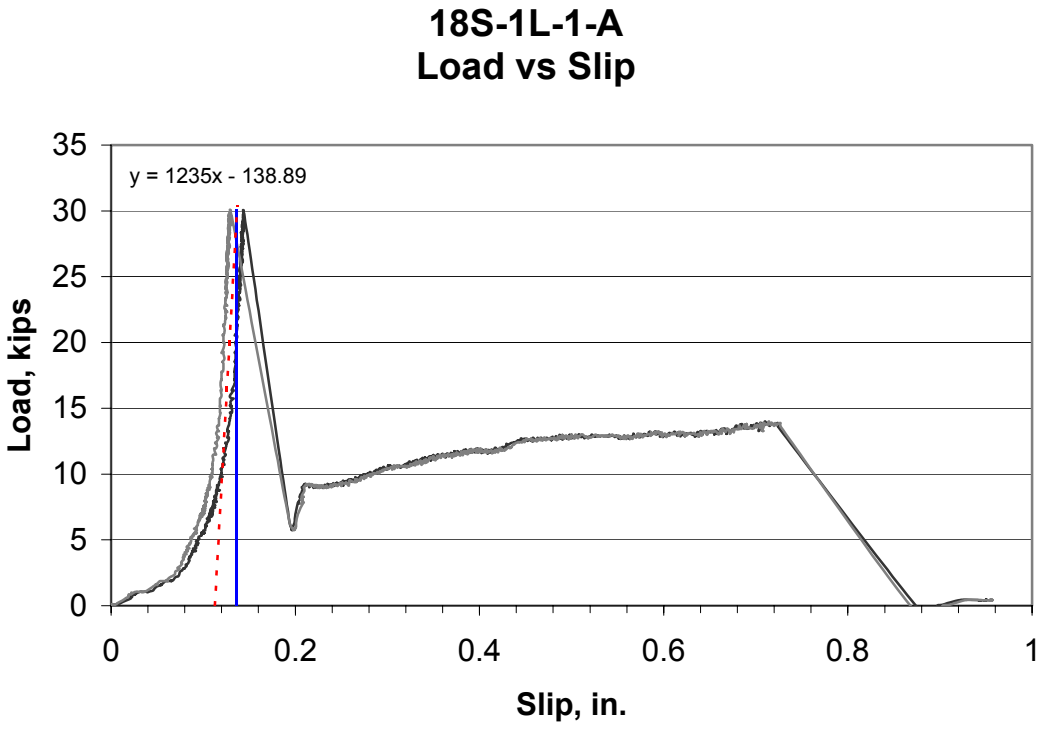

Figure 4.9 Typical Load versus Slip Plot for the Single Leg Specimens

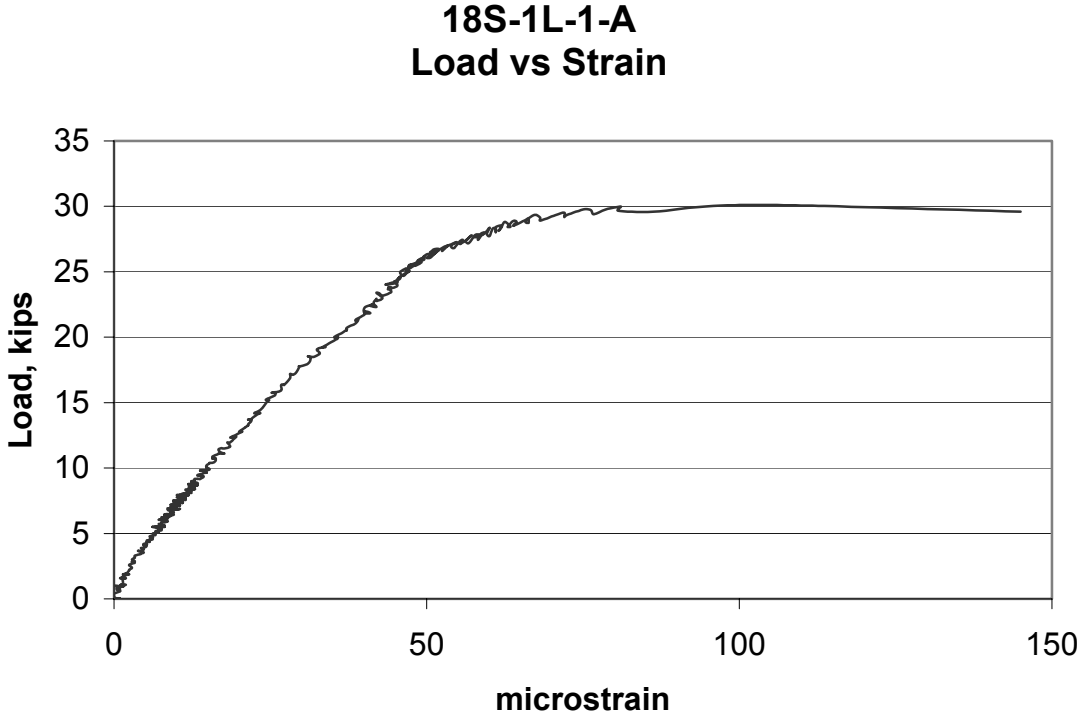

Figure 4.10 Typical Load versus Strain Plot for the Single Leg Specimens

Table 4.7 Test Results for a Typical 18 in. Double Leg Specimen

Reinforcing	2 legs of No. 3 bar
Area of Reinforcing, A_{vh}	0.22 in^2
Yield Stress of reinforcing	72 ksi
Normal force, P_n	256 lbs
Width of interface, b_v	10 in
Length of interface, s	16 in
f'c, lightweight concrete	5862 psi
Surface type	Smooth
f'c, ductile concrete	32.3 ksi
Slip Load	19.00 kips
Ultimate Load	23.36 kips
Displacement at Slip Load	0.041 in
Displacement at Ultimate Load	0.585 in

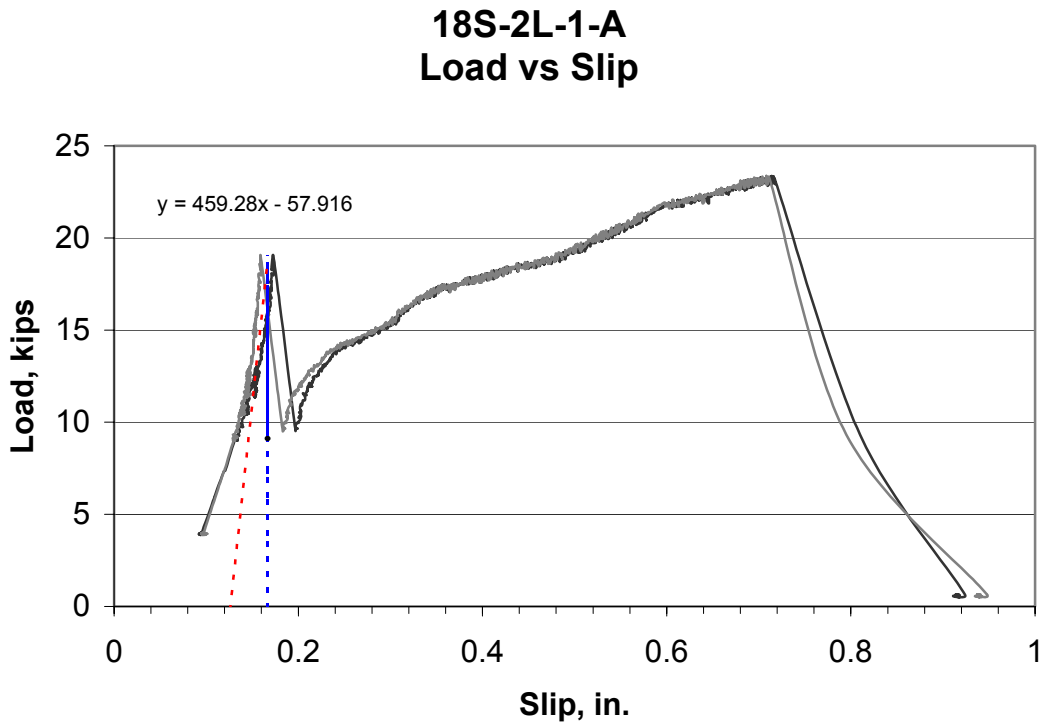

Figure 4.11 Typical Load versus Slip Plot for the Double Leg Specimens

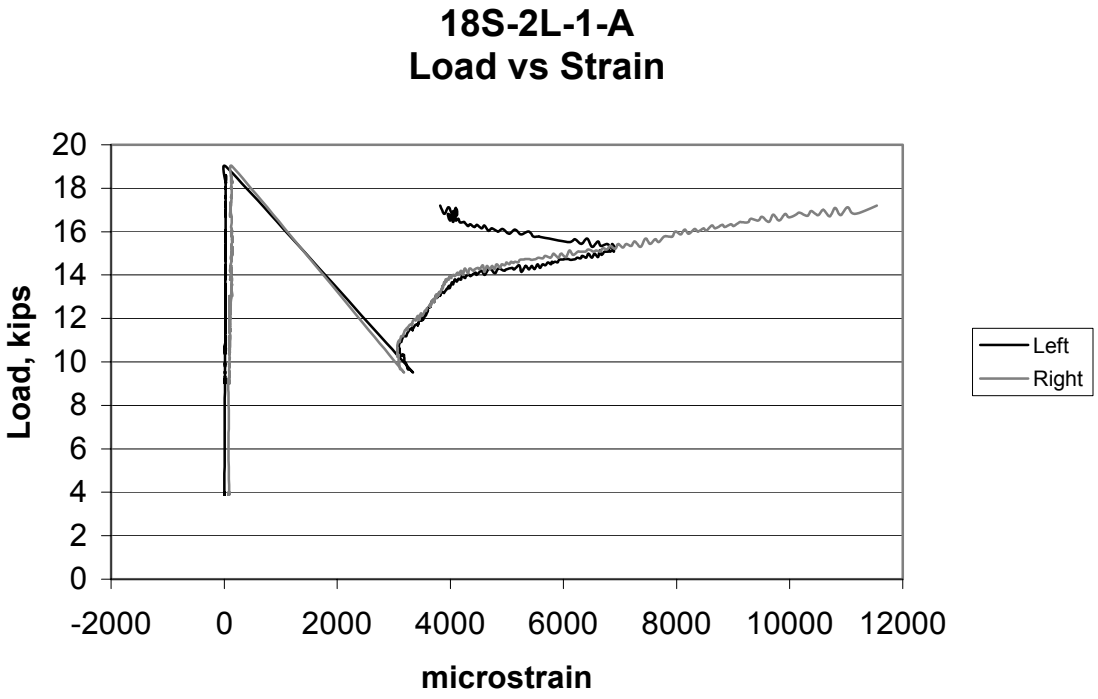

Figure 4.12 Typical Load versus Strain Plot for the Double Leg Specimens

It was found that in the lightweight concrete blocks, the concrete immediately adjacent to the reinforcing steel was crushed. Due to the extremely high compressive strength of the Ductal® blocks, no such crushing occurred. The only failure of the concrete in the Ductal® blocks was slight spalling of the surface around the ruptured reinforcing steel. The crushed concrete on the L-Shaped lightweight blocks is located between the sheared off reinforcing steel and the black circular lines. The black lines drawn on the surface of the Ductal® blocks identify the boundary of the spalled concrete. Figures 4.13 through 4.17 show typical single and double leg specimens after testing.

Figure 4.13 Lightweight Side of Single Leg Specimen (After Testing)

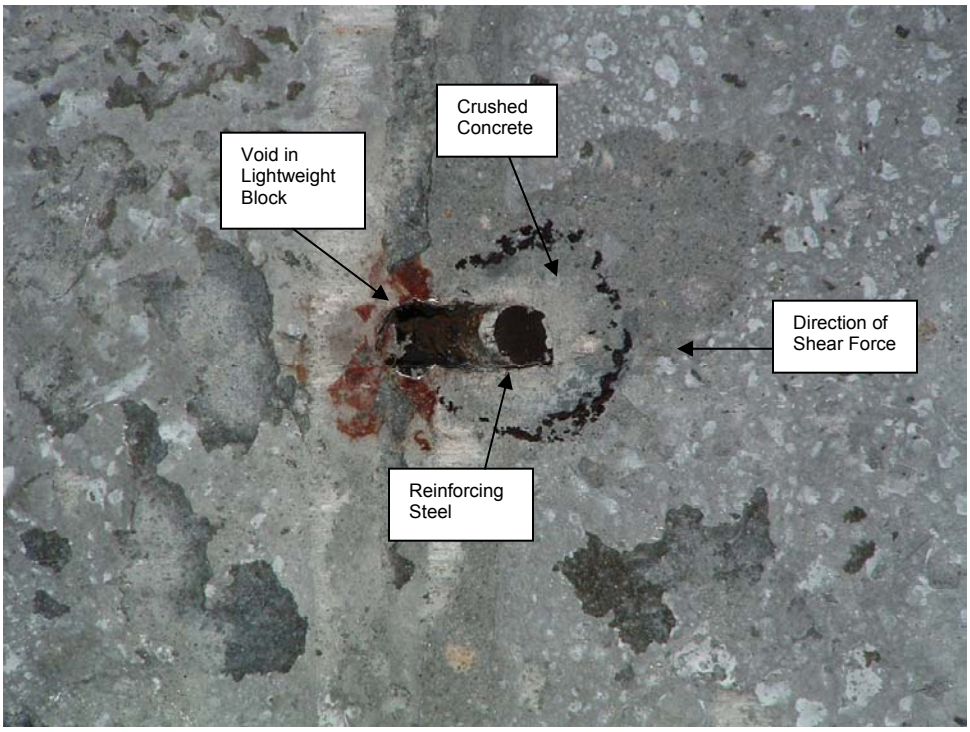

Figure 4.14 Close-up of Lightweight Side of Single Leg Specimen (After Testing)

Figure 4.15 Ductal® Side of Single Leg Specimen (After Testing)

Figure 4.16 Lightweight Side of Double Leg Specimen (After Testing)

Figure 4.17 Undamaged Ductal® Side of Double Leg Specimen (After Testing)

Specimens with four to six legs of reinforcing steel exhibited very unique behavior during testing. For these specimens, there was no clearly defined initial slip. The load was applied and increased until the reinforcing steel ruptured. The failure modes were different for each specimen. Some specimens had each leg of reinforcing steel rupture at individual times, and some had multiple legs rupture simultaneously. The ruptures of the reinforcing steel can be easily seen in the load versus slip plots for each specimen. The load increases to the rupture point, and subsequently drops. If reinforcing steel remained un-ruptured, then the load again increased until the next leg or legs of reinforcing steel ruptured. This cycle repeated itself until all of the reinforcing steel crossing the interface ruptured.

As with the specimens with only one or two legs, the reinforcing steel in the specimens with four to six legs experienced very little strain until the initial slip occurred. To adequately determine the load at which the initial slip occurred, the data from the strain gages had to be used. It was determined that the load at which the first significant jump in strain occurred was the initial slip load. It was also found that during these tests, prior to initial slip, the strain in the reinforcing steel closest to the applied load experienced the highest tensile forces. During some of the tests, the legs of reinforcing steel closest to the fixed buttress, prior to slip, experienced compressive forces. Figure 3.14 illustrates the location of the reinforcing steel crossing the interface.

During the testing of each specimen, the forces acting across the shear interface were transferred into the testing frame approximately ½ in. below the interface. Figure 3.1 illustrates where the applied load enters the testing frame. This slight moment arm did not induce enough moment to significantly affect the tests. Figures 4.18 through 4.21 show the load versus slip plots and the load versus strain plots for the four and six leg specimens. Figures 4.22 through 4.24 show the four and six leg specimens after testing. Figure 4.23 shows scrapes on the face of the lightweight block after testing. This is where deformations on the surface of the Ductal® block scraped off portions of the lightweight concrete

during testing. Tables 4.8 and 4.9 show the test results for typical 18 in. smooth surface specimens with four and six legs of reinforcing steel crossing the interface.

Table 4.8 Test Results for a Typical 18 in. Four Leg Specimen

Reinforcing	4 legs of No. 3 bar
Area of Reinforcing, A_{vh}	0.44 in^2
Yield Stress of reinforcing	72 ksi
Normal force, P_n	256 lbs
Width of interface, b_v	10 in
Length of interface, s	16 in
f'c, lightweight concrete	5862 psi
Surface type	Smooth
f'c, ductile concrete	32.3 ksi
Slip Load	21.73 kips
Ultimate Load	46.97 kips
Displacement at Slip Load	0.031 in
Displacement at Ultimate Load	0.410 in

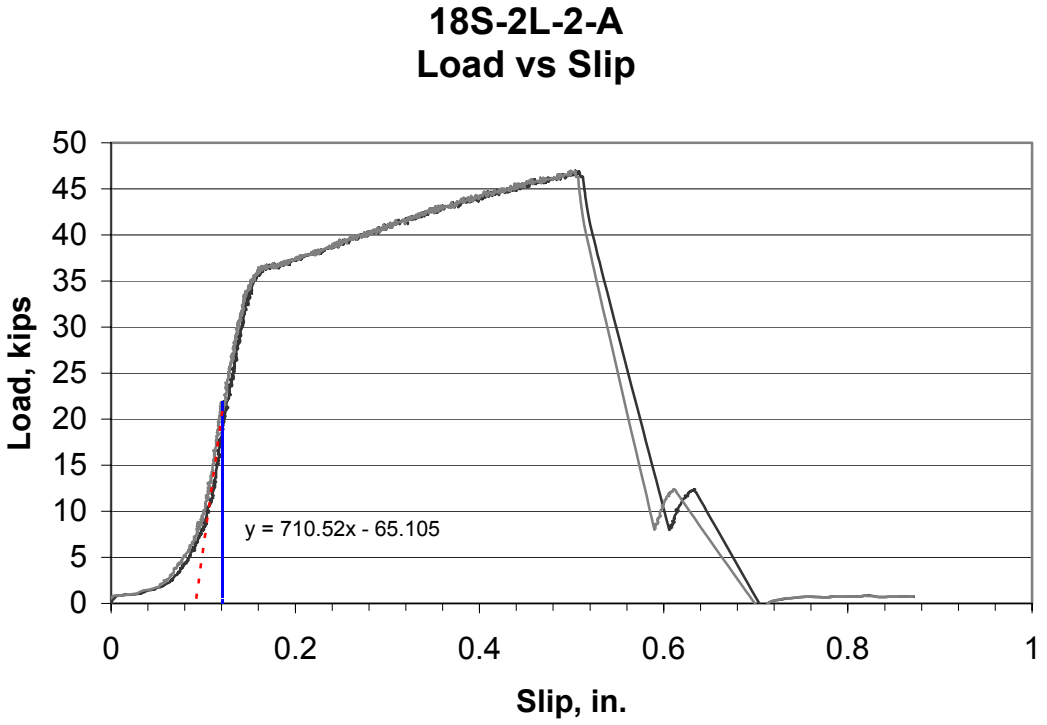

Figure 4.18 Typical Load versus Slip Plot for the Four Leg Specimens

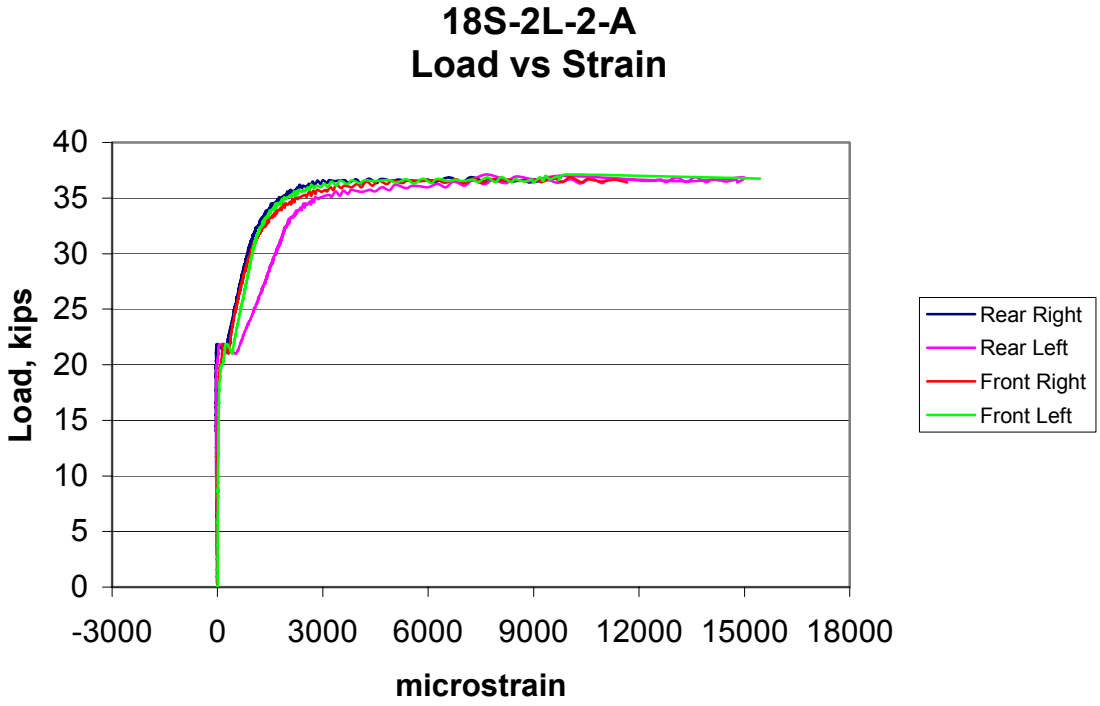

Figure 4.19 Typical Load versus Strain Plot for the Four Leg Specimens

Table 4.9 Test Results for a Typical 18 in. Six Leg Specimen

Reinforcing	6 legs of No. 3 bar
Area of Reinforcing, A_{vh}	0.66 in^2
Yield Stress of reinforcing	72 ksi
Normal force, P_n	256 lbs
Width of interface, b_v	10 in
Length of interface, s	16 in
f'c, lightweight concrete	5862 psi
Surface type	Smooth
f'c, ductile concrete	32.3 ksi
Slip Load	12.62 kips
Ultimate Load	56.33 kips
Displacement at Slip Load	0.031 in
Displacement at Ultimate Load	0.380 in

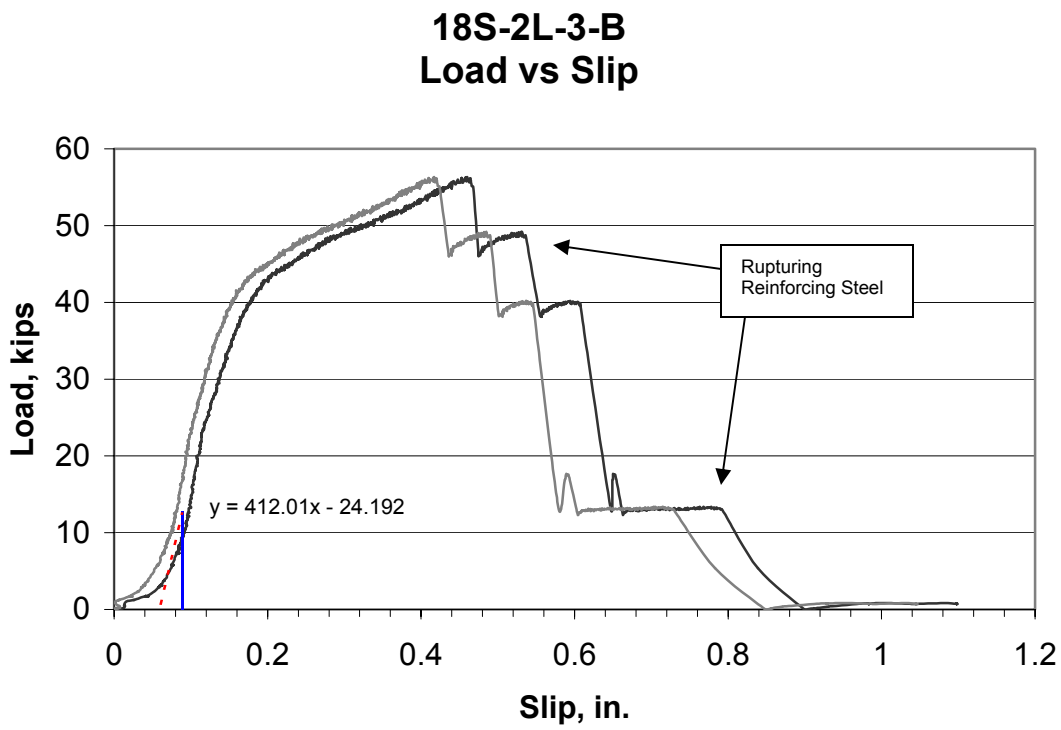

Figure 4.20 Typical Load versus Slip Plot for the Six Leg Specimens

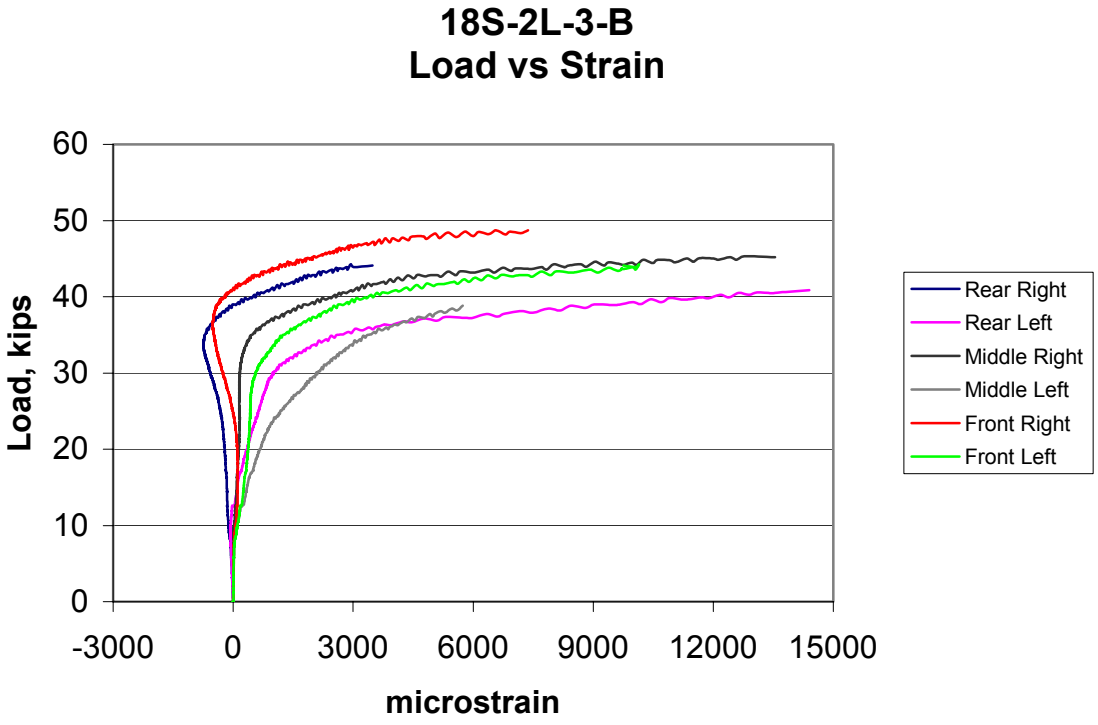

Figure 4.21 Typical Load versus Strain Plot for the Six Leg Specimens

Figure 4.22 Lightweight Side of Four Leg Specimen (After Testing)

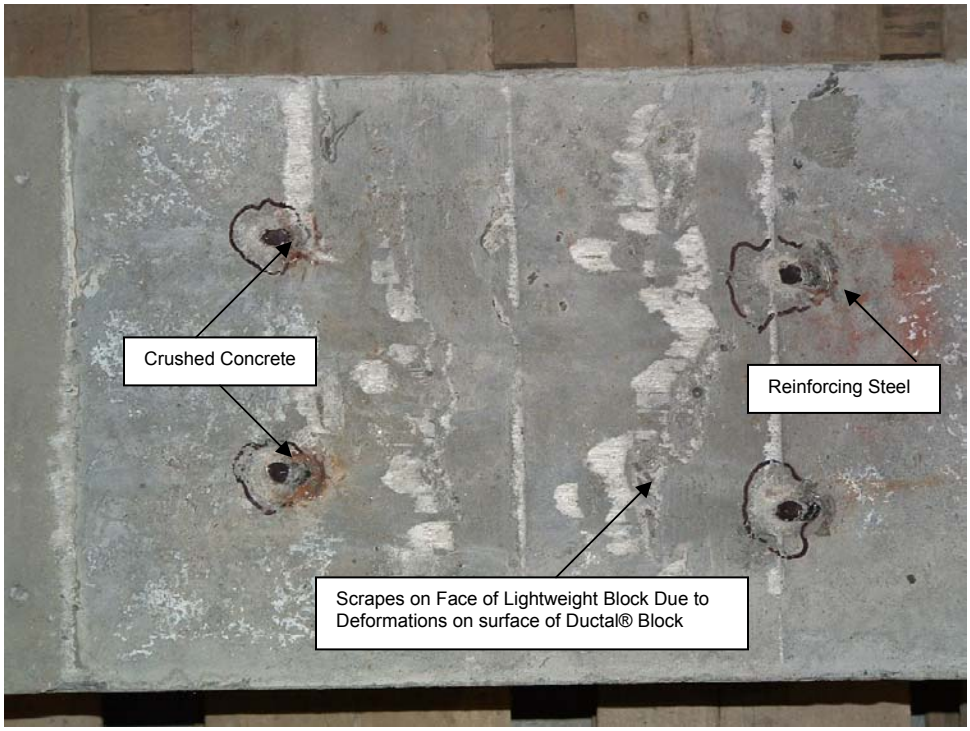

Figure 4.23 Close-up of Lightweight Side of Four Leg Specimen (After Testing)

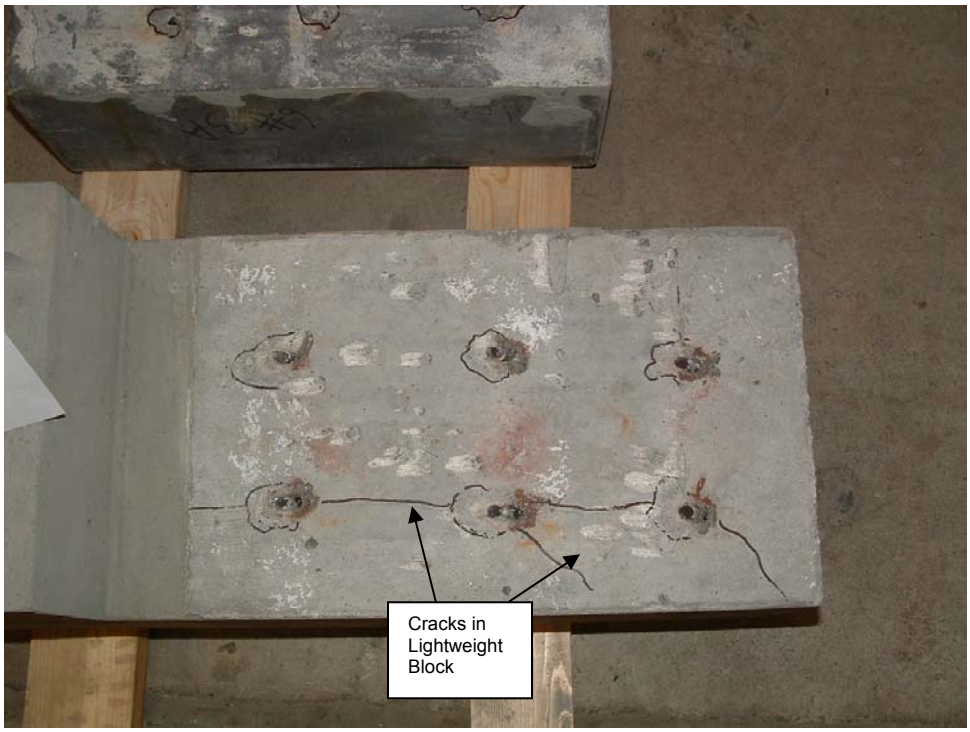

Figure 4.24 Lightweight Side of Six Leg Specimen (After Testing)

4.1.4 Tests with Varying Interface Areas

One hypothesis that was studied during this research was the possibility that the aspect ratio of a test specimen would influence the horizontal shear resistance. As the interface area increased in length, the angle of the principal compressive strut decreases. This decrease in angle could significantly affect the horizontal shear resistance. Figure 4.25 illustrates this principal.

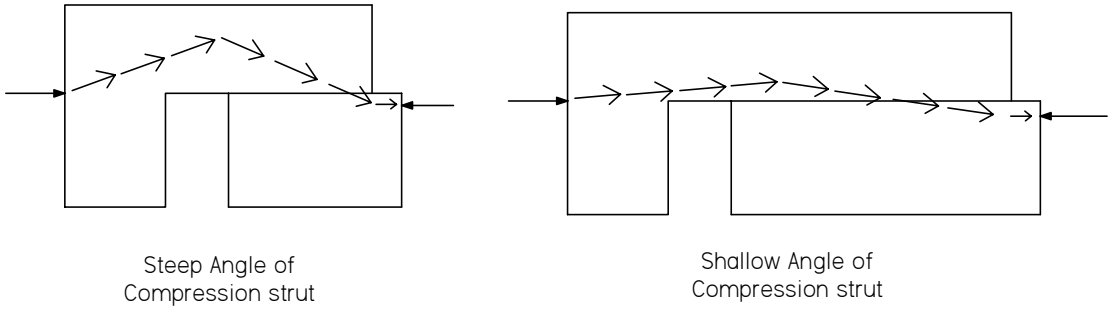

Figure 4.25 Compression Strut Angles

For beams used in bridge construction, the ratio between the deck thickness and the beam length is very small. These long interface areas cause very shallow compression strut angles. For this reason, it was important to examine how aspect ratio affects the ultimate horizontal shear resistance. To determine these effects, blocks with identical amounts of reinforcing steel crossing the interface were tested. These blocks had interface lengths of 12 in., 18 in. and 24 in.

The results from tests were inconclusive. No clear relationship between aspect ratio and the horizontal shear resistance could be determined from testing. The smooth surface specimens had varying maximum shear stresses, and the reinforced specimens did not follow this trend.

The specimens with 4 legs of No. 3 reinforcing had very consistent maximum horizontal shearing loads, but the maximum horizontal shearing stresses decreased as the interface area increased. Table 4.10 shows the maximum horizontal shearing loads and stresses for the four legged specimens. One possible reason for this trend is that the ultimate failure mode was the rupture of the reinforcing steel crossing the interface. This would explain the consistent failure loads for the specimens with identical amounts of reinforcing steel. At slip load, the concrete to concrete bond is providing most of the horizontal shear resistance. This was proven by the strain gage measurements on each leg of reinforcing steel. When the shearing stresses at slip loads for the 4 legs of No. 3 specimens was plotted against the interface area, results similar to the smooth surface specimens were obtained. Further research should be performed to more accurately determine if any relationship exists between aspect ratio and horizontal shear resistance. Figure 4.26 shows a plot of the shear stress versus the interface area for the smooth surface and 4 Legs of No. 3 specimens.

Table 4.10 Maximum Horizontal Shearing Loads and Stresses for Four Leg Specimens

Spcimen	Maximum Load	Maximum Shear Stress
	kips	***psi***
12S-2L-2-A	41.59	415.87
12S-2L-2-B	40.95	409.52
18S-2L-2-A	46.97	293.58
18S-2L-2-B	41.78	261.13
24S-2L-2-A	43.55	197.94
24S-2L-2-B	41.45	188.40

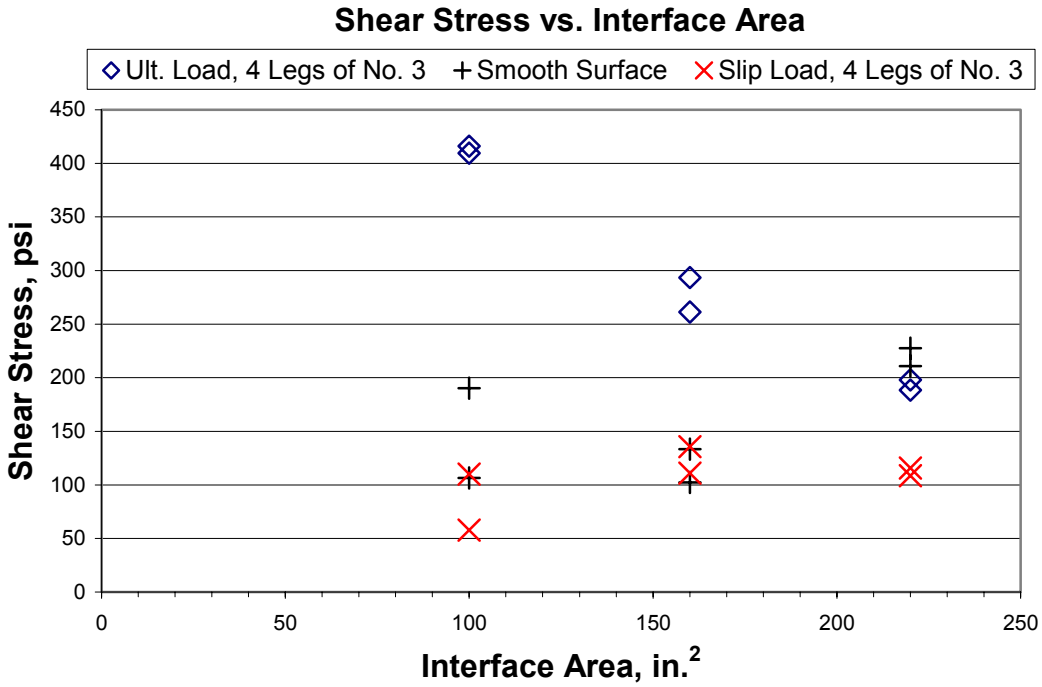

Figure 4.26 Shear Stress versus Interface Area

4.2 Strut and Tie Modeling

One method commonly used to determine the horizontal shear transfer across an interface is with the use of strut and tie modeling. For this method, a three dimensional object is modeled as a two dimensional truss. The tensile forces flowing through the specimen are represented by solid lines. These "tension ties" are typically representative of the reinforcing steel. The compressive forces flowing through the specimen are represented by dashed

lines. These “compression struts” are representative of the compressive forces acting through the concrete matrix.

Two types of strut and tie models are represented in Figures 4.27 and 4.28. These models are representative of only one possible strut and tie configuration. Figure 4.27 illustrates a possible strut and tie configuration for the single or double leg 18 in. specimen. From the geometry shown in Figure 4.27, the following relationship can be used to calculate P.

$$P = A_v f_y \tan\theta$$

where:

A_v = Area of reinforcing steel crossing the interface

f_y = Yield stress of the reinforcing steel

θ = Angle of compression strut

For this particular model, the angle theta (θ) can vary depending on the configuration of the compression struts. Differing values for θ were examined, and tested for their ability to predict values of P that closely represented those values found in the lab. Table 4.11 shows those calculations for angles from 50 to 56 degrees. For angles up to 55.5 degrees, the estimated values of P are less than the actual values found in the lab for both the single and double leg specimens. The estimated values of P found using this strut and tie model configuration can be considered conservative for design, provided θ is less than or equal to 55.5 degrees.

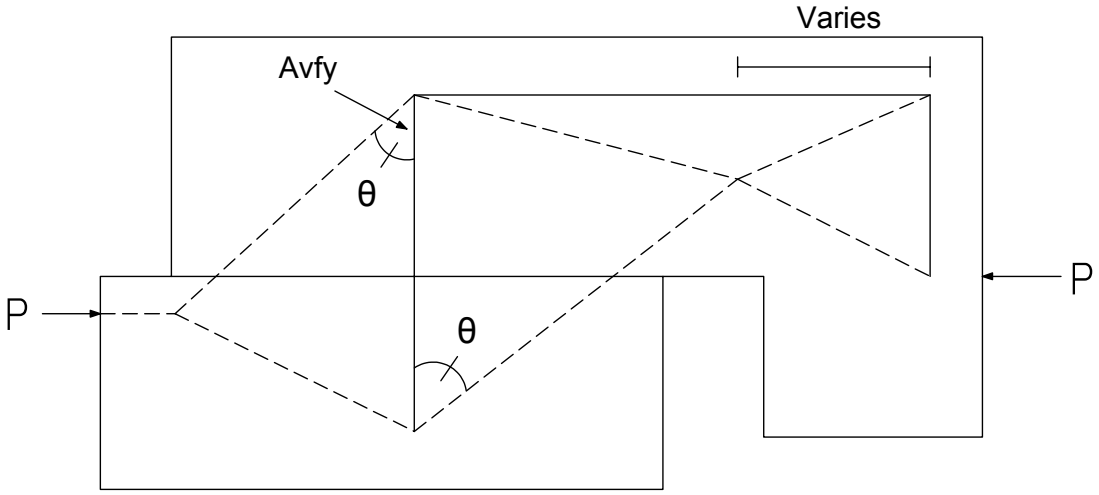

Figure 4.27 Strut and Tie Model for 18 in. Single or Double Leg Specimen

Table 4.11 Predicted Values for Horizontal Shear Resistance Using Strut and Tie Modeling

18 in. Strut and Tie Model					
		Single Leg		Double Leg	
	Av =	0.11	in	0.22	in
	fy =	72	ksi	72	ksi
	P_{actual} =	13.74	kips	23.19	kips
θ	tan(θ)	$P_{estimated}$	$P_{estimated}/P_{actual}$	P(estimated)	estimated/actual
50.0	1.19	9.44	0.69	18.88	0.81
50.5	1.21	9.61	0.70	19.22	0.83
51.0	1.23	9.78	0.71	19.56	0.84
51.5	1.26	9.96	0.72	19.91	0.86
52.0	1.28	10.14	0.74	20.27	0.87
52.5	1.30	10.32	0.75	20.64	0.89
53.0	1.33	10.51	0.77	21.02	0.91
53.5	1.35	10.70	0.78	21.41	0.92
54.0	1.38	10.90	0.79	21.80	0.94
54.5	1.40	11.10	0.81	22.21	0.96
55.0	1.43	11.31	0.82	22.62	0.98
55.5	1.46	11.52	0.84	23.05	0.99
56.0	1.48	11.74	0.85	23.48	1.01

From the geometry shown in Figure 4.28, the following relationship can be used to calculate P.

$$P = \frac{A_v f_y}{2}(\tan\beta + \tan\phi + \tan\theta)$$

where:

A_v = The total area of reinforcing steel crossing the interface

f_y = Yield stress of the reinforcing steel

θ = Angle of compression strut

β = 20.6 degrees for this configuration

Φ = 24.4 degrees for this configuration

For this model, the angle theta (θ) can vary depending on the configuration of the compression struts. Angles beta (β) and phi (Φ) remain constant for this configuration. Their values remain constant due to the geometry of the strut and tie model. Table 4.12 shows calculations for angles of θ from 56.0 to 63.5 degrees. For angles up to 63 degrees, the estimated values of P are less than or equal to the actual values found in the lab for the 4 leg specimens. The estimated values of P found using this strut and tie model configuration can be considered conservative for design, provided θ is less than or equal to 63.0 degrees.

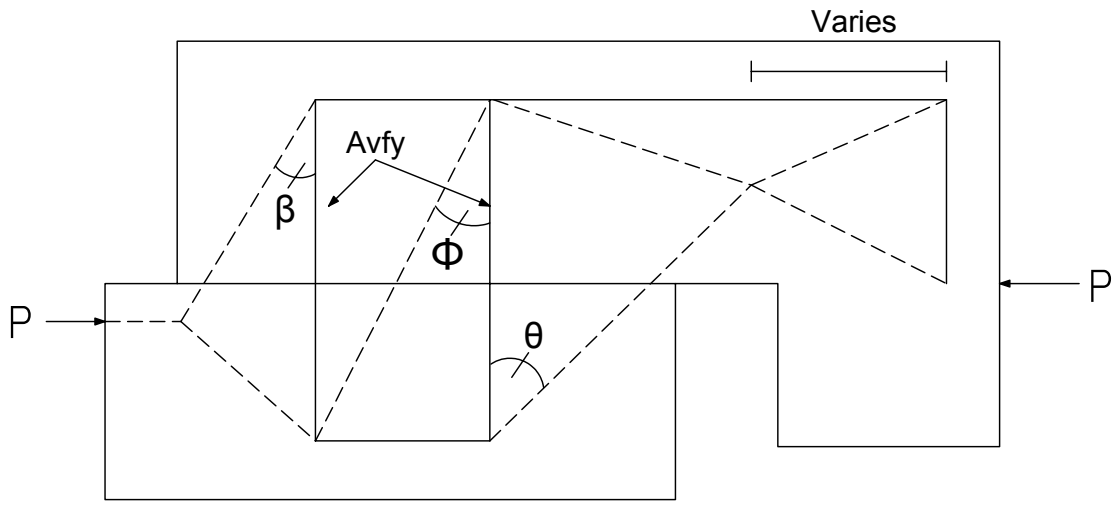

Figure 4.28 Strut and Tie Model for 18 in. Four Leg Specimen

Table 4.12 Predicted Values for Horizontal Shear Resistance Using Strut and Tie Modeling

18 in. Strut and Tie Model			
		4 legs	
	Av =	0.44	in
	fy =	72	ksi
	P_{actual} =	44.38	kips
θ	tan(θ)	$P_{estimated}$	$P_{estimated}/P_{actual}$
56.0	1.48	36.62	0.83
56.5	1.51	37.07	0.84
57.0	1.54	37.53	0.85
57.5	1.57	38.00	0.86
58.0	1.60	38.49	0.87
58.5	1.63	38.99	0.88
59.0	1.66	39.50	0.89
59.5	1.70	40.03	0.90
60.0	1.73	40.57	0.91
60.5	1.77	41.14	0.93
61.0	1.80	41.72	0.94
61.5	1.84	42.31	0.95
62.0	1.88	42.93	0.97
62.5	1.92	43.57	0.98
63.0	1.96	44.23	1.00
63.5	2.01	44.91	1.01

The two strut and tie models presented in this thesis show that this type of analysis can conservatively predict the horizontal shear resistance of a composite section. One significant downfall however is that the correct geometry for the compression struts and tension ties needs to be used. Further research in this area needs to be performed.

4.3 Results Compared to Existing Equations

The results from the 24 push-off tests were compared to the equations for calculating horizontal shear strengths found in ACI 318 (2002), AASHTO *Standard Specifications* (2002) and AASHTO LRFD Specifications (2004). Only the smooth surface unreinforced and reinforced specimens were used for this comparison. The comparison data is presented in Table 4.13. It can be seen that all of the present design equations are conservative for determining the horizontal shear strengths for the composite Ductal® and lightweight concrete sections. Equations from ACI 318 provided the least conservative horizontal shear strength estimate, and the equations from the AASHTO Standard Specifications provided the most conservative estimate. It has been shown that the design equations are conservative without utilizing the lightweight concrete adjustment factor (λ).

It must be noted that the wording in ACI 318 (2002) does not allow for additional horizontal shearing capacity to be given to smooth surface specimens with more than the minimum amount of reinforcing steel crossing the interface. For the purposes of this research, it has been assumed that the horizontal shearing capacity for a smooth surface specimen increases as the amount of reinforcing steel increases. The equation presented for rough surface specimens was modified for use with smooth surface specimens. This was done to account for the lower cohesion between the concrete interfaces. The data from testing showed that this assumption was valid.

Figures 4.29 and 4.30 present plots of the maximum shear stress versus the clamping stress. The three lines below the plotted specimen data in Figure 4.29 represent the three aforementioned design equations. Figure 4.30

illustrates that the AASHTO LRFD equation for smooth surfaces is a reasonable lower bound for this data set. The AASHTO LRFD equation for rough surfaces represents a rough upper bound for this data set. It should be noted that for all of the design equations shown in Figures 4.28 and 4.29, λ is equal to 1.0.

Table 4.13 Test Results Compared Against Predicted Values

Specimen	Surface	Max Load	λ = 1.0, Φ = 1.0			Test Results/Predicted Values		
			ACI 318	AASHTO Standard Spec	AASHTO LRFD Spec	ACI 318	AASHTO Standard Spec	AASHTO LRFD Spec
-	-	*kips*	*Vn (kips)*	*Vn (kips)*	*Vn (kips)*			
18S-1L-1-A	Smooth	29.6	17.6	16.0	16.9	1.69	1.85	1.75
18S-1L-1-B	Smooth	25.8	17.6	16.0	16.9	1.47	1.61	1.52
18S-2L-1-A	Smooth	23.4	22.3	19.2	21.7	1.05	1.22	1.08
18S-2L-1-B	Smooth	23.0	22.3	19.2	21.7	1.03	1.20	1.06
12S-2L-2-A	Smooth	41.6	27.1	20.7	26.7	1.54	2.01	1.56
12S-2L-2-B	Smooth	41.0	27.1	20.7	26.7	1.51	1.98	1.53
18S-2L-2-A	Smooth	47.0	31.9	25.5	31.2	1.47	1.84	1.50
18S-2L-2-B	Smooth	41.8	31.9	25.5	31.2	1.31	1.64	1.34
24S-2L-2-A	Smooth	43.5	36.7	30.3	35.8	1.19	1.44	1.22
24S-2L-2-B	Smooth	41.4	36.7	30.3	35.8	1.13	1.37	1.16
18S-2L-3-A	Smooth	64.4	41.4	31.9	40.8	1.56	2.02	1.58
18S-2L-3-B	Smooth	56.3	41.4	31.9	40.8	1.36	1.77	1.38
12S-0L-0-A	Smooth	10.7	8.00	8.00	7.60	1.33	1.33	1.40
12S-0L-0-B	Smooth	19.0	8.00	8.00	7.60	2.38	2.38	2.50
18S-0L-0-A	Smooth	21.3	12.8	12.8	12.2	1.67	1.66	1.75
18S-0L-0-B	Smooth	16.4	12.8	12.8	12.2	1.28	1.28	1.35
24S-0L-0-A	Smooth	46.4	17.6	17.6	16.7	2.64	2.64	2.78
24S-0L-0-B	Smooth	50.0	17.6	17.6	16.7	2.84	2.84	2.99
					Average =	1.58	1.78	1.64
					Standard Deviation =	0.52	0.48	0.56
					95% Confidence Interval =	1.34	1.56	1.38
						1.82	2.00	1.90

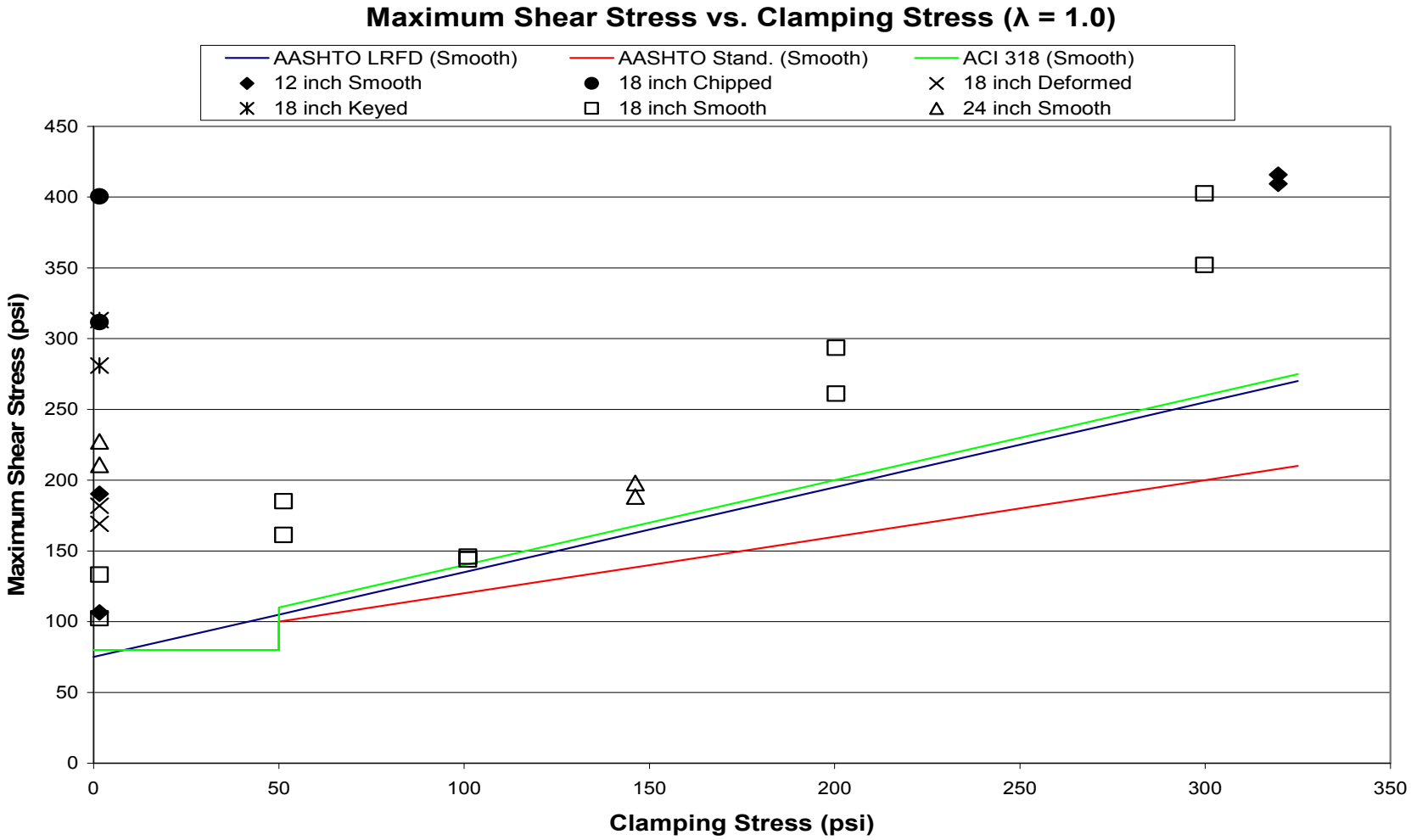

Figure 4.29 Measured Maximum Shear Stress versus Clamping Stress Compared to Equations for Smooth Interfaces

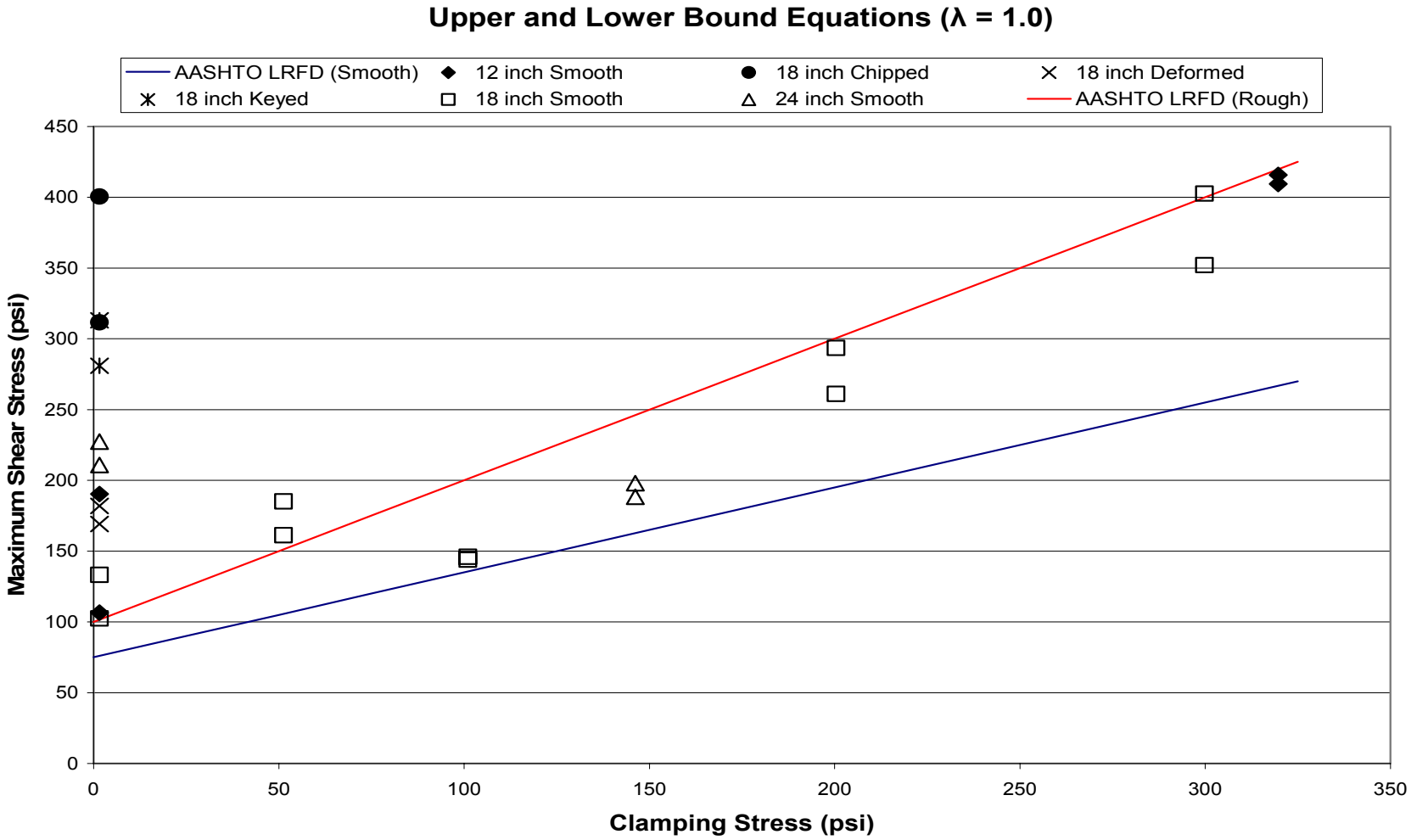

Figure 4.30 Measured Maximum Shear Stress versus Clamping Stress Compared to Equations for Rough and Smooth Interfaces

4.3.1 Strain Hardening of Shear Stirrups

Strain data gathered during testing showed that prior to ultimate failure, the stress in the reinforcing steel was greater than yield. It was assumed that in most cases the steel was experiencing strain hardening. For all of the equations used for analysis, the clamping stress is a function of the area of reinforcing times the yield stress. It can be assumed that the actual clamping stress for each reinforced specimen was higher than the calculated value used for comparison of results. Further research needs to be performed to determine how this added clamping stress affects the horizontal shear resistance. The present design equations can still be considered conservative without taking this added clamping stress into account.

4.3.2 Relating Slip Stress to Service Loads

For all of the reinforced specimens, the initial bond at the concrete interface released before the ultimate failure of the specimen. Prior to this initial slip, the horizontal shearing forces were resisted by the concrete bond. Strain data from the reinforcing steel reveals that prior to the initial concrete bond failure, very little force was transferred into the horizontal shear reinforcement. After failure, the reinforcing steel began taking on load quickly until the yield stress was reached. Beyond the yield stress, strain hardening of the reinforcing steel was experienced, and continued loading eventually led to the failure of the specimen. Although the reinforced specimens behaved similarly under loading, there was variation in the ratio between ultimate and slip shear stresses. Figure 4.31 illustrates this variation between the ultimate and first slip shear stresses.

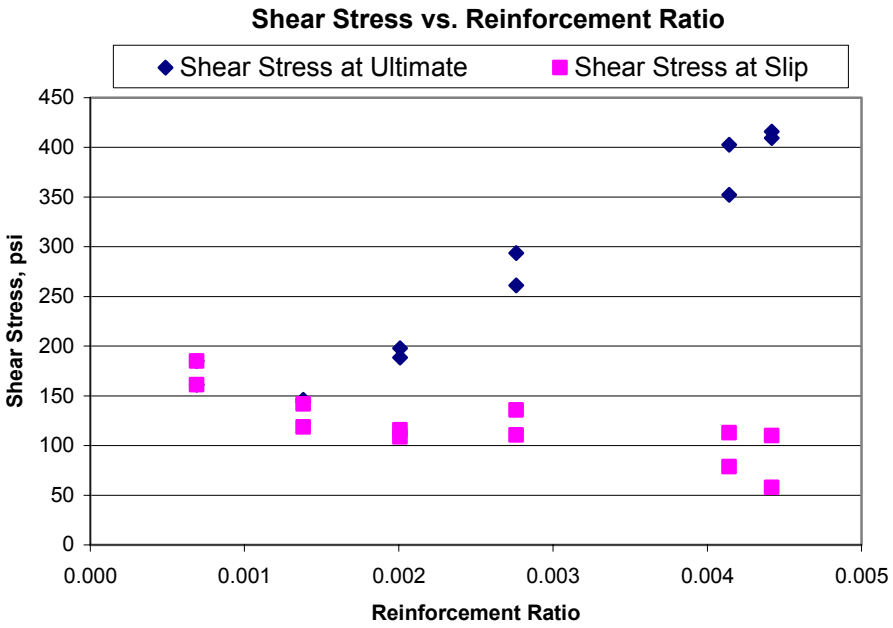

Figure 4.31 Ultimate and Slip Shear Stresses versus Reinforcement Ratio

For a typical bridge design, the ratio between live and dead loads is approximately 60:40 or 40:60 respectively. By applying these ratios to the Strength I equation in AASHTO LRFD the following relationship can be shown:

$$U = 1.25D + 1.75L$$

where:

$$U_1 = 1.25(0.4) + 1.75(0.6) = 1.55$$

$$U_2 = 1.25(0.6) + 1.75(0.4) = 1.45$$

From this relationship, we can assume that the factored load is approximately equal to 1.5 times the service load. Figure 4.32 shows a plot of the maximum shear stress divided by the shear stress at slip versus reinforcement ratio.

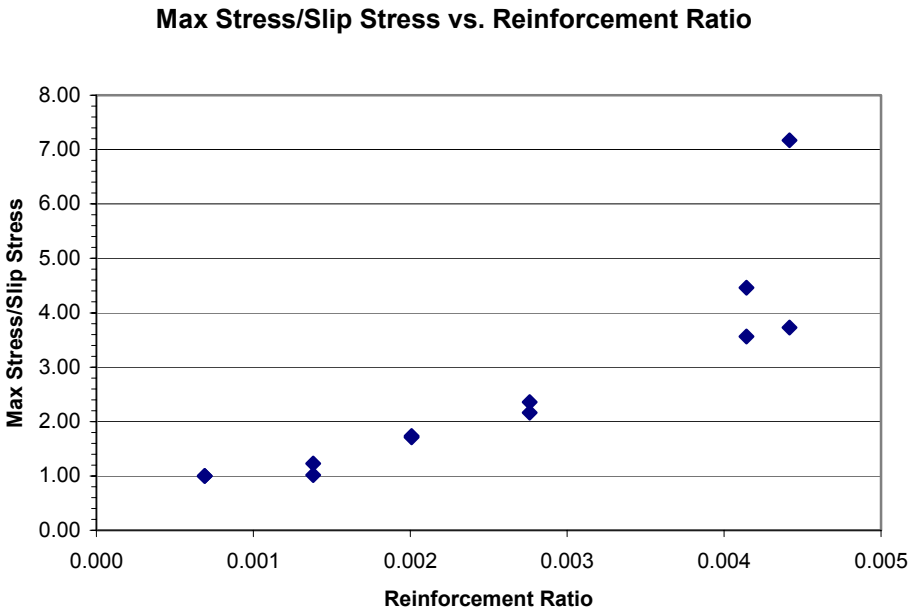

Figure 4.32 Maximum Shear Stress/Shear Stress at First Slip Versus Reinforcement Ratio

The above figure illustrates that for small reinforcement ratios, the ratio of maximum load to load at slip is less than 1.5. It can be assumed that for these reinforcement ratios, the typical service load will be less than the slip load. Therefore the interface will be uncracked at service loading. For specimens with higher reinforcement ratios, the service load may be greater than the slip load. This could cause premature cracking along the interface. If higher reinforcement ratios are required, while at the same time minimal cracking along the interface is desired, surface deformations may need to be utilized.

CHAPTER 5: SUMMARY, CONCLUSIONS AND RECOMMENDATIONS

5.1 Summary

As materials used in bridge construction have become stronger and more durable, engineers are increasingly pushing the boundaries of design. By using lighter and stronger materials, longer spans can be crossed with less material. Along with the use of new materials, comes the need for testing and validation of design assumptions. One such assumption that needed to be tested for The Virginia Department of Transportation was that the present design equations for determining horizontal shear resistance would be valid for composite Ductal® concrete beams. The composite sections in questions consist of Ductal® concrete beams with a lightweight concrete bridge deck attached.

The present design equations do not provided guidance as to the best method for determining the horizontal shear strength of a Ductal® concrete composite section. The purpose of this research was to test the horizontal shear strength of specimens with varying interface surface treatments, sizes, and reinforcement ratios. 24 push-off tests were carried out and provided varying results. From these tests, recommendations about what factors to use in design, and which of the following equations will best predict the nominal horizontal shear strength of a composite Ductal® section were made. The equations in question came from ACI 318 (2002), AASHTO Standard Specifications (2002), and AASHTO LRFD Specifications (2004). Recommendations are set forth in the following section.

5.2 Conclusions

From the research performed on the push-off tests, it has been proven that each of the design methods in question conservatively predicts the horizontal shear strength of composite Ductal® concrete sections. The AASHTO Standard Specifications provided the most conservative results. The ACI 318 design equations yielded the least conservative results, but were still acceptable for design. The design equations utilized a lightweight concrete adjustment

factor λ equal to 1.0. If more conservative results are desired, a λ equal to either 0.85 or 0.75 can be used. The equations from both ACI 318 (2002) and AASHTO LRFD Specification (2004) provide similar results when determining the horizontal shear resistance of a Ductal® and lightweight concrete composite section. For its ability to incorporate various cohesion and friction factors, it is recommended that the equation from AASHTO LRFD Specification (2004) be used for design.

If designers desire that surface deformations should be incorporated into the top flange of the Ductal® concrete beams, the most effective solution is the chipped surface. This surface treatment was the least time consuming to produce, and could be done at any point in the construction process prior to deck placement. By removing a very thin layer of concrete from the surface of the flange, the reinforcing fibers in the matrix were exposed. This allowed for extra mechanical bond between the deck and beam concrete. Two possible methods could be used to chip the surface of the beam. Hydraulic demolition or jackhammers could be used on site to expose the fibers in the top surface of the beam. The feasibility of using either method would depend on the site conditions and the geometry of the beam. If chipping the surface will place too much stress on the beam, then the top flange should remain unaltered, or other surface deformations can be used. Each of the other surface deformations are time consuming to form, and provided limited increases in the overall horizontal shear resistance. The benefits of increasing the horizontal shear resistance versus spending the time on fabricating surface deformations has to be weighed carefully by each designer.

In general, the design equations used for determining horizontal shear resistance are applicable for use in Ductal® concrete design. Lightweight adjustment factors do not need to be used, and surface deformations should not be required.

5.3 Recommendations for Future Research

- Further research needs to be performed to better test the influence that aspect ratio has on the horizontal shear resistance.
- More detailed strut and tie modeling needs to be performed to better determine the flow of forces through the Ductal® blocks.
- More testing is required to provide better modeling of the ultimate load versus the slip loads.
- Testing needs to be performed on more specimens to determine what influence strain hardening has on the horizontal shear resistance of a specimen.
- Further testing into predicting the forces acting in the reinforcing steel crossing the interface prior to slip loads needs to be performed.

REFERENCES

AASHTO LRFD Bridge Design Specification (2004). American Associate of State Highway and Transportation Officials, Washington D.C.

Anderson, A.R. (1960), "Composite Designs in Precast and Cast-in-Place Concrete", *Progressive Architecture,* V. 41, No. 9, 172 – 179.

Birkeland, P.W., and Birkeland, H.W. (1966), "Connections in Pre-cast Concrete Construction", *ACI Journal*, V. 63, No. 3, 345 – 367.

Building Code Requirements for Structural Concrete, ACI 318-02 (2002). American Concrete Institute, Farmington Hills, Michigan.

Ferdinand, P.B. and Johnston, R. (1992), *Mechanics of Materials, Second Edition.* McGraw-Hill, Inc. New York.

Graybeal, B.A and Hartmann, J.L. (2003), "Strength and Durability of Ultra-High Performance Concrete", *3rd International Symposium on High Performance Concrete/PCI National Bridge Conference, Proceedings*, Precast/Prestressed Concrete Institute, Orlando, FL, 2003. (on CD).

Hajar, Z., Simon, A., Lecointre, D., and Petitjean, J. (2003), "Construction of the First Road Bridges Made of Ultra-High-Performance Concrete", *3rd International Symposium on High Performance Concrete/PCI National Bridge Conference, Proceedings*, Precast/Prestressed Concrete Institute, Orlando, FL, 2003. (on CD).

Hanson, N.W. (1960), "Precast – Prestressed Concrete Bridges", *Journal PCA Research and Development Laboratories*, V. 2, No. 3, 38 – 58.

Hsu, T.T.C., Mau, S.T., and Chen, B. (1987), "Theory of Shear Transfer Strength of Reinforced Concrete", *ACI Journal,* V. 84, No. 2, 149-160.

Hwang, S.J., Yu, H.W., and Lee, H.J. (2000), "Interface Shear Capacity of Reinforced Concrete", *Journal of Structural Engineering,* V. 126, No. 6, 700 – 707.

Kumar, N.P. and Ramirez, J.A. (1996), "Interface Horizontal Shear Strength in Composite Decks With Precast Concrete Panels", *PCI Journal*, V. 41, No. 2, 42 – 55.

Loov, R.E. (1978), "Design of Precast Connections", Paper Presented at a Seminar Organized by Compa International Pte, Ltd.

Loov, R.E., Patnaik, A.K. (1994), “Horizontal Shear Strength of Composite Concrete Beams with a Rough Interface”, *PCI Journal*, V. 39, No. 1, 48 – 66.

MacGregor, J.G. (1997), *Reinforced Concrete Mechanics and Designs,* Third Edition. Prentice Hall, Inc. Upper Saddle River, New Jersey.

Mast, R.F. (1968), “Auxiliary Reinforcement in Concrete Connections”, *ASCE Journal*, V. 94, No. ST6, 1485 – 1504.

Mattock, A.H., (1974), “Shear Transfer in Concrete Having Reinforcement at an Angle to the Shear Plane”, *Shear in Reinforced Concrete*, ACI Special Publication SP-42, V.1, American Concrete Institute, Detroit, MI, 17-42.

Mattock, A.H., and Hawkins, N.M. (1972), “Shear Transfer in Reinforced Concrete – Recent Research”, *PCI Journal,* V. 17, No. 2, 55 – 75.

Mattock, A.H., Johal, L., and Chow, H.C. (1975), “Shear Transfer in Reinforced Concrete with Moment or Tension Across the Shear Plane”, *PCI Journal*, V. 20, No. 4, 76 – 93.

Mattock, A.H., Li, W.K., and Wang, T.C. (1976), “Shear Transfer in Lightweight Reinforced Concrete”, *PCI Journal*, V. 21, No. 1, 20 – 39.

Menkulasi, F. (2002), “Horizontal Shear Connectors for Precast Prestressed Bridge Deck Panels”, Masters of Science Thesis, Department of Civil and Environmental Engineering, The Virginia Polytechnic Institute and State University, Blacksburg, Virginia.

Park, H., Ulm, F.J., and Chuang, E. (2003), “Model-Based Optimization of Ultra High Performance Concrete Highway Bridge Girders”, Department of Civil Engineering, Massachusetts Institute of Technology, CEE Report R03-01, Cambridge, MA.

Patnaik, A.K. (2001), “Behavior of Composite Concrete Beams with Smooth Interface”, *Journal of Structural Engineering,* V. 127, No. 4, 359 – 366.

PCI Design Handbook – Precast and Prestressed Concrete (1992), Fourth Edition, Precast/Prestressed Concrete Institute, Chicago, IL.

Perry, V.H., and Zakariasen, D. (2003), “Overview of UHPC Technology, Materials, Properties, Markets and Manufacturing”, Concrete Bridge Conference.

Resplendino, J., and Petitjean, J. (2003), "Ultra-High-Performance Concrete: First Recommendations and Examples of Application", *3rd International Symposium on High Performance Concrete/PCI National Bridge Conference, Proceedings*, Precast/Prestressed Concrete Institute, Orlando, FL, 2003. (on CD).

Saemann, J. C., and Washa, G.W. (1964), "Horizontal Shear Connections Between Precast Beams and Cast-in-Place Slabs", *ACI Journal*, V. 61, No. 11, 1383 – 1408.

Salmon, C.G. and Johnson, J.E. (1996), *Steel Structures, Design and Behavior,* Fourth Edition, Prentice Hall, Inc. Upper Saddle River, New Jersey.

Shaikh, A.F. (1978), "Proposed Revisions to Shear-Friction Provisions", *PCI Journal*, V. 23, No. 2, 12 – 21.

Standard Specification for Highway Bridges, Seventeenth Edition (2002). American Association of State Highway and Transportation Officials, Washington D.C.

Walraven, J., Frenay, J., and Pruijssers, A. (1987), "Influence of Concrete Strength and Load History on the Shear Friction Capacity of Concrete Members", *PCI Journal*, V. 32, No. 1, 66 – 84.

Appendix A
Test Results

Test 12S-0L-0-A

Specimen Details

Reinforcing	none
Area of Reinforcing, A_{vh}	-
Yield Stress of reinforcing	-
Normal force, P_n	160 lbs
Width of interface, b_v	10 in
Length of interface, s	10 in
f'c, lightweight concrete	5862 psi
Surface type	Smooth
f'c, ductile concrete	32.3 ksi
Slip Load	10.66 kips
Ultimate Load	10.66 kips
Displacement at Slip Load	0.057 in
Displacement at Ultimate Load	0.057 in

12S-0L-0-A
Load vs Slip

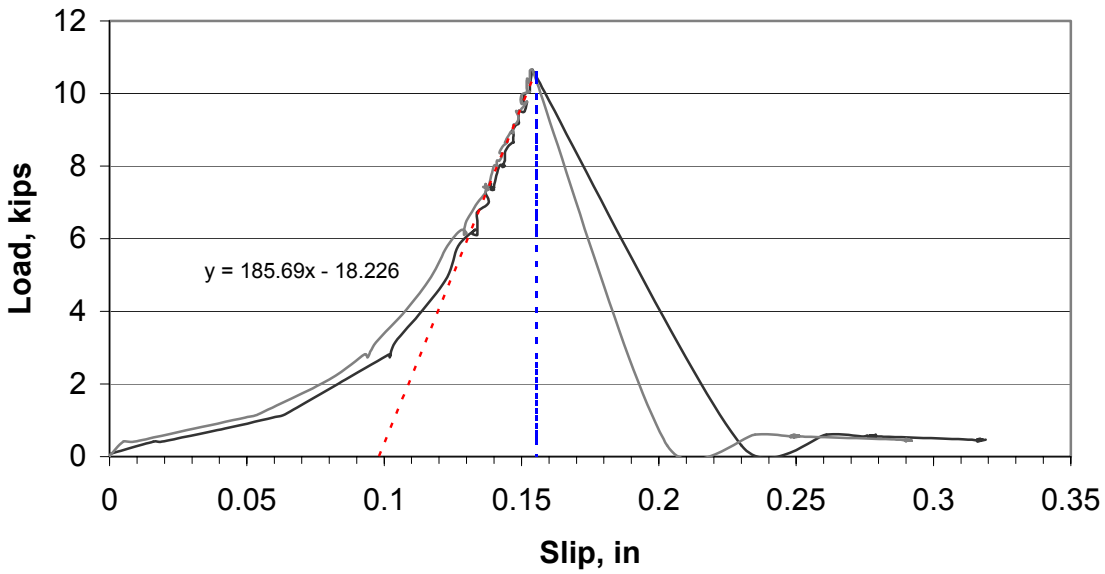

Test 12S-0L-0-B

Specimen Details

Reinforcing	none
Area of Reinforcing, A_{vh}	-
Yield Stress of reinforcing	-
Normal force, P_n	160 lbs
Width of interface, b_v	10 in
Length of interface, s	10 in
f'c, lightweight concrete	5862 psi
Surface type	Smooth
f'c, ductile concrete	32.3 ksi
Slip Load	19.03 kips
Ultimate Load	19.03 kips
Displacement at Slip Load	0.023 in
Displacement at Ultimate Load	0.023 in

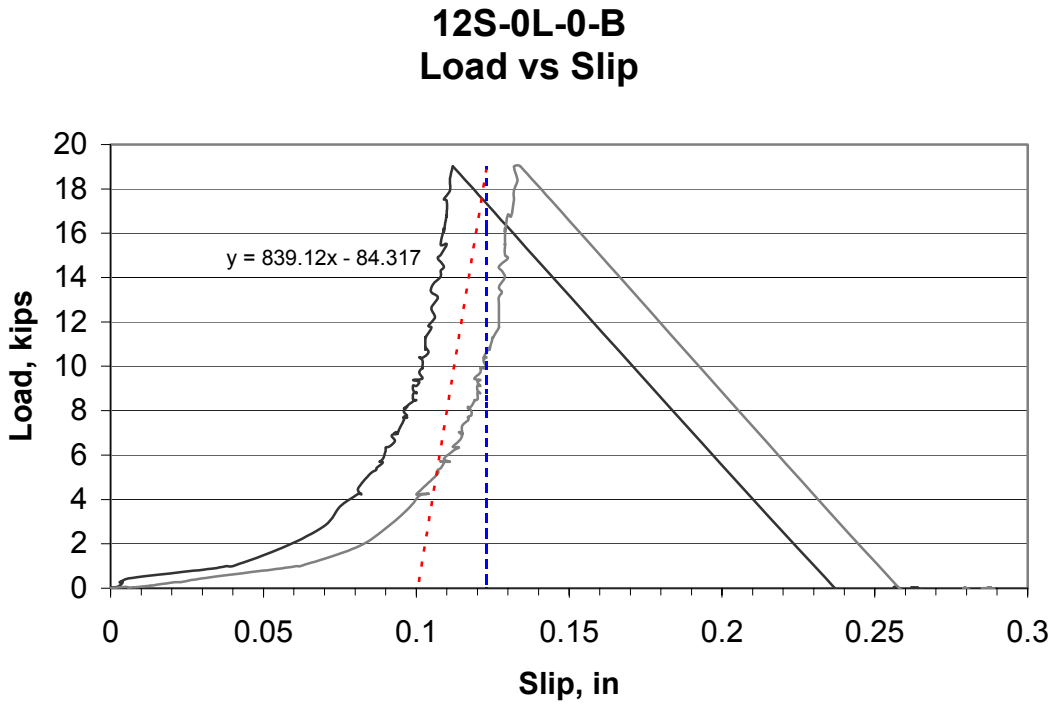

Test 12S-2L-2-A

Specimen Details

Reinforcing	4 legs of No. 3 bar
Area of Reinforcing, A_{vh}	0.44 in^2
Yield Stress of reinforcing	72 ksi
Normal force, P_n	160 lbs
Width of interface, b_v	10 in
Length of interface, s	10 in
f'c, lightweight concrete	5862 psi
Surface type	Smooth
f'c, ductile concrete	32.3 ksi
Slip Load	5.80 kips
Ultimate Load	41.59 kips
Displacement at Slip Load	0.031 in
Displacement at Ultimate Load	0.574 in

12S-2L-2-A
Load vs Slip

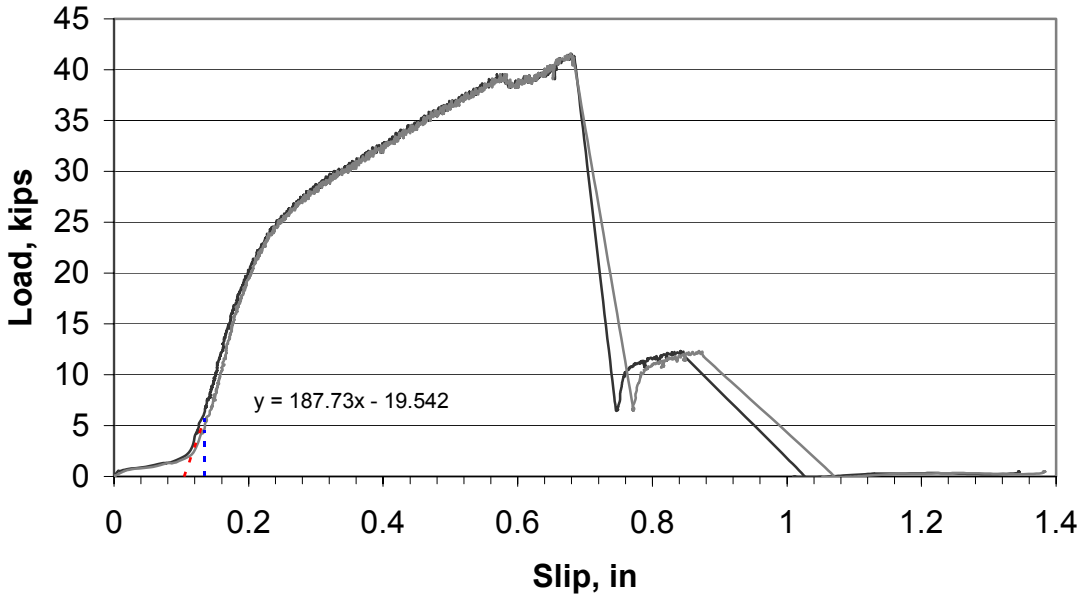

12S-2L-2-A
Load vs Strain

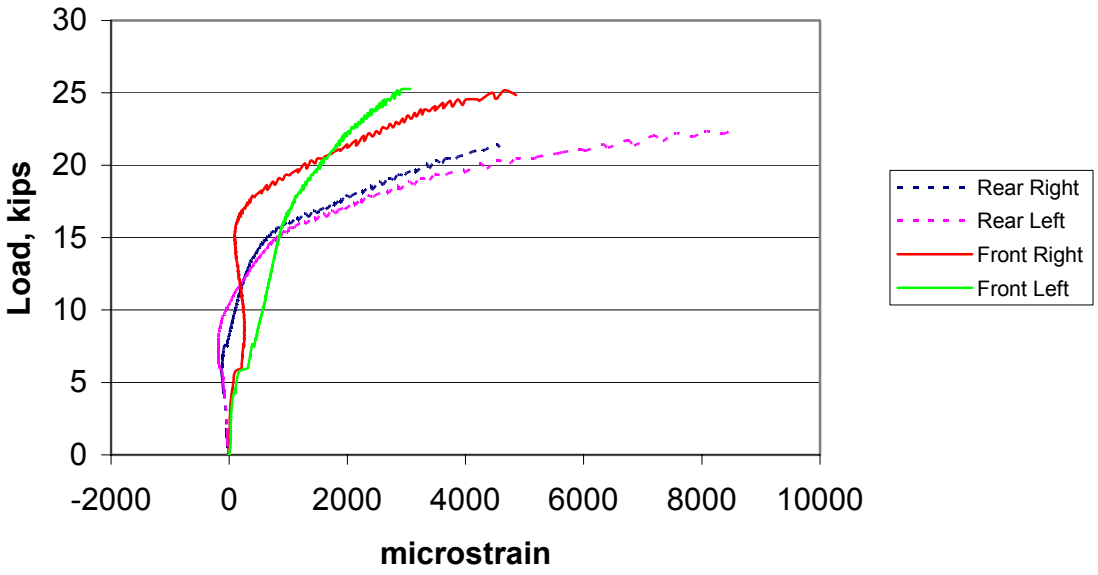

12S-2L-2-A
Load vs Strain
(Rear Legs)

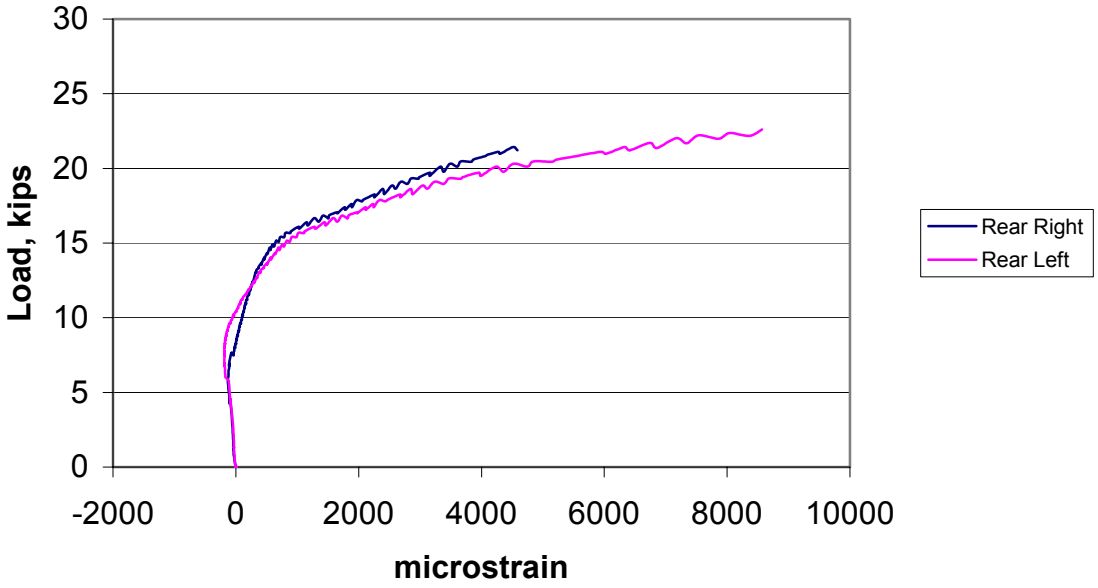

12S-2L-2-A
Load vs Strain
(Front Legs)

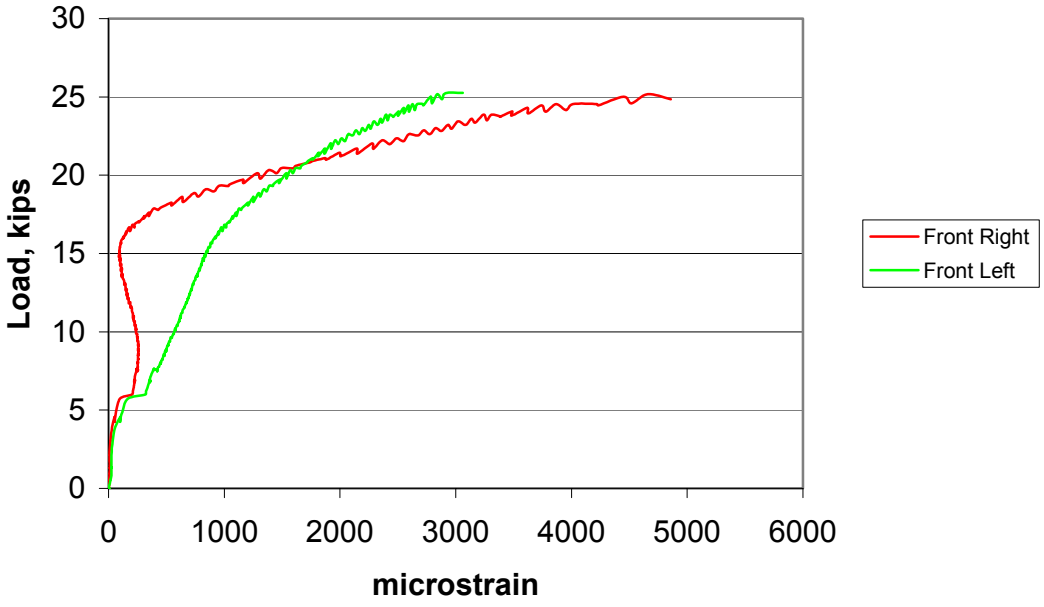

Test 12S-2L-2-B

Specimen Details

Reinforcing	4 legs of No. 3 bar
Area of Reinforcing, A_{vh}	0.44 in^2
Yield Stress of reinforcing	72 ksi
Normal force, P_n	160 lbs
Width of interface, b_v	10 in
Length of interface, s	10 in
f'c, lightweight concrete	5862 psi
Surface type	Smooth
f'c, ductile concrete	32.3 ksi
Slip Load	10.99 kips
Ultimate Load	40.95 kips
Displacement at Slip Load	0.029 in
Displacement at Ultimate Load	0.470 in

12S-2L-2-B
Load vs Slip

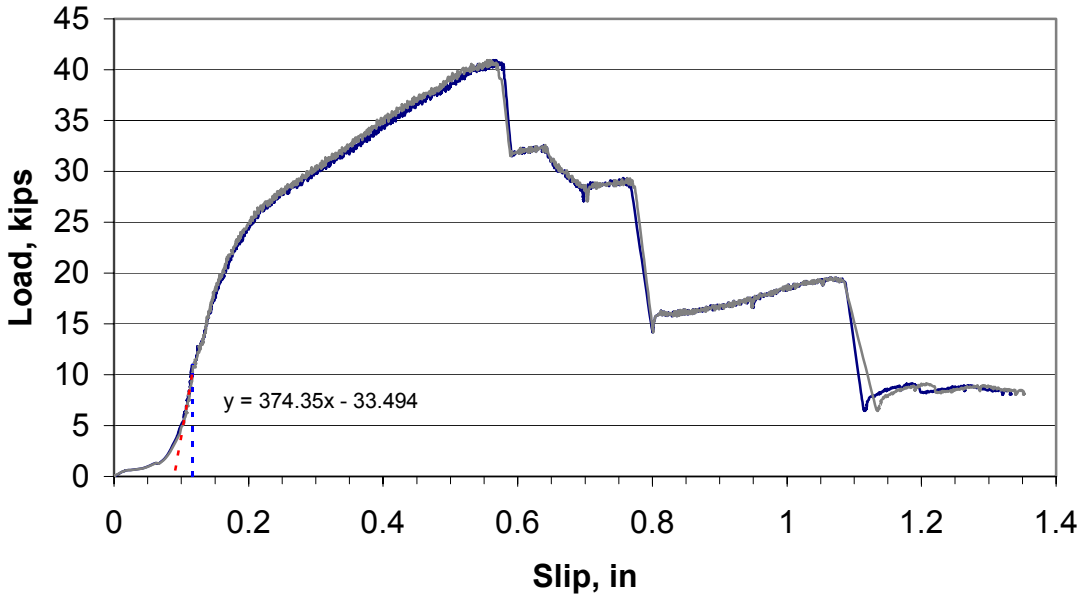

12S-2L-2-B
Load vs Strain

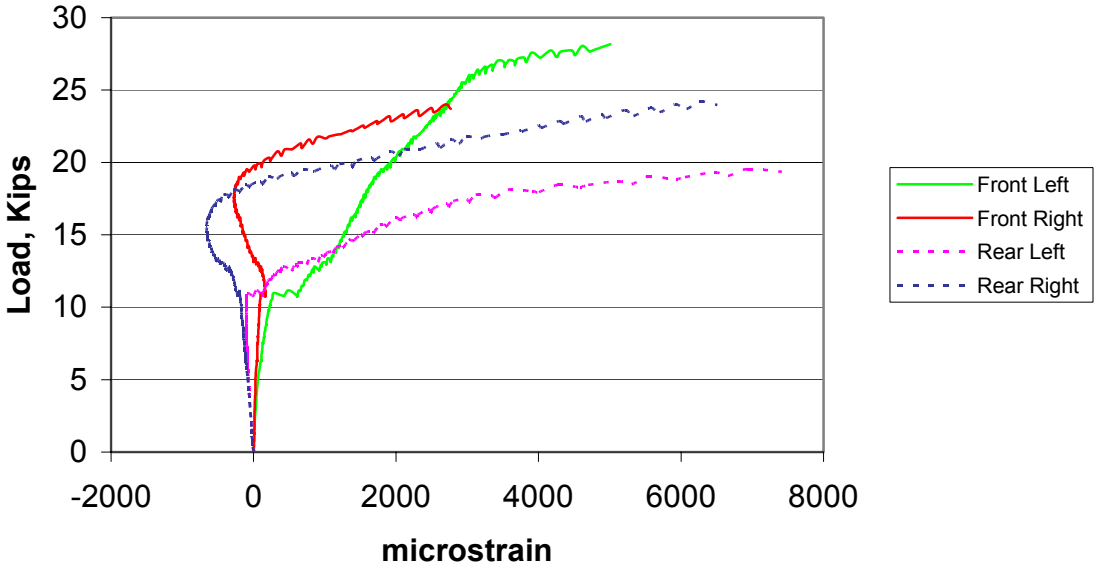

12S-2L-2-B
Load vs Strain
(Rear Legs)

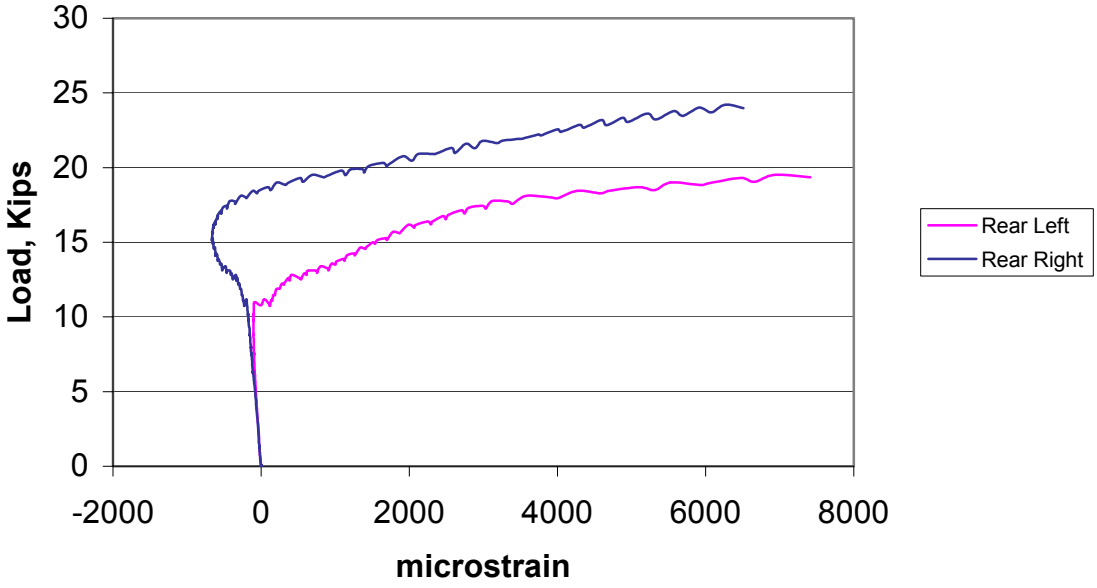

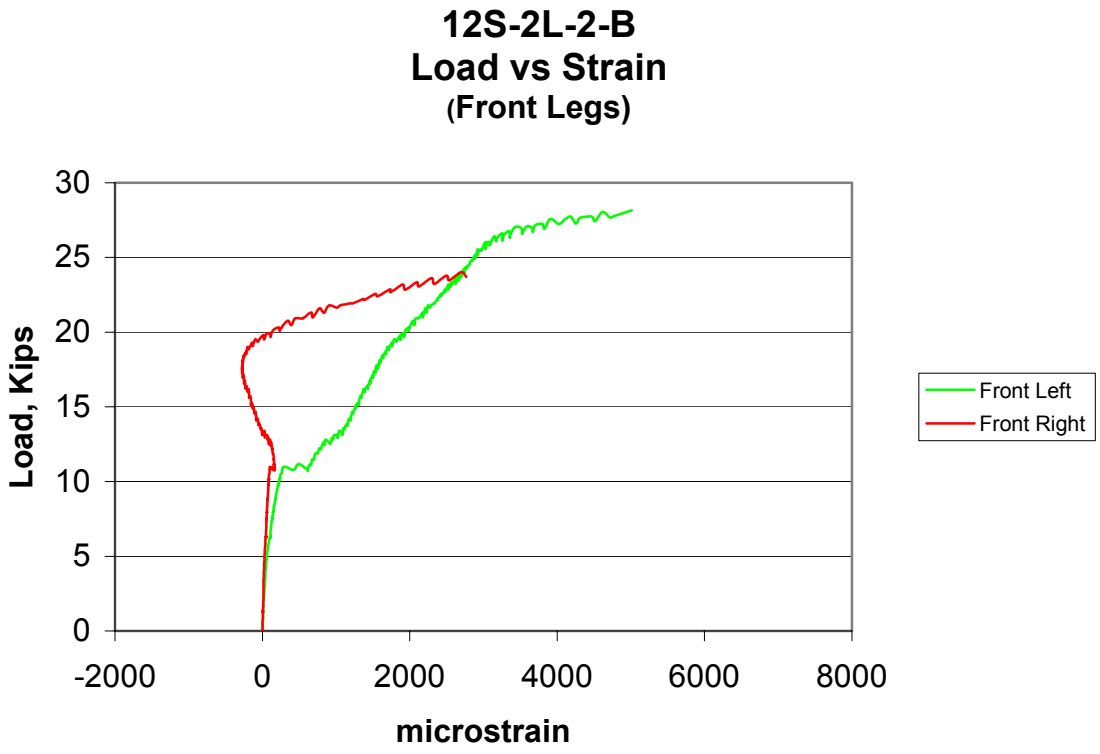
12S-2L-2-B
Load vs Strain
(Front Legs)
Load, Kips
30
25
20
15
10
5
0
-2000
0
2000
4000
6000
8000
microstrain
Front Left
Front Right

Test 18S-1L-1-A

Specimen Details

Reinforcing	1 leg of No. 3 bar
Area of Reinforcing, A_{vh}	0.11 in^2
Yield Stress of reinforcing	72 ksi
Normal force, P_n	256 lbs
Width of interface, b_v	10 in
Length of interface, s	16 in
f'c, lightweight concrete	5862 psi
Surface type	Smooth
f'c, ductile concrete	32.3 ksi
Slip Load	29.60 kips
Ultimate Load	13.61 kips
Displacement at Slip Load	0.024 in
Displacement at Ultimate Load	0.613 in

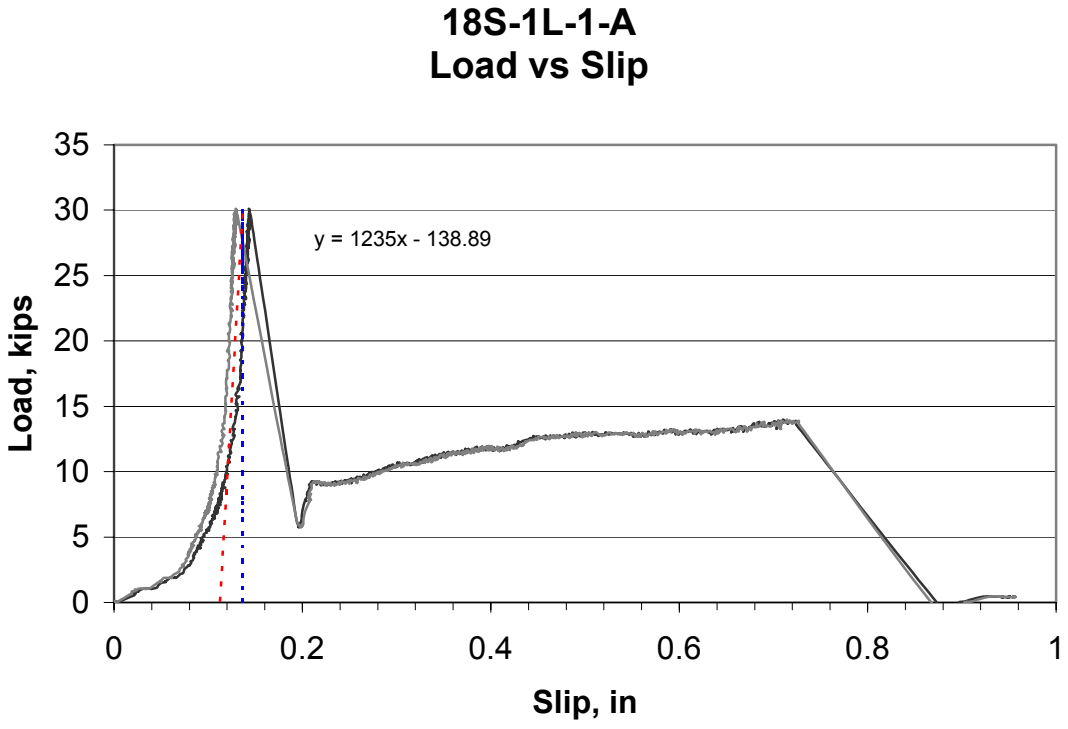

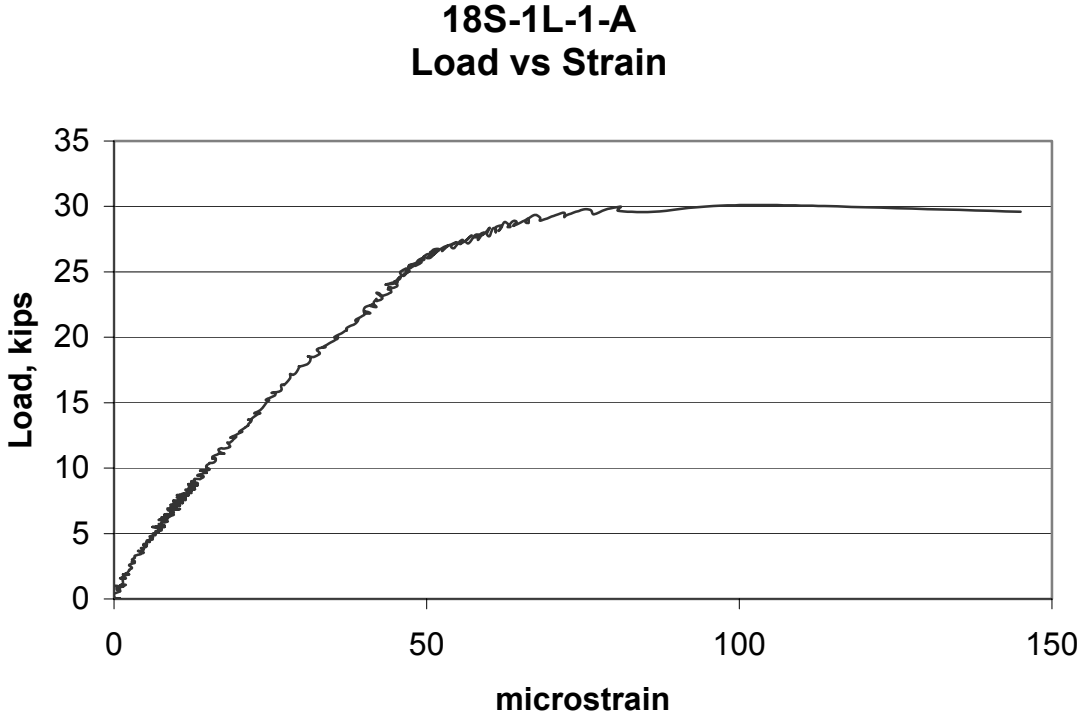
18S-1L-1-A
Load vs Strain
Load, kips
35
30
25
20
15
10
5
0
0
50
100
150
microstrain

Test 18S-1L-1-B

Specimen Details

Reinforcing	1 leg of No. 3 bar
Area of Reinforcing, A_{vh}	0.11 in^2
Yield Stress of reinforcing	72 ksi
Normal force, P_n	256 lbs
Width of interface, b_v	10 in
Length of interface, s	16 in
f'c, lightweight concrete	5862 psi
Surface type	Smooth
f'c, ductile concrete	32.3 ksi
Slip Load	25.79 kips
Ultimate Load	13.86 kips
Displacement at Slip Load	0.028 in
Displacement at Ultimate Load	0.747 in

18S-1L-1-B
Load vs Slip

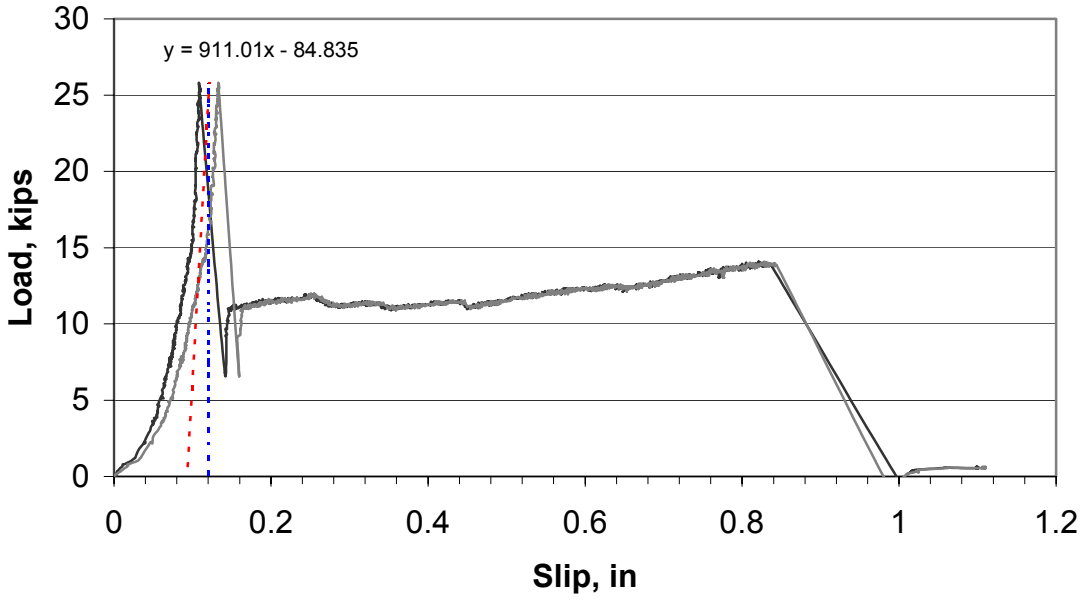

18S-1L-1-B
Load vs Strain

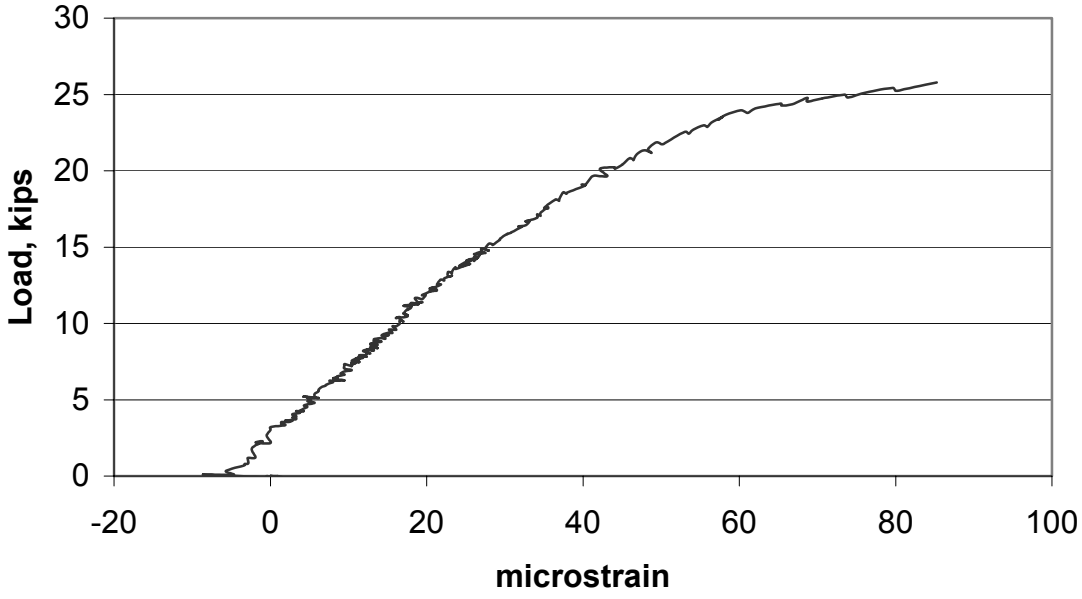

Test 18S-2L-1-A

Specimen Details

Reinforcing	2 legs of No. 3 bar
Area of Reinforcing, A_{vh}	0.22 in^2
Yield Stress of reinforcing	72 ksi
Normal force, P_n	256 lbs
Width of interface, b_v	10 in
Length of interface, s	16 in
f'c, lightweight concrete	5862 psi
Surface type	Smooth
f'c, ductile concrete	32.3 ksi
Slip Load	19.00 kips
Ultimate Load	23.36 kips
Displacement at Slip Load	0.041 in
Displacement at Ultimate Load	0.585 in

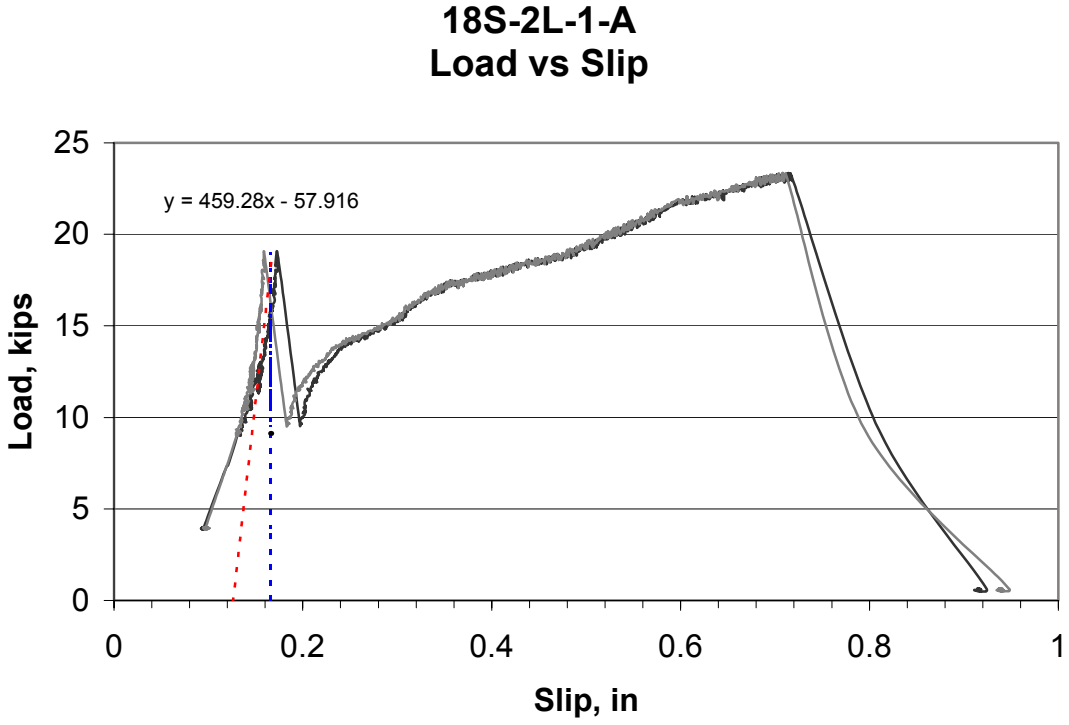

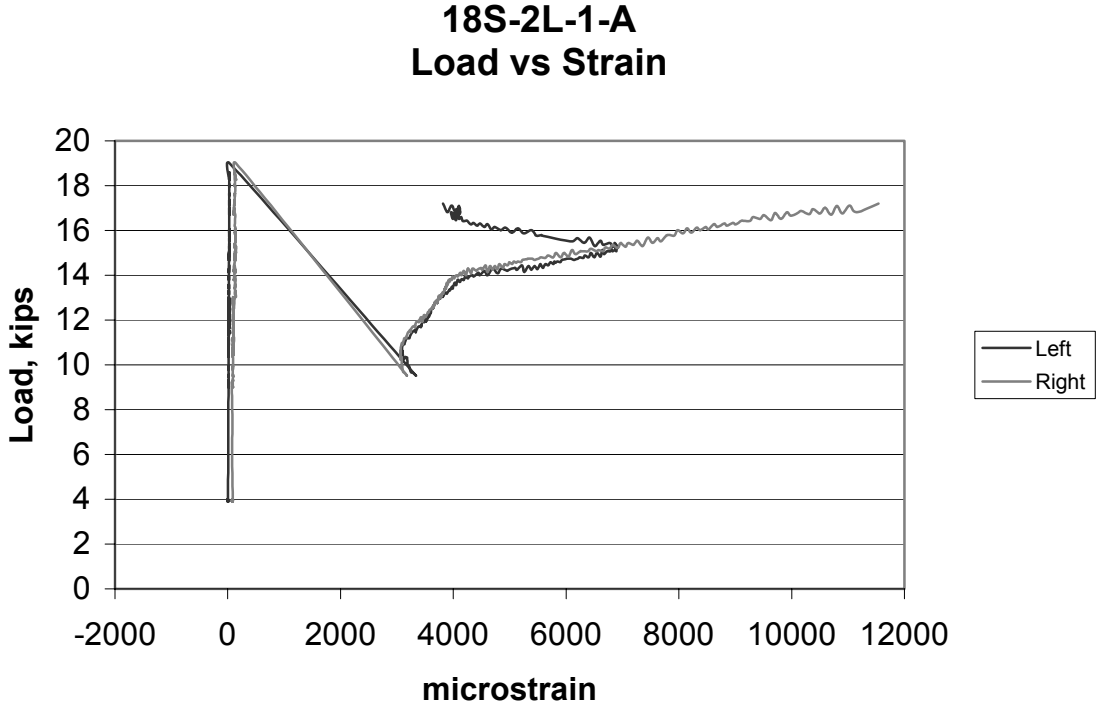
18S-2L-1-A
Load vs Strain
Load, kips
20
18
16
14
12
10
8
6
4
2
0
-2000
0
2000
4000
6000
8000
10000
12000
microstrain
Left
Right

Test 18S-2L-1-B

Specimen Details

Reinforcing	2 legs of No. 3 bar
Area of Reinforcing, A_{vh}	0.22 in^2
Yield Stress of reinforcing	72 ksi
Normal force, P_n	256 lbs
Width of interface, b_v	10 in
Length of interface, s	16 in
f'c, lightweight concrete	5862 psi
Surface type	Smooth
f'c, ductile concrete	32.3 ksi
Slip Load	22.67 kips
Ultimate Load	23.03 kips
Displacement at Slip Load	0.024 in
Displacement at Ultimate Load	0.376 in

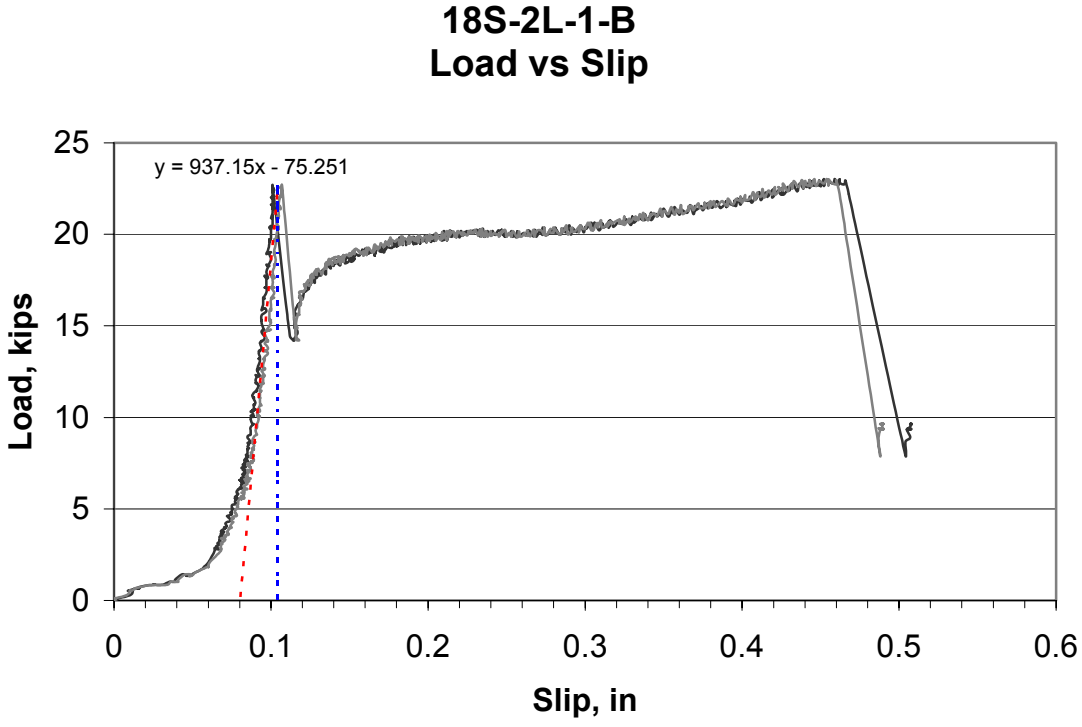

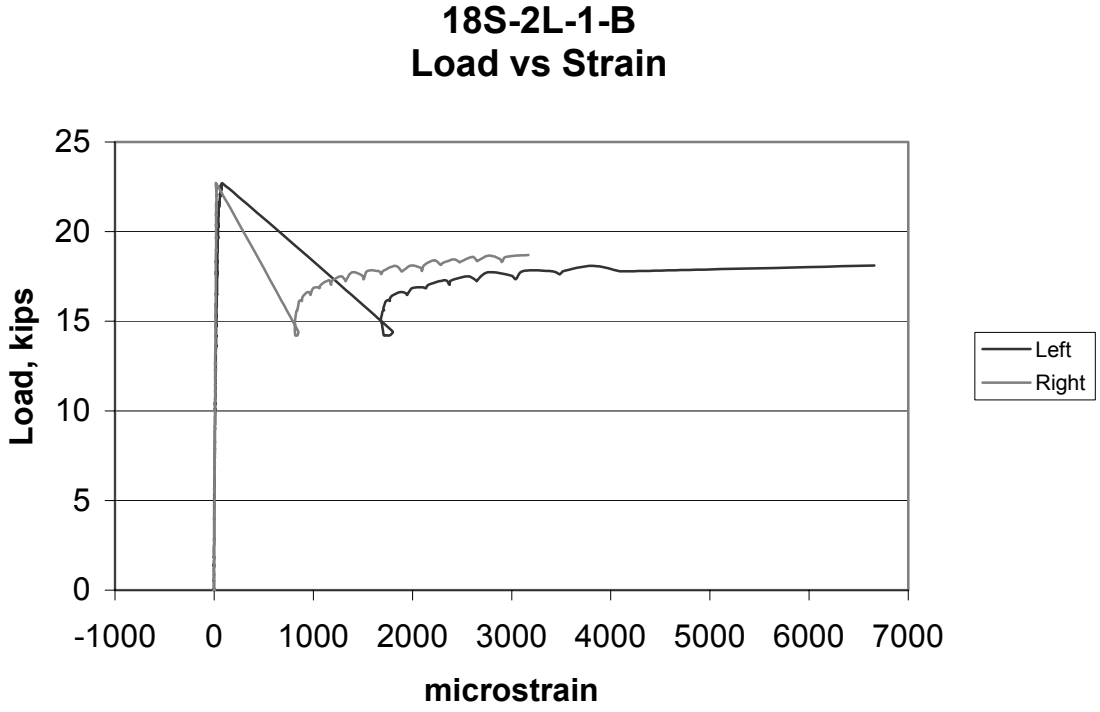
18S-2L-1-B
Load vs Strain
Load, kips
25
20
15
10
5
0
-1000
0
1000
2000
3000
4000
5000
6000
7000
microstrain
Left
Right

Test 18S-2L-2-A

Specimen Details

Reinforcing	4 legs of No. 3 bar
Area of Reinforcing, A_{vh}	0.44 in^2
Yield Stress of reinforcing	72 ksi
Normal force, P_n	256 lbs
Width of interface, b_v	10 in
Length of interface, s	16 in
f'c, lightweight concrete	5862 psi
Surface type	Smooth
f'c, ductile concrete	32.3 ksi
Slip Load	21.73 kips
Ultimate Load	46.97 kips
Displacement at Slip Load	0.031 in
Displacement at Ultimate Load	0.410 in

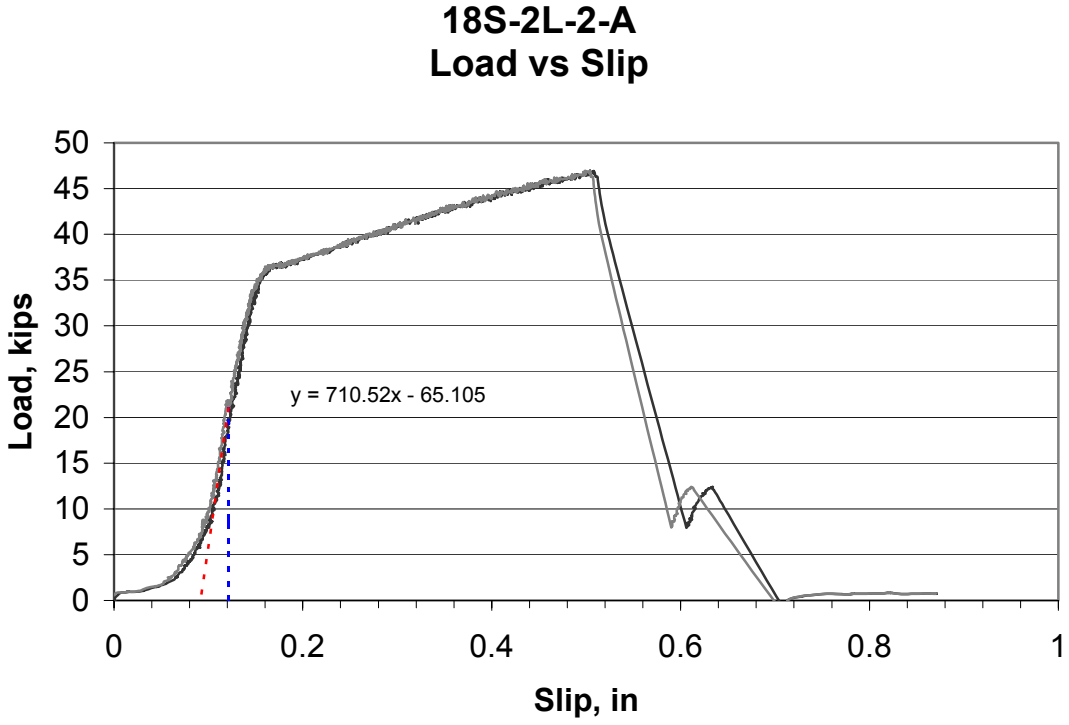

18S-2L-2-A
Load vs Strain

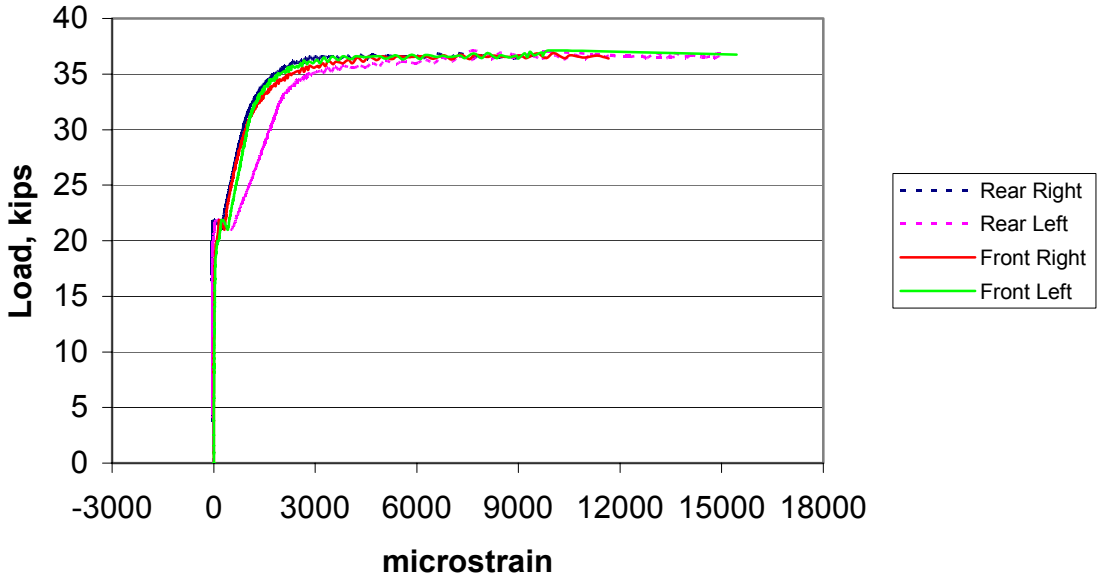

18S-2L-2-A
Load vs Strain
(Rear Legs)

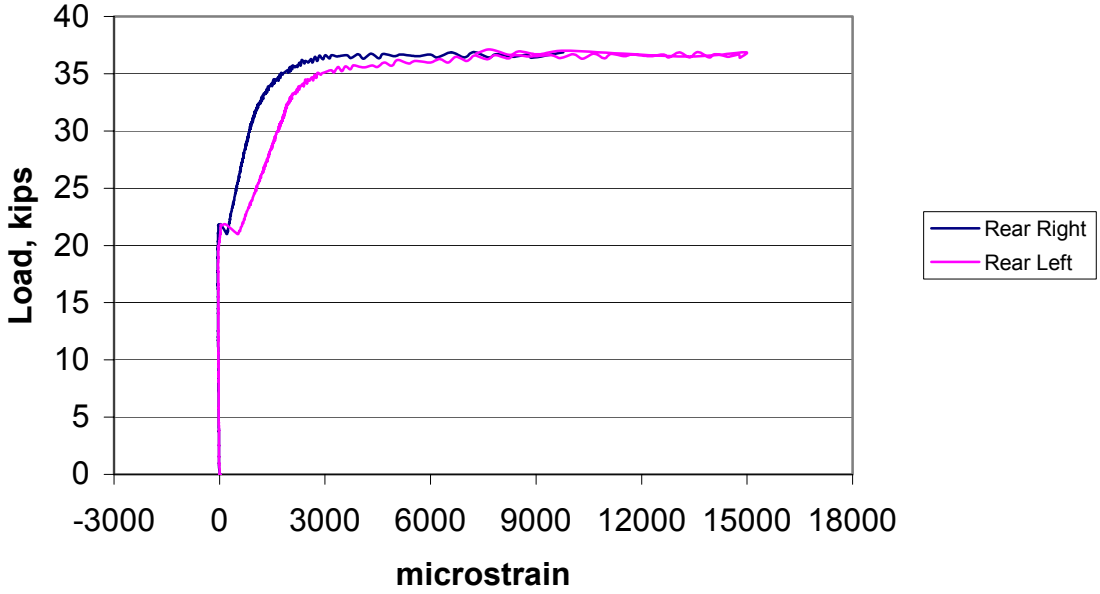

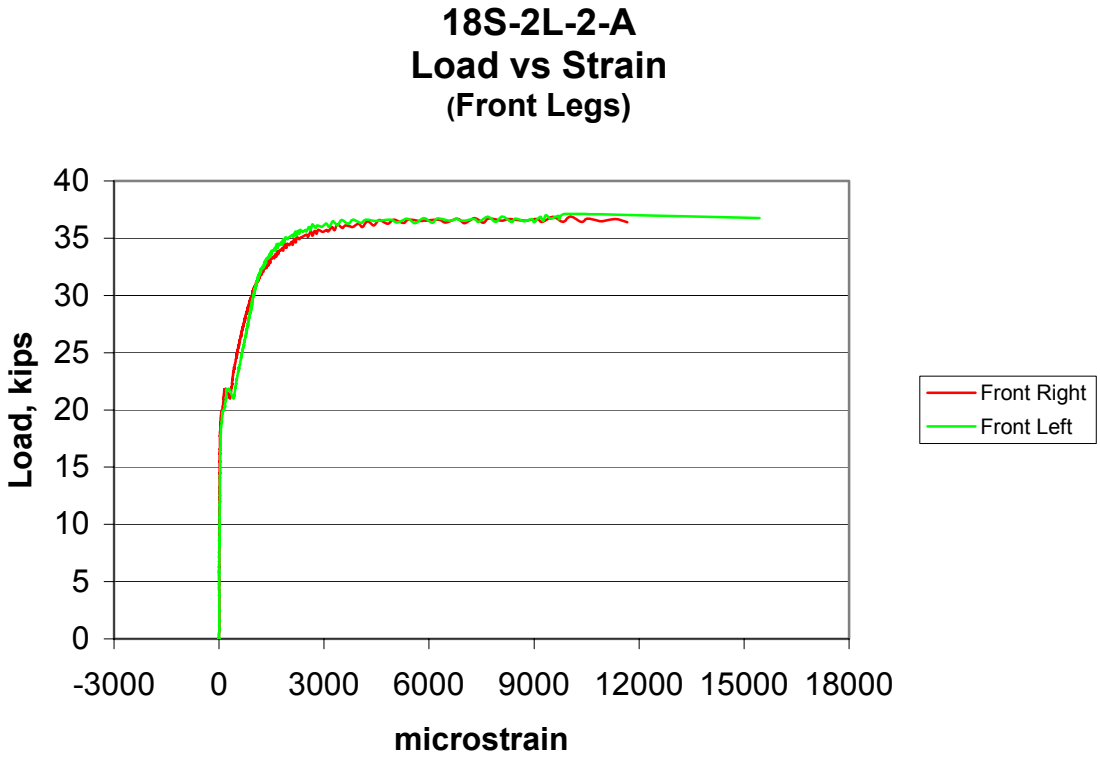
18S-2L-2-A
Load vs Strain
(Front Legs)
Load, kips
40
35
30
25
20
15
10
5
0
-3000
0
3000
6000
9000
12000
15000
18000
microstrain
Front Right
Front Left

Test 18S-2L-2-B

Specimen Details

Reinforcing	4 legs of No. 3 bar
Area of Reinforcing, A_{vh}	0.44 in^2
Yield Stress of reinforcing	72 ksi
Normal force, P_n	256 lbs
Width of interface, b_v	10 in
Length of interface, s	16 in
f'c, lightweight concrete	5862 psi
Surface type	Smooth
f'c, ductile concrete	32.3 ksi
Slip Load	17.73 kips
Ultimate Load	41.78 kips
Displacement at Slip Load	0.057 in
Displacement at Ultimate Load	0.398 in

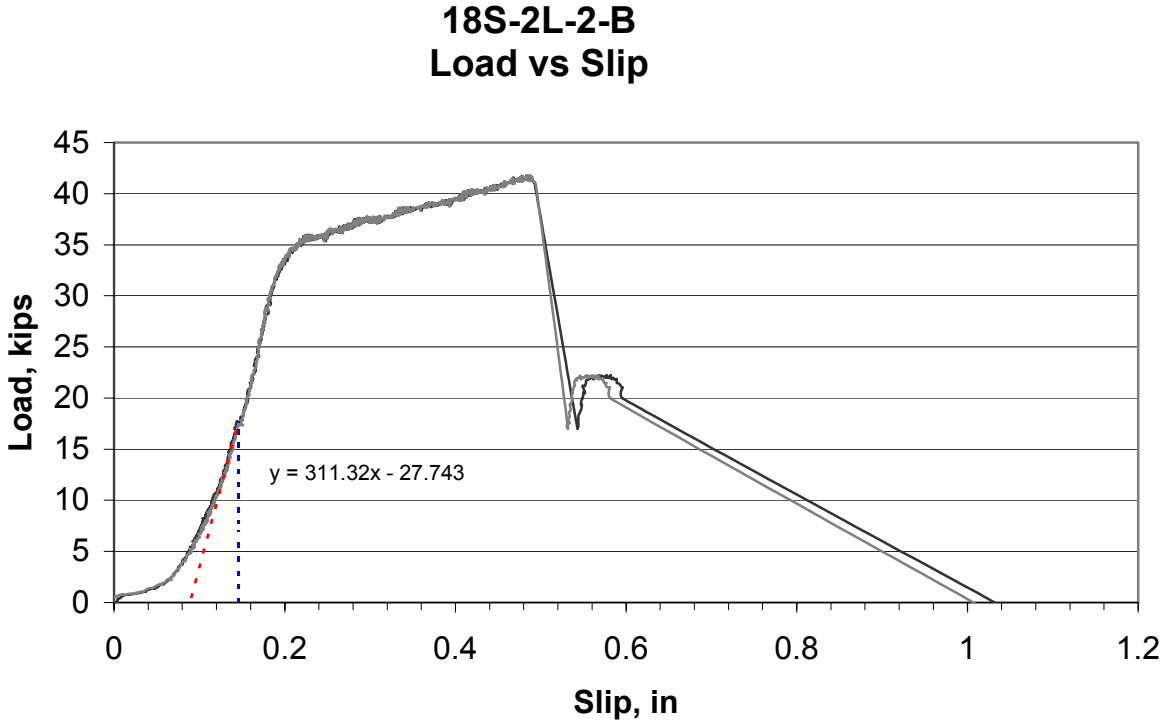

18S-2L-2-B
Load vs Strain

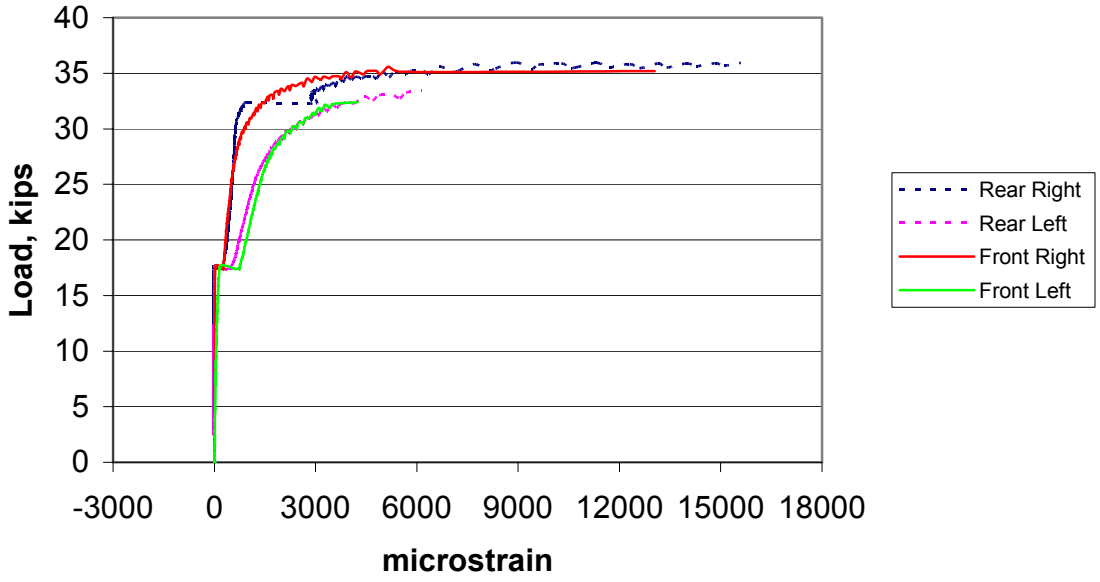

18S-2L-2-B
Load vs Strain
(Rear Legs)

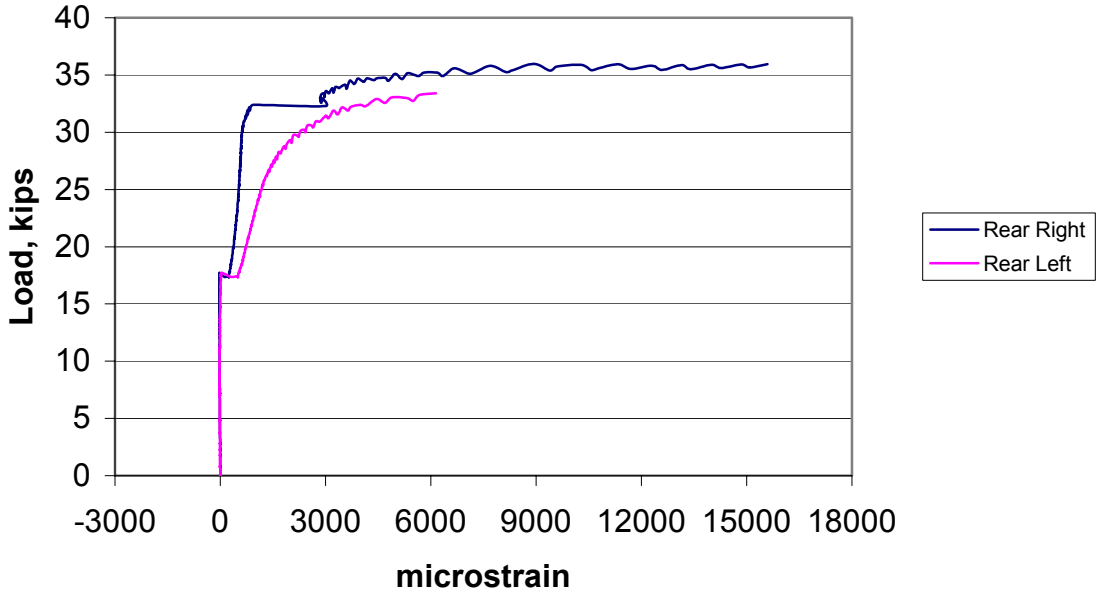

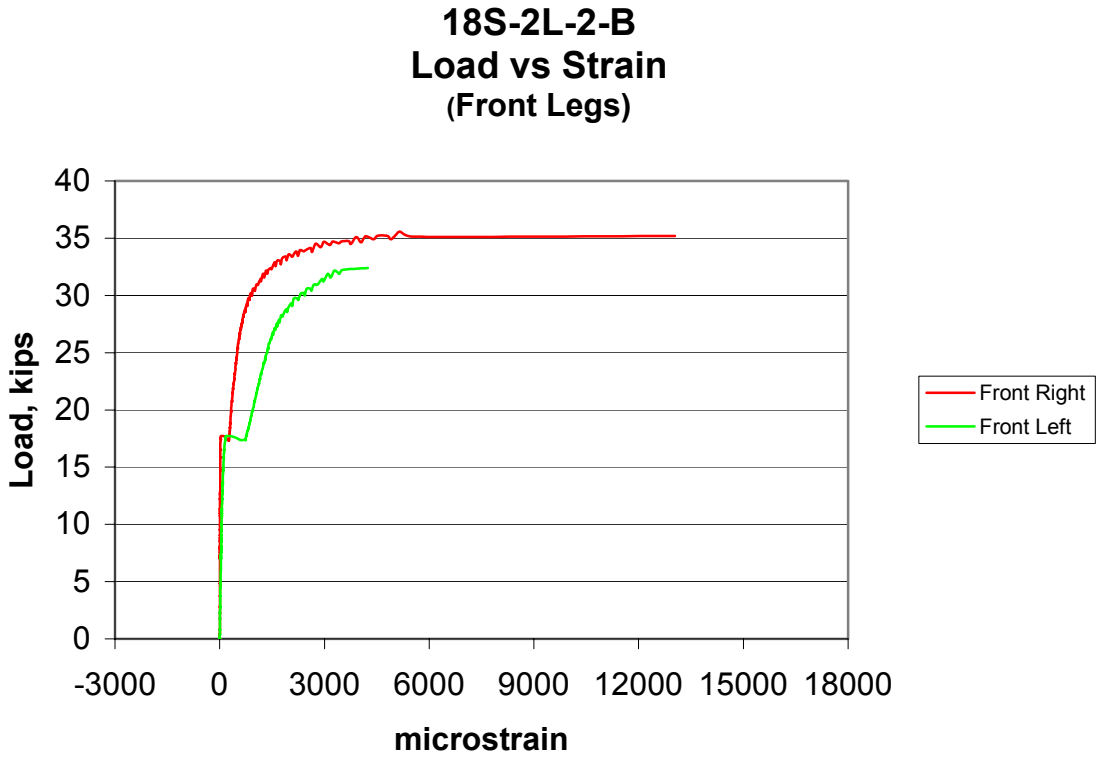
18S-2L-2-B
Load vs Strain
(Front Legs)
Load, kips
40
35
30
25
20
15
10
5
0
-3000
0
3000
6000
9000
12000
15000
18000
microstrain
Front Right
Front Left

Test 18S-2L-3-A

Specimen Details

Reinforcing	6 legs of No. 3 bar
Area of Reinforcing, A_{vh}	0.66 in^2
Yield Stress of reinforcing	72 ksi
Normal force, P_n	256 lbs
Width of interface, b_v	10 in
Length of interface, s	16 in
f'c, lightweight concrete	5862 psi
Surface type	Smooth
f'c, ductile concrete	32.3 ksi
Slip Load	18.09 kips
Ultimate Load	64.42 kips
Displacement at Slip Load	0.028 in
Displacement at Ultimate Load	0.480 in

18S-2L-3-A
Load vs Slip

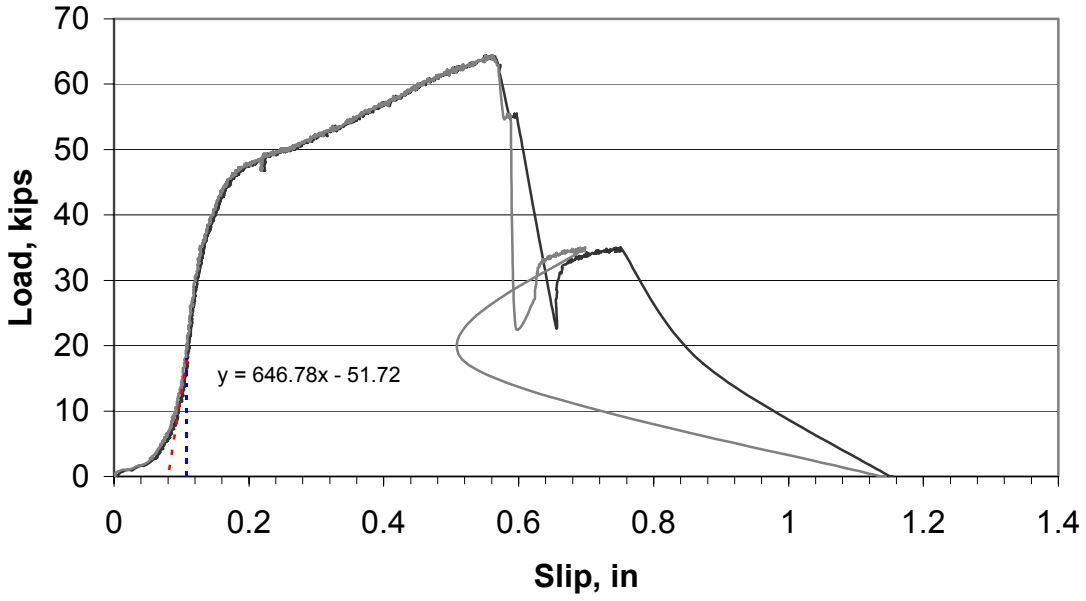

18S-2L-3-A
Load vs Strain

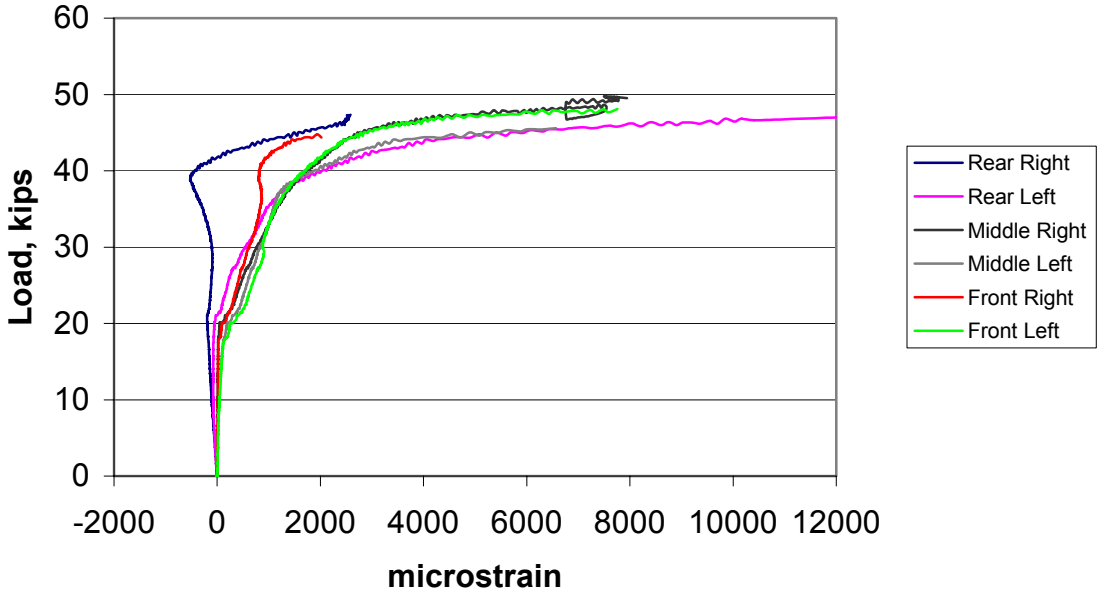

18S-2L-3-A
Load vs Strain
(Rear Legs)

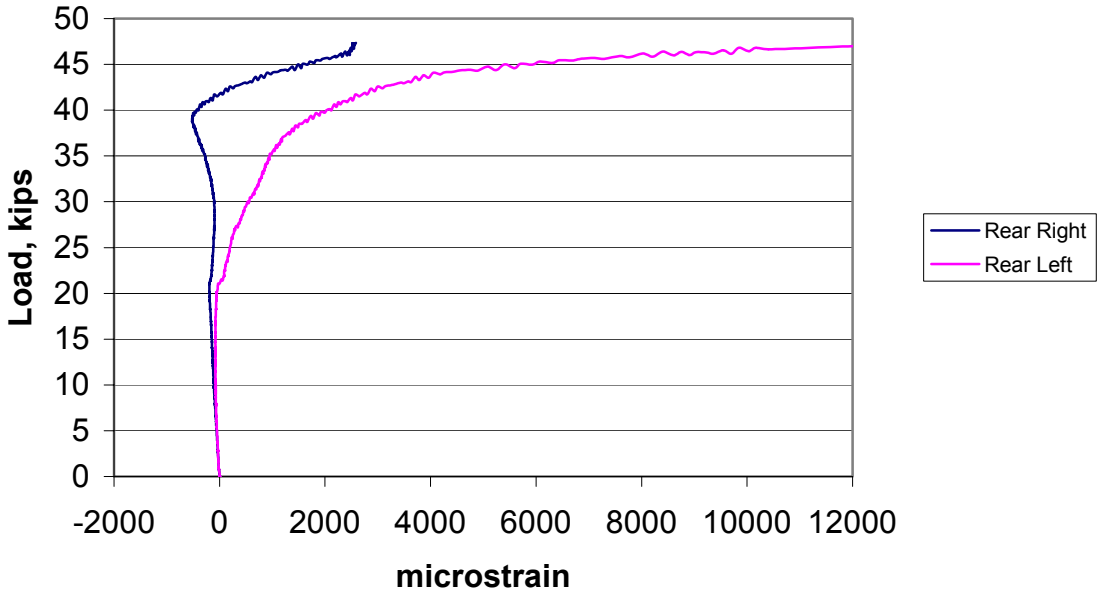

18S-2L-3-A
Load vs Strain
(Middle Legs)

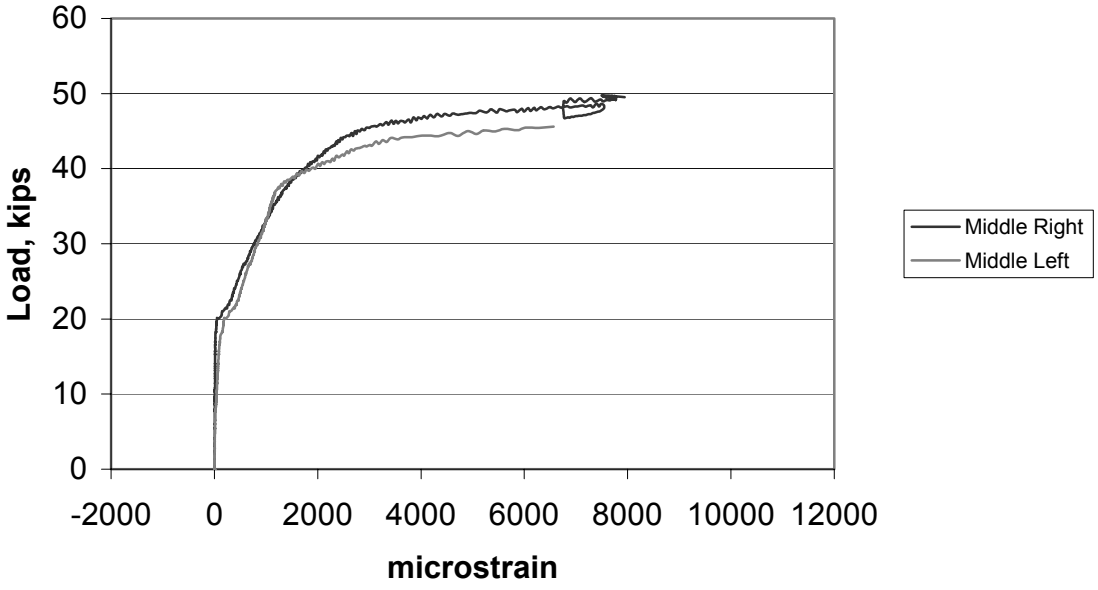

18S-2L-3-A
Load vs Strain
(Front Legs)

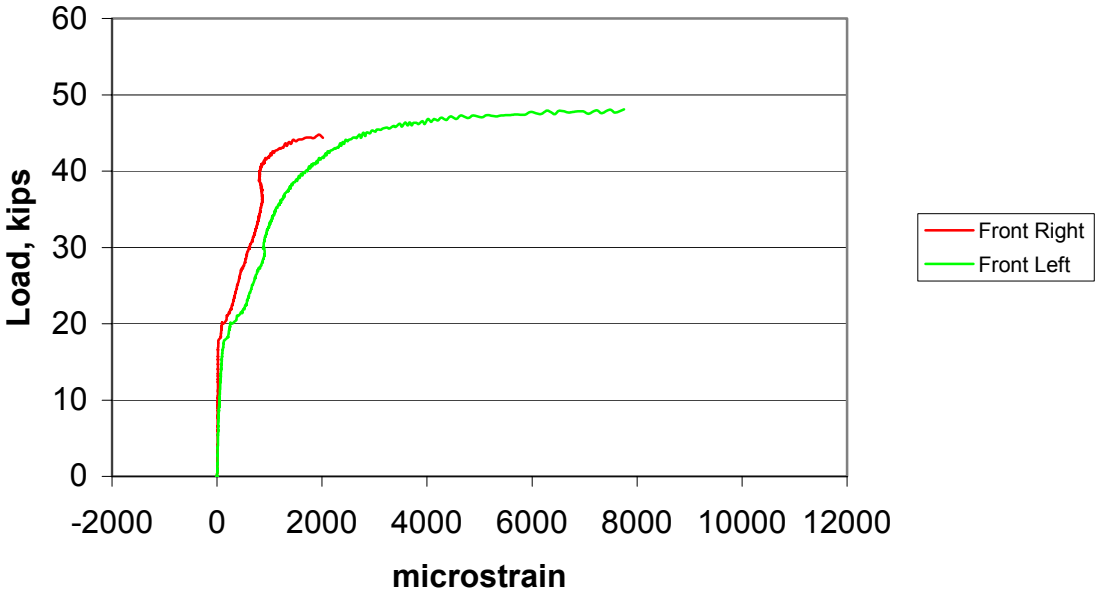

Test 18S-2L-3-B

Specimen Details

Reinforcing	6 legs of No. 3 bar
Area of Reinforcing, A_{vh}	0.66 in^2
Yield Stress of reinforcing	72 ksi
Normal force, P_n	256 lbs
Width of interface, b_v	10 in
Length of interface, s	16 in
f'c, lightweight concrete	5862 psi
Surface type	Smooth
f'c, ductile concrete	32.3 ksi
Slip Load	12.62 kips
Ultimate Load	56.33 kips
Displacement at Slip Load	0.031 in
Displacement at Ultimate Load	0.380 in

18S-2L-3-B
Load vs Slip

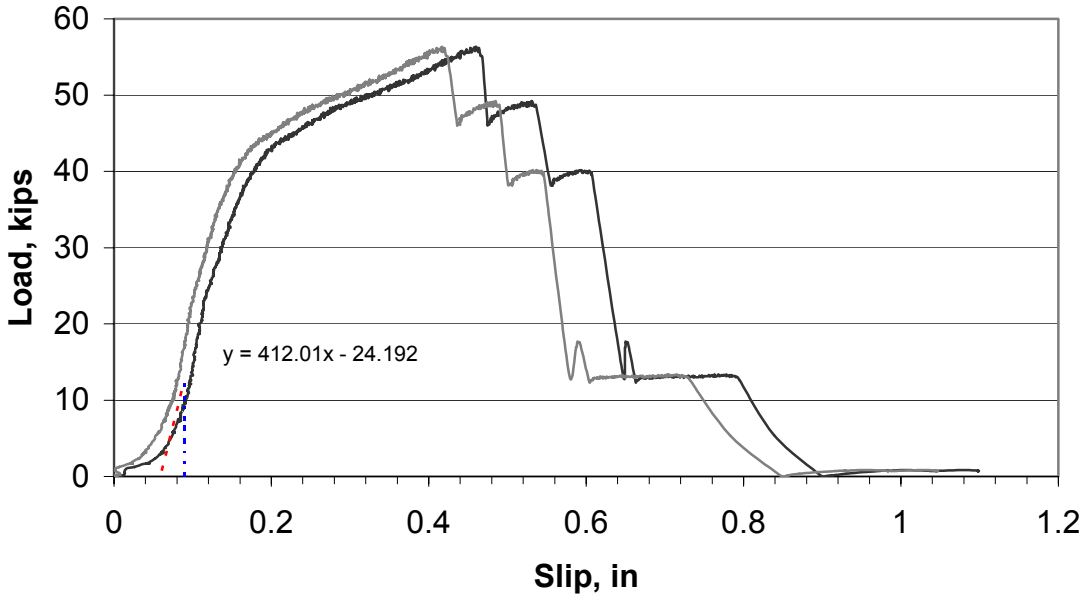

18S-2L-3-B
Load vs Strain

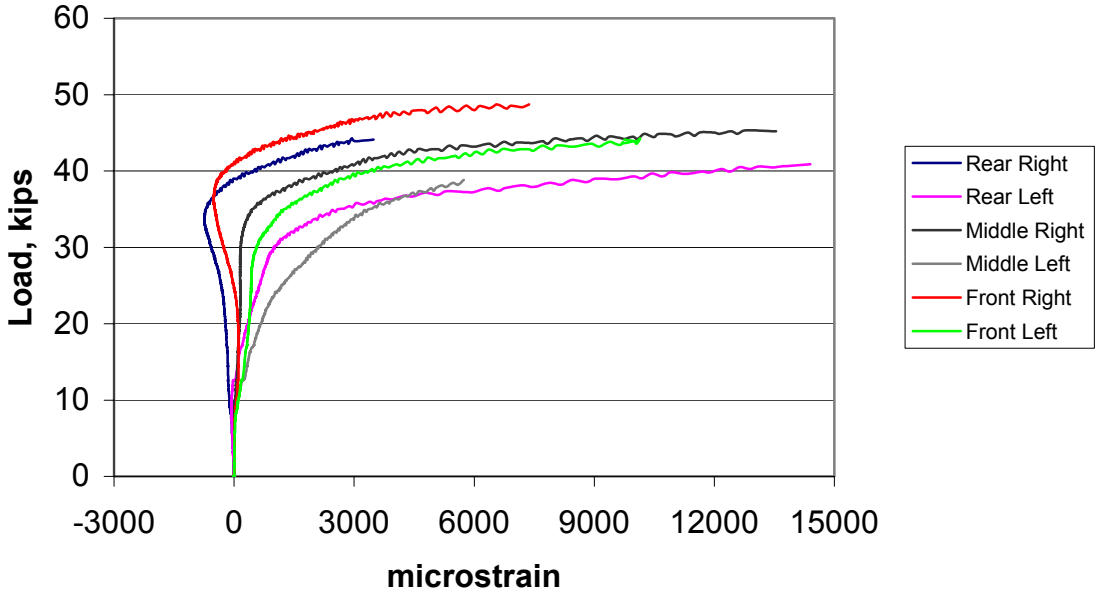

18S-2L-3-B
Load vs Strain
(Rear Legs)

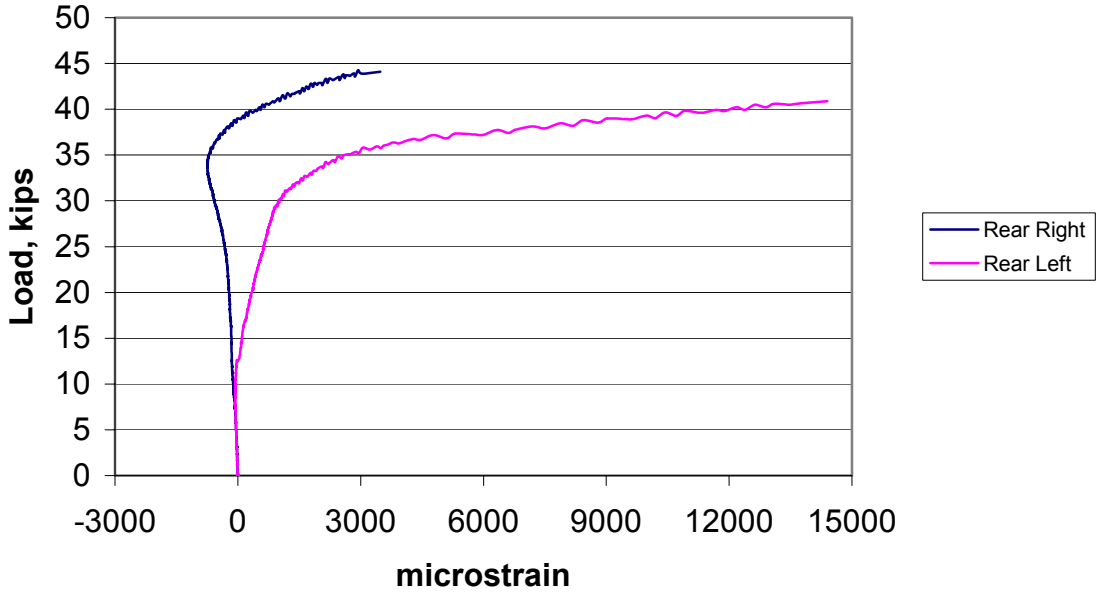

18S-2L-3-B
Load vs Strain
(Middle Legs)

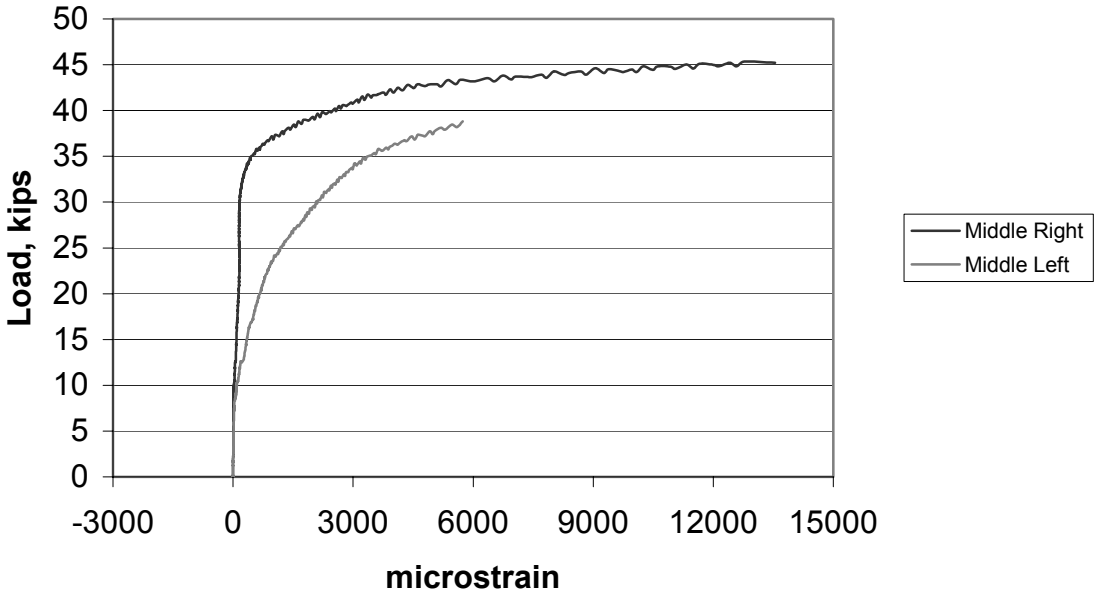

18S-2L-3-B
Load vs Strain
(Front Legs)

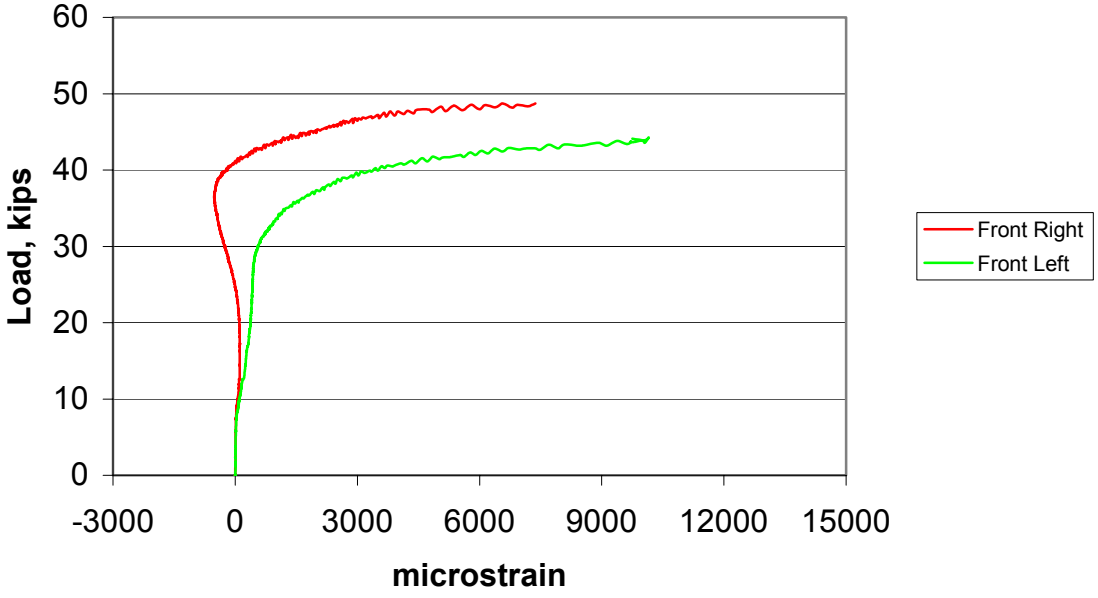

Test 18S-0L-0-A

Specimen Details

Reinforcing	none
Area of Reinforcing, A_{vh}	-
Yield Stress of reinforcing	-
Normal force, P_n	256 lbs
Width of interface, b_v	10 in
Length of interface, s	16 in
f'c, lightweight concrete	5862 psi
Surface type	Smooth
f'c, ductile concrete	32.3 ksi
Slip Load	21.32 kips
Ultimate Load	21.32 kips
Displacement at Slip Load	0.026 in
Displacement at Ultimate Load	0.026 in

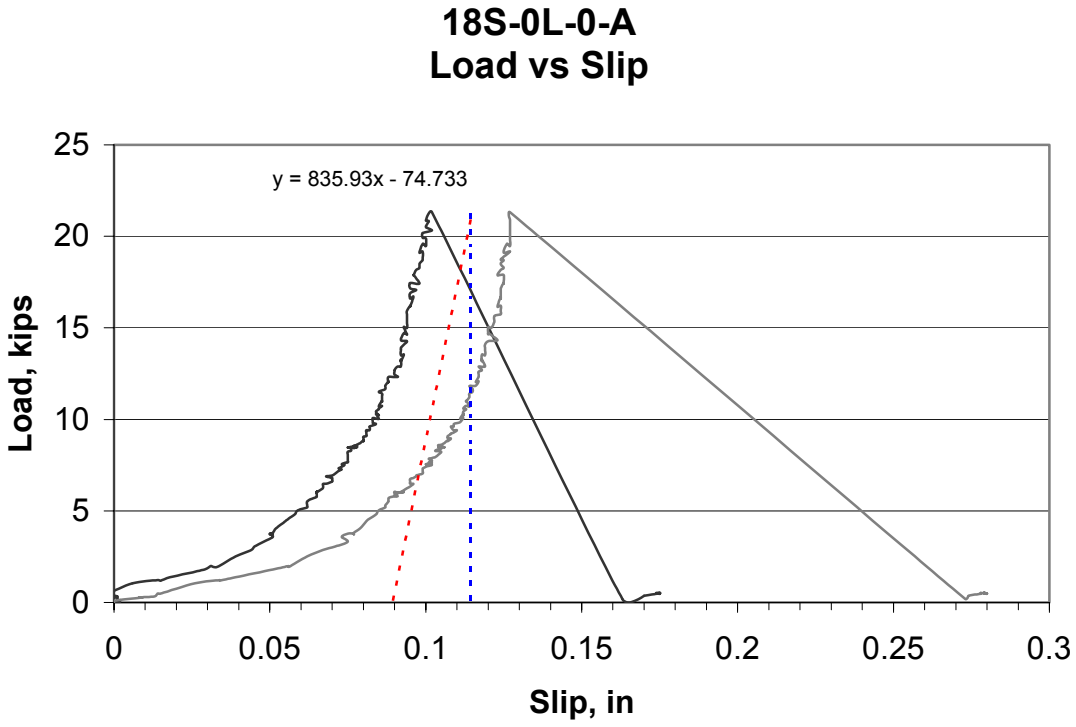

Test 18S-0L-0-B

Specimen Details

Reinforcing	none
Area of Reinforcing, A_{vh}	-
Yield Stress of reinforcing	-
Normal force, P_n	256 lbs
Width of interface, b_v	10 in
Length of interface, s	16 in
f'c, lightweight concrete	5862 psi
Surface type	Smooth
f'c, ductile concrete	32.3 ksi
Slip Load	16.38 kips
Ultimate Load	16.38 kips
Displacement at Slip Load	0.034 in
Displacement at Ultimate Load	0.034 in

18S-0L-0-B
Load vs Slip

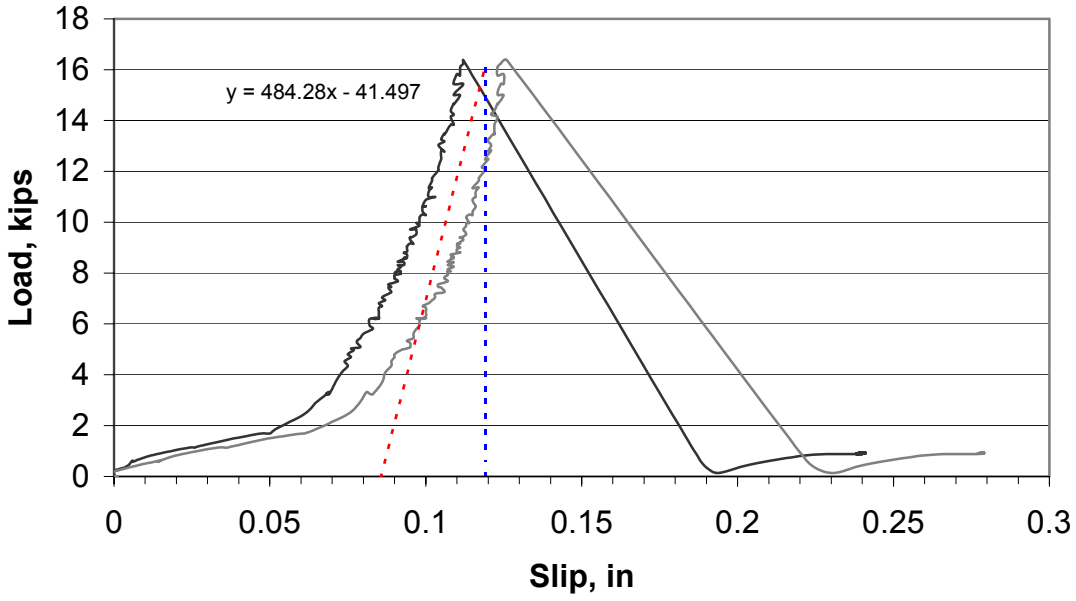

Test 18D-0L-0-A

Specimen Details

Reinforcing	none
Area of Reinforcing, A_{vh}	-
Yield Stress of reinforcing	-
Normal force, P_n	256 lbs
Width of interface, b_v	10 in
Length of interface, s	16 in
f'c, lightweight concrete	5862 psi
Surface type	Deformed
f'c, ductile concrete	32.3 ksi
Slip Load	27.06 kips
Ultimate Load	27.06 kips
Displacement at Slip Load	0.018 in
Displacement at Ultimate Load	0.018 in

18D-0L-0-A
Load vs Slip

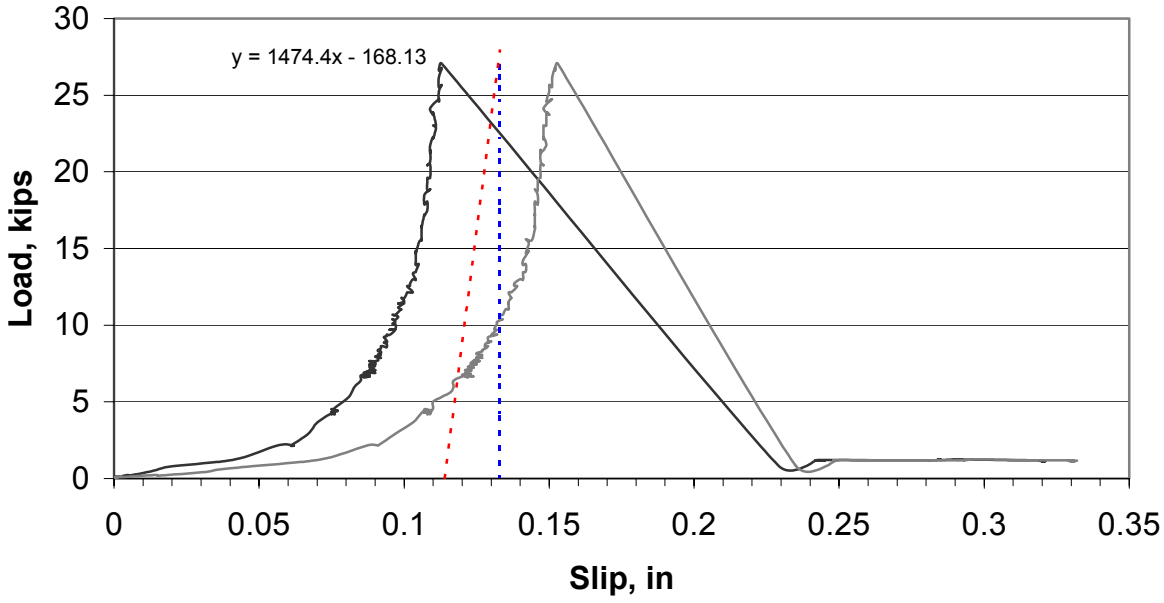

Test 18D-0L-0-B

Specimen Details

Reinforcing	none
Area of Reinforcing, A_{vh}	-
Yield Stress of reinforcing	-
Normal force, P_n	256 lbs
Width of interface, b_v	10 in
Length of interface, s	16 in
f'c, lightweight concrete	5862 psi
Surface type	Deformed
f'c, ductile concrete	32.3 ksi
Slip Load	29.11 kips
Ultimate Load	29.11 kips
Displacement at Slip Load	0.034 in
Displacement at Ultimate Load	0.034 in

18D-0L-0-B
Load vs Slip

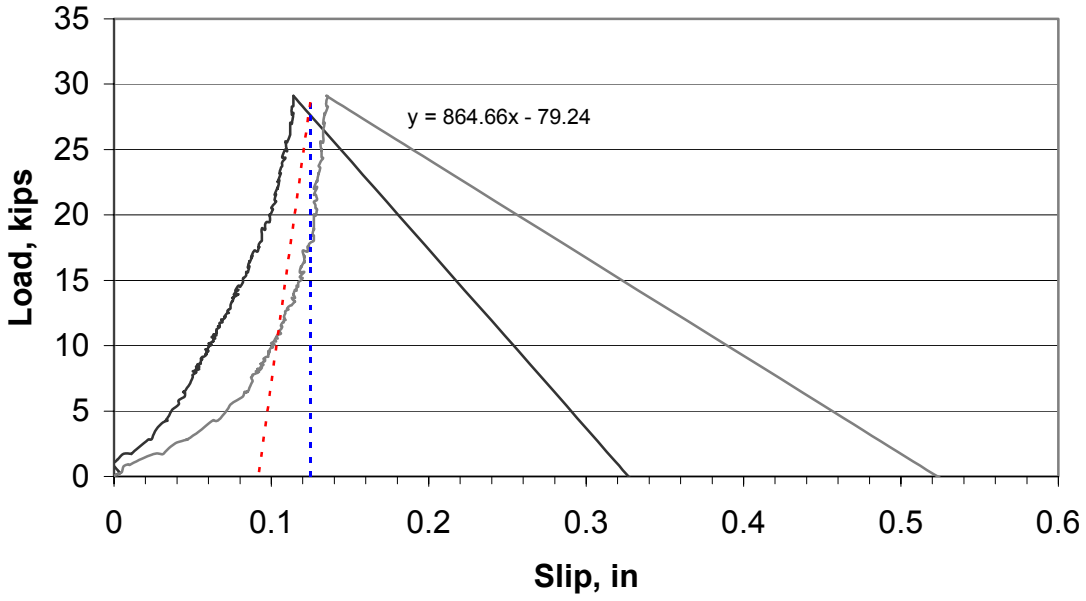

Test 18K-0L-0-A

Specimen Details

Reinforcing	none
Area of Reinforcing, A_{vh}	-
Yield Stress of reinforcing	-
Normal force, P_n	256 lbs
Width of interface, b_v	10 in
Length of interface, s	16 in
f'c, lightweight concrete	5862 psi
Surface type	Keyed
f'c, ductile concrete	32.3 ksi
Slip Load	50.09 kips
Ultimate Load	50.09 kips
Displacement at Slip Load	0.035 in
Displacement at Ultimate Load	0.035 in

18K-0L-0-A
Load vs Slip

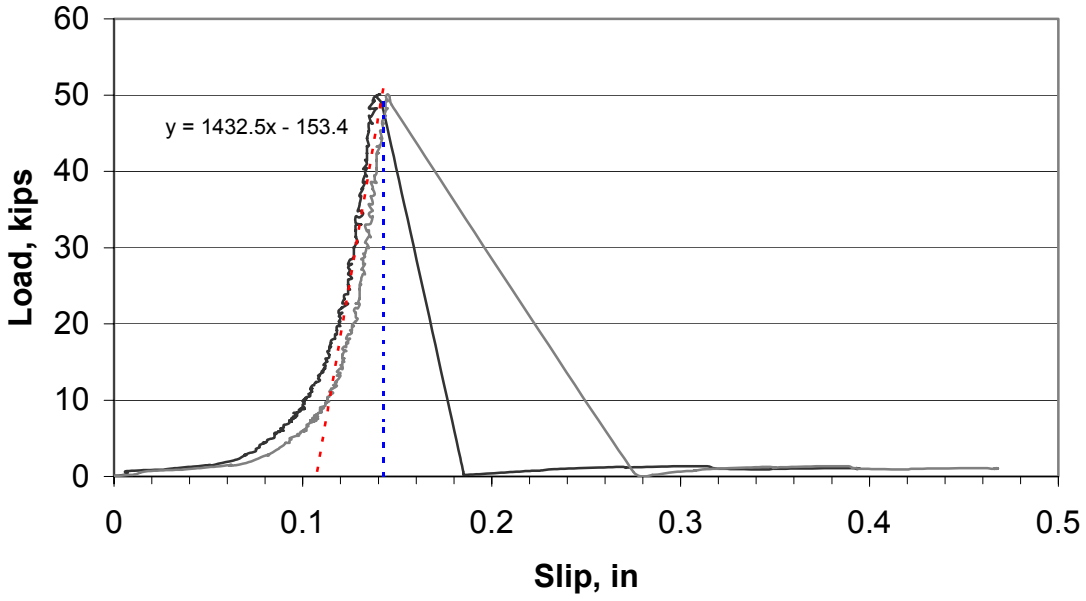

Test 18K-0L-0-B

Specimen Details

Reinforcing	none
Area of Reinforcing, A_{vh}	-
Yield Stress of reinforcing	-
Normal force, P_n	256 lbs
Width of interface, b_v	10 in
Length of interface, s	16 in
f'c, lightweight concrete	5862 psi
Surface type	Keyed
f'c, ductile concrete	32.3 ksi
Slip Load	44.96 kips
Ultimate Load	44.96 kips
Displacement at Slip Load	0.038 in
Displacement at Ultimate Load	0.038 in

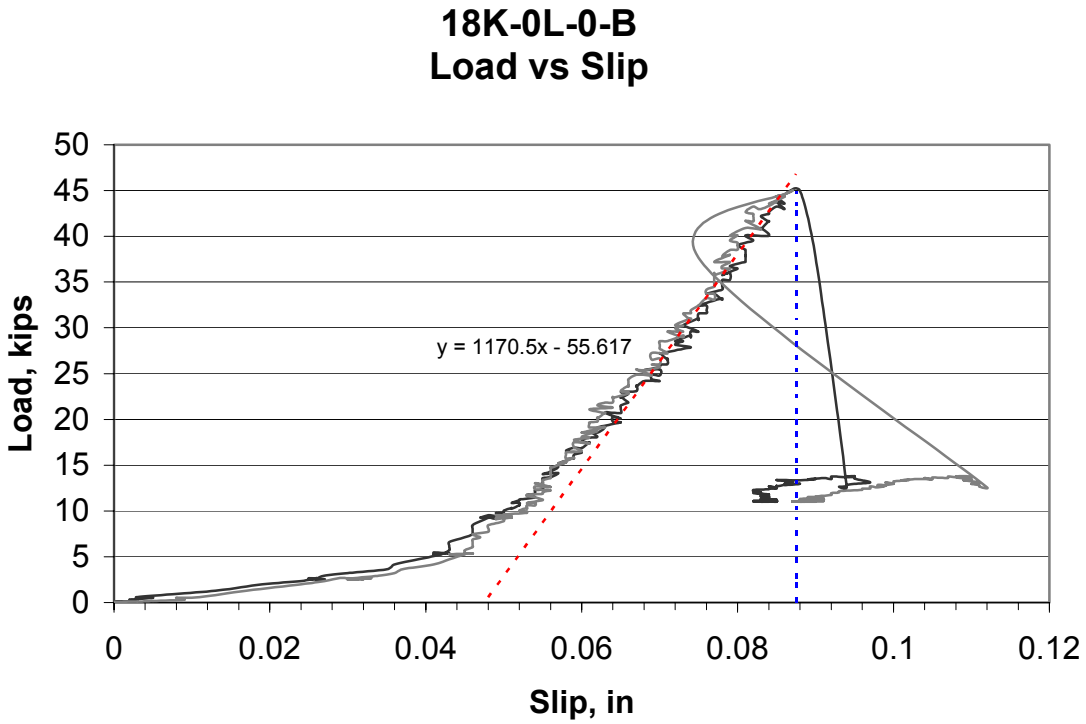

Test 18C-0L-0-A

Specimen Details

Reinforcing	none
Area of Reinforcing, A_{vh}	-
Yield Stress of reinforcing	-
Normal force, P_n	256 lbs
Width of interface, b_v	10 in
Length of interface, s	16 in
f'c, lightweight concrete	5862 psi
Surface type	Chipped
f'c, ductile concrete	32.3 ksi
Slip Load	64.09 kips
Ultimate Load	64.09 kips
Displacement at Slip Load	0.046 in
Displacement at Ultimate Load	0.046 in

18C-0L-0-A
Load vs Slip

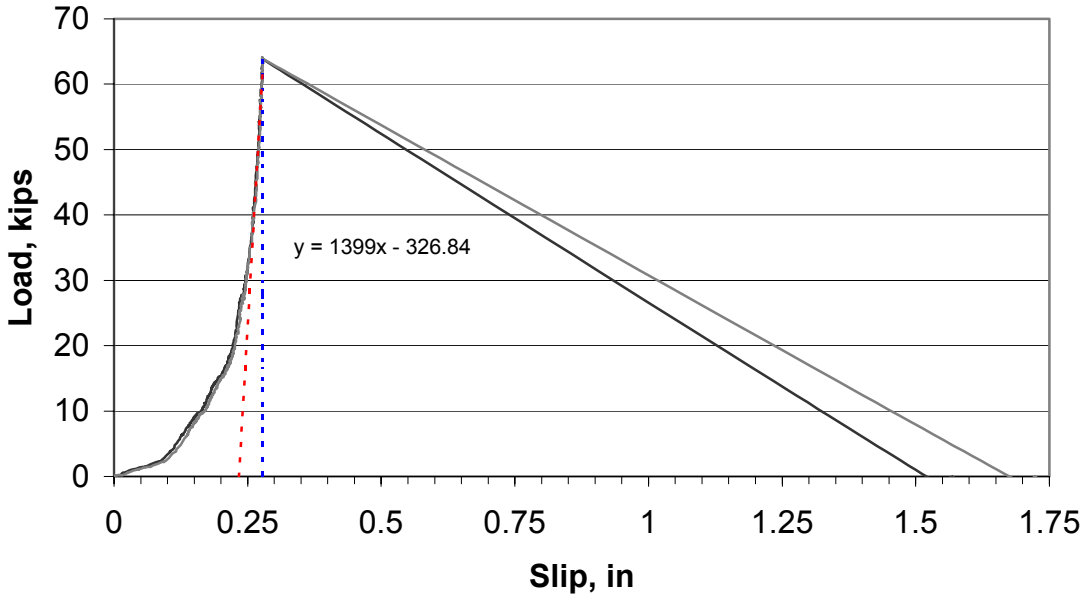

Test 18C-0L-0-B

Specimen Details

Reinforcing	none
Area of Reinforcing, A_{vh}	-
Yield Stress of reinforcing	-
Normal force, P_n	256 lbs
Width of interface, b_v	10 in
Length of interface, s	16 in
f'c, lightweight concrete	5862 psi
Surface type	Chipped
f'c, ductile concrete	32.3 ksi
Slip Load	49.87 kips
Ultimate Load	49.87 kips
Displacement at Slip Load	0.036 in
Displacement at Ultimate Load	0.036 in

18C-0L-0-B
Load vs Slip

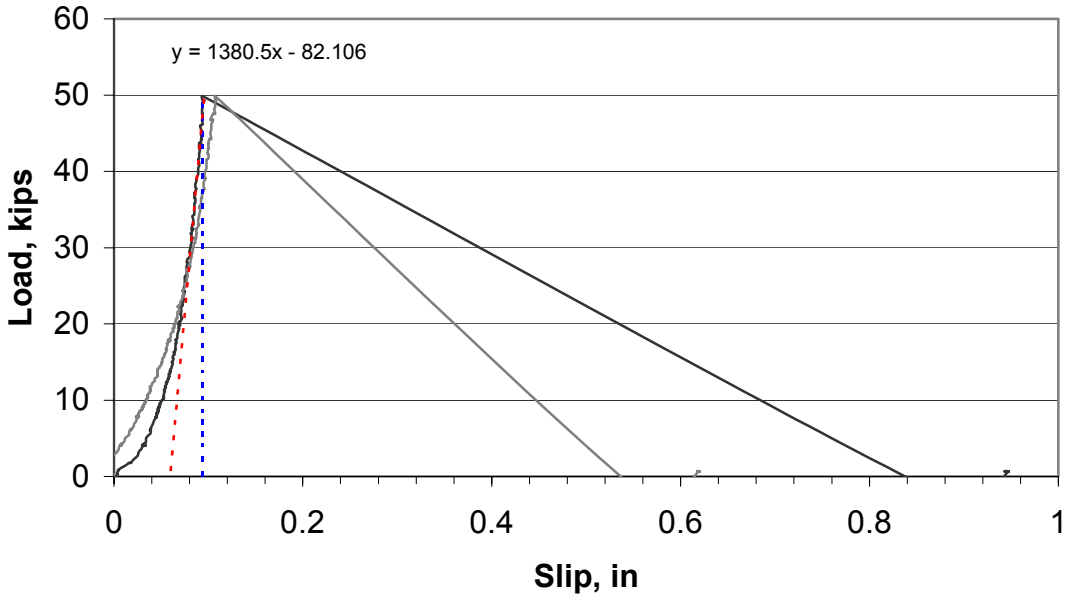

Test 24S-0L-0-A

Specimen Details

Reinforcing	none
Area of Reinforcing, A_{vh}	-
Yield Stress of reinforcing	-
Normal force, P_n	352 lbs
Width of interface, b_v	10 in
Length of interface, s	22 in
f'c, lightweight concrete	5862 psi
Surface type	Smooth
f'c, ductile concrete	32.3 ksi
Slip Load	46.39 kips
Ultimate Load	46.39 kips
Displacement at Slip Load	0.028 in
Displacement at Ultimate Load	0.028 in

24S-0L-0-A
Load vs Slip

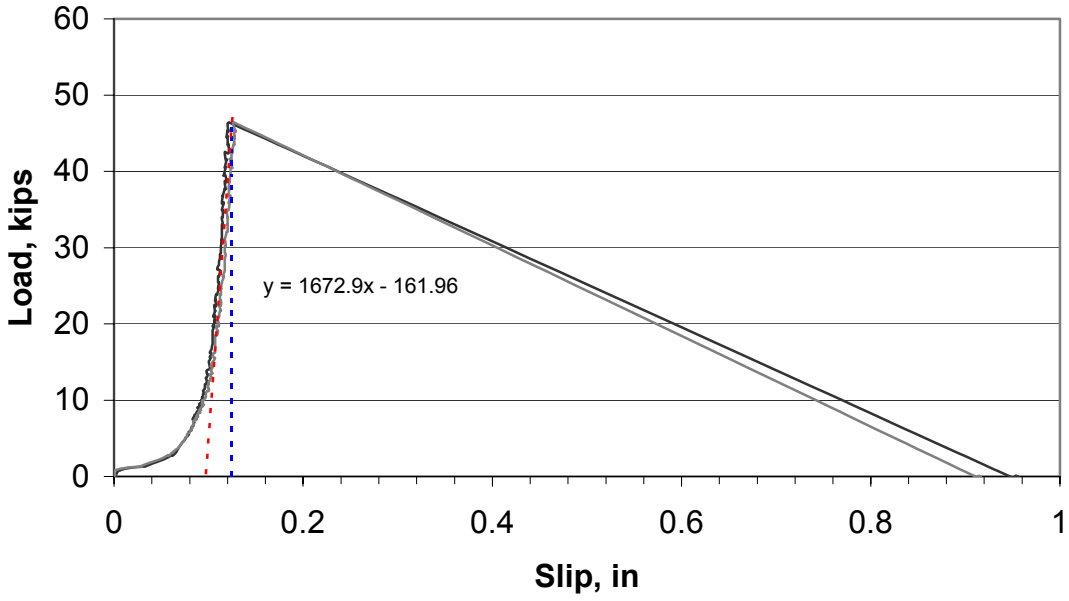

Test 24S-0L-0-B

Specimen Details

Reinforcing	none
Area of Reinforcing, A_{vh}	-
Yield Stress of reinforcing	-
Normal force, P_n	352 lbs
Width of interface, b_v	10 in
Length of interface, s	22 in
f'c, lightweight concrete	5862 psi
Surface type	Smooth
f'c, ductile concrete	32.3 ksi
Slip Load	50.04 kips
Ultimate Load	50.04 kips
Displacement at Slip Load	0.031 in
Displacement at Ultimate Load	0.031 in

24S-0L-0-B
Load vs Slip

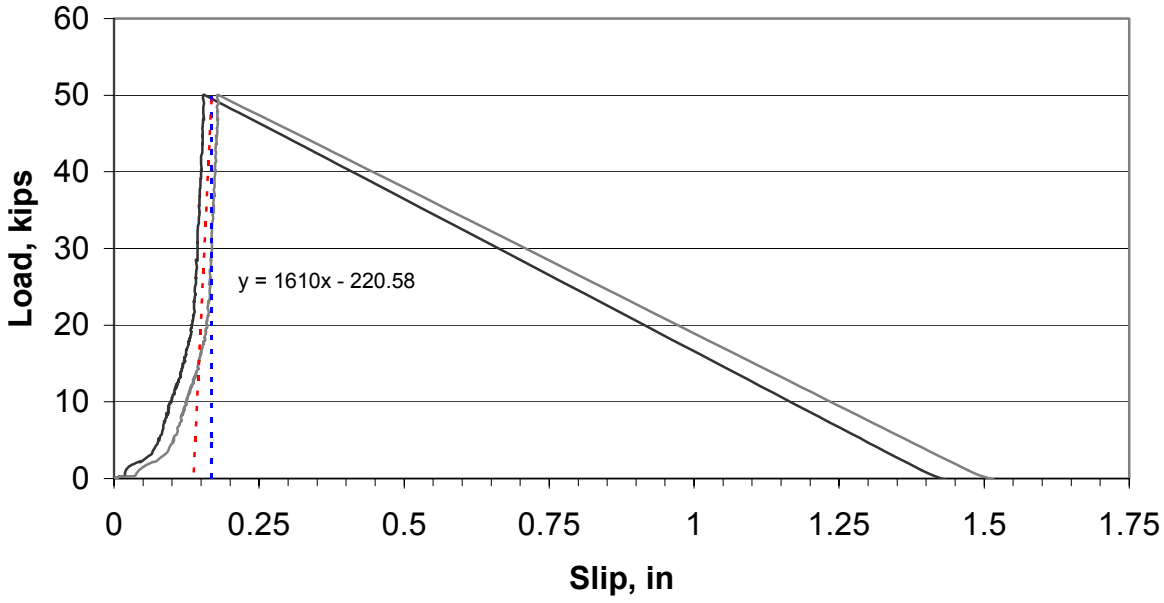

Test 24S-2L-2-A

Specimen Details

Reinforcing	4 legs of #3 bar
Area of Reinforcing, A_{vh}	0.44 in^2
Yield Stress of reinforcing	72
Normal force, P_n	352 lbs
Width of interface, b_v	10 in
Length of interface, s	22 in
f'c, lightweight concrete	5862 psi
Surface type	Smooth
f'c, ductile concrete	32.3 ksi
Slip Load	25.46 kips
Ultimate Load	43.55 kips
Displacement at Slip Load	0.034 in
Displacement at Ultimate Load	0.418 in

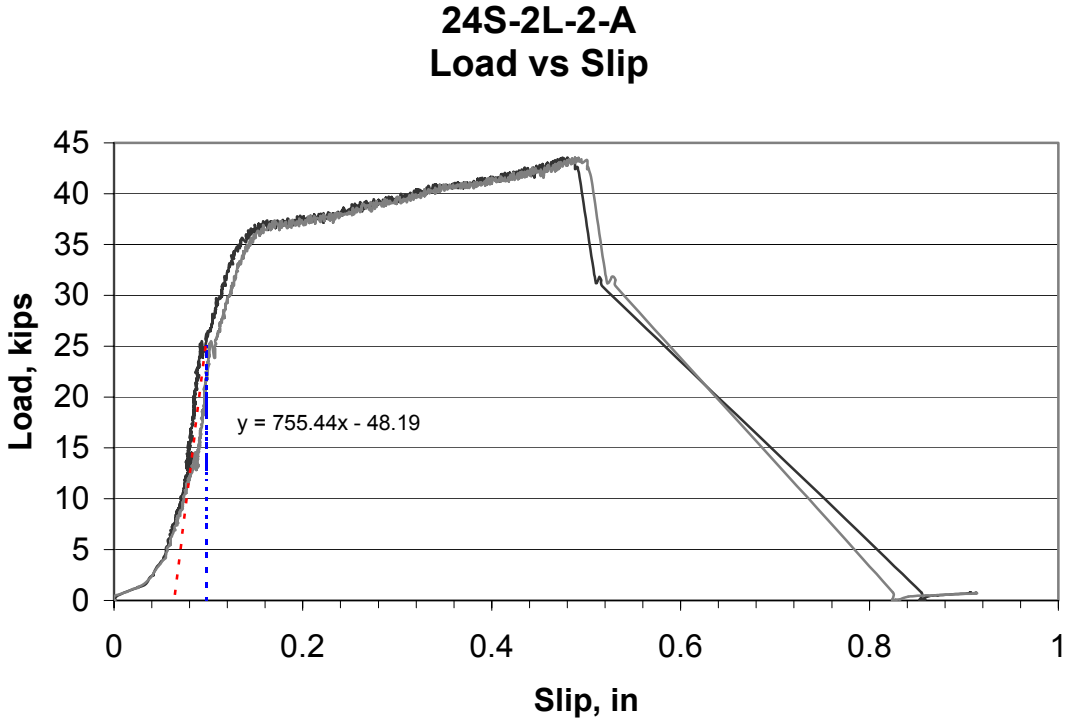

24S-2L-2-A
Load vs Strain

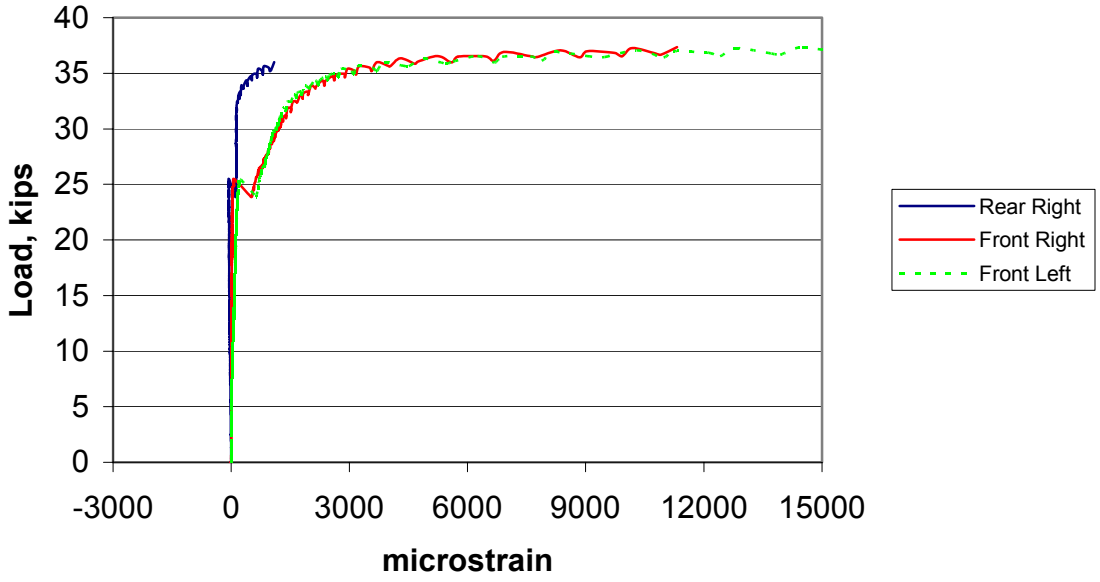

24S-2L-2-A
Load vs Strain
(Rear Legs)

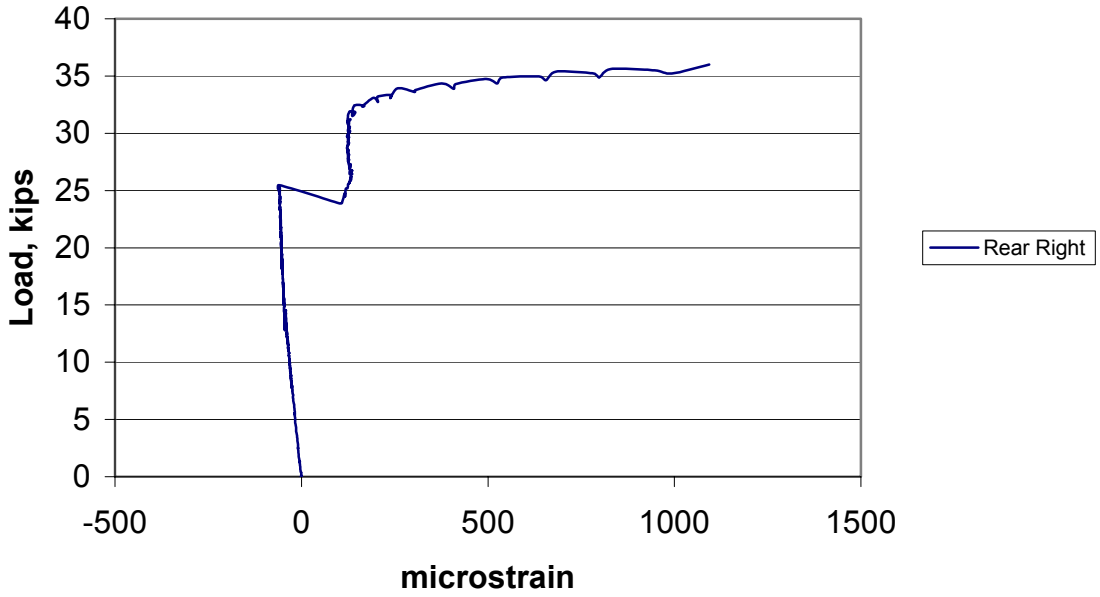

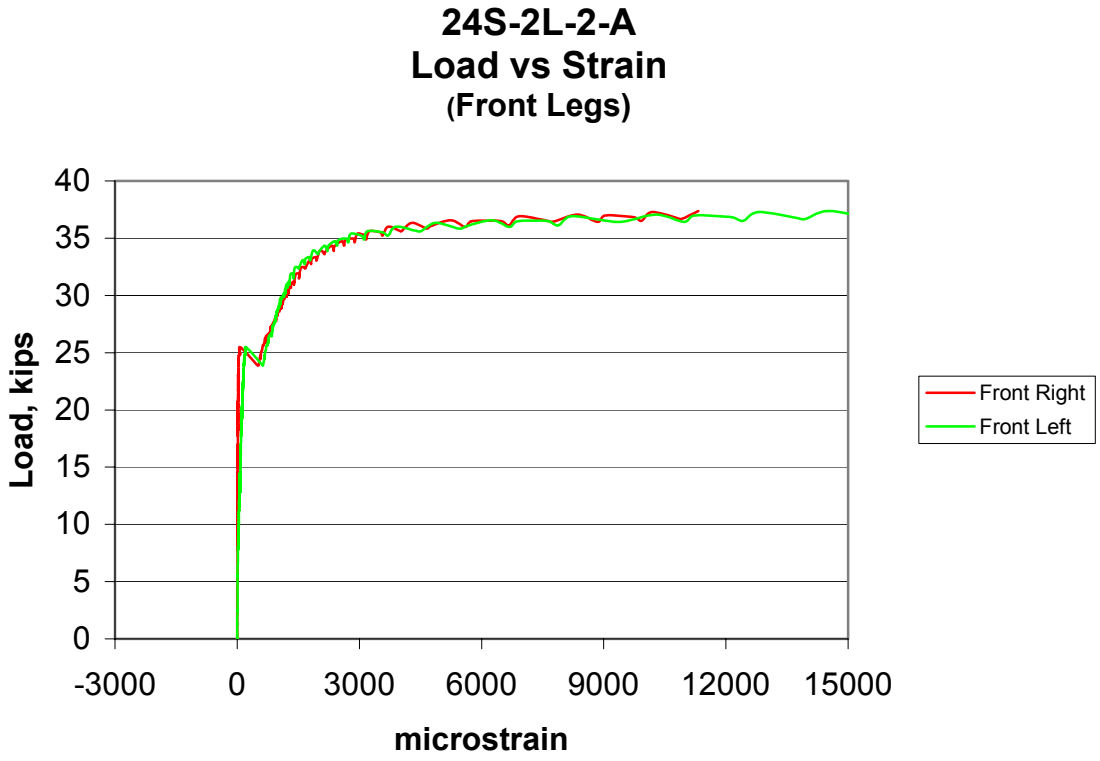
24S-2L-2-A
Load vs Strain
(Front Legs)
Load, kips
40
35
30
25
20
15
10
5
0
-3000
0
3000
6000
9000
12000
15000
microstrain
Front Right
Front Left

Test 24S-2L-2-B

Specimen Details

Reinforcing	4 legs of #3 bar
Area of Reinforcing, A_{vh}	0.44 in^2
Yield Stress of reinforcing	72
Normal force, P_n	352 lbs
Width of interface, b_v	10 in
Length of interface, s	22 in
f'c, lightweight concrete	5862 psi
Surface type	Smooth
f'c, ductile concrete	32.3 ksi
Slip Load	23.89 kips
Ultimate Load	23.89 kips
Displacement at Slip Load	0.019 in
Displacement at Ultimate Load	0.375 in

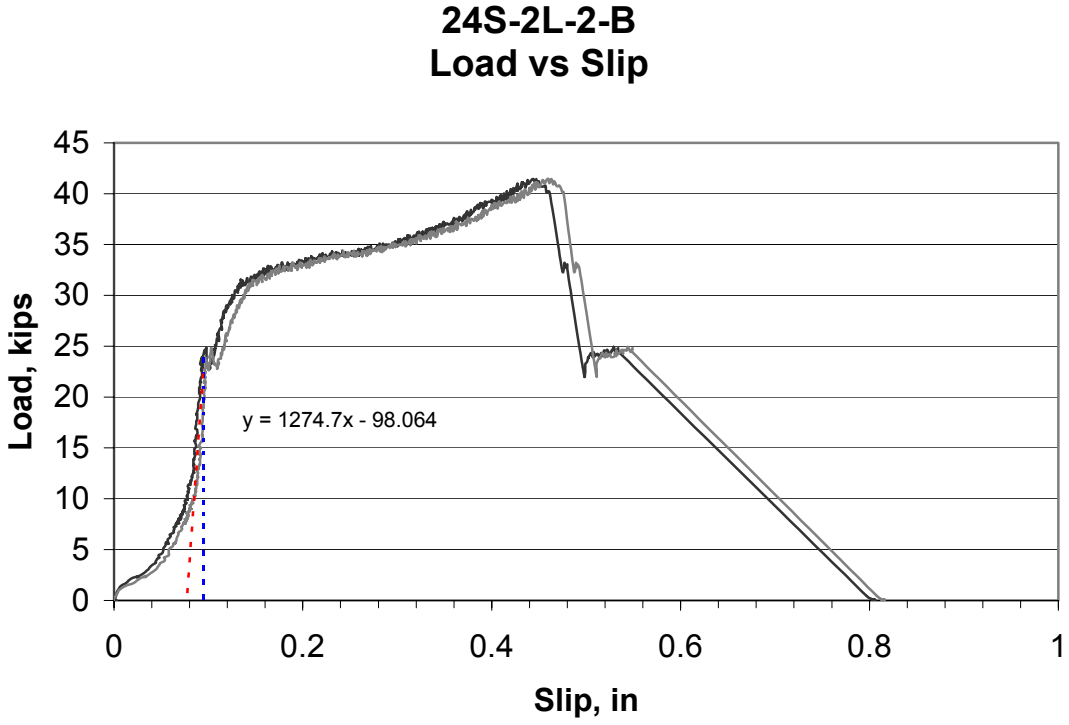

24S-2L-2-B
Load vs Strain

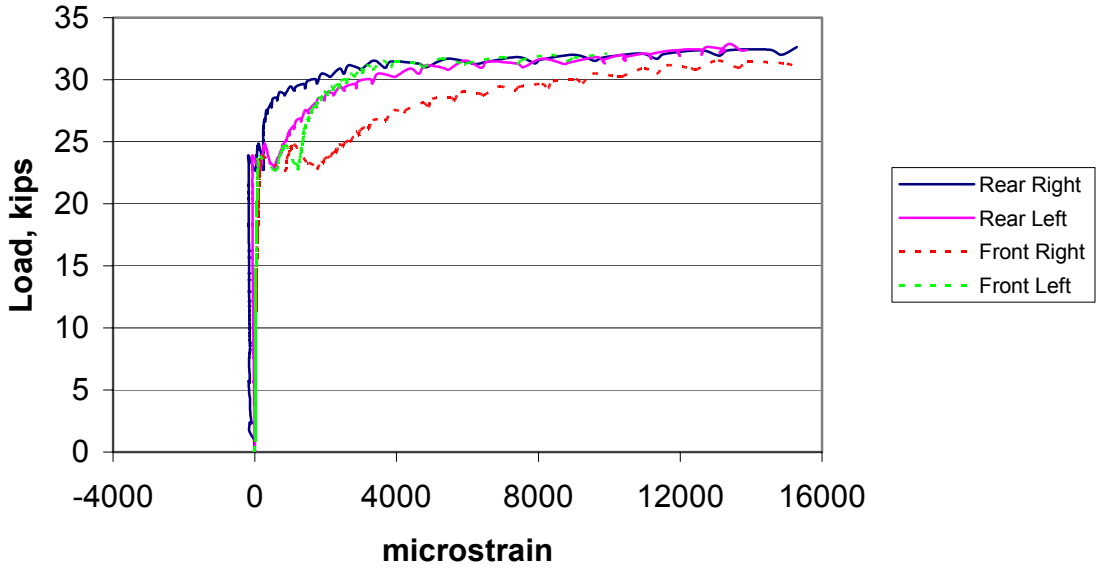

24S-2L-2-B
Load vs Strain
(Rear Legs)

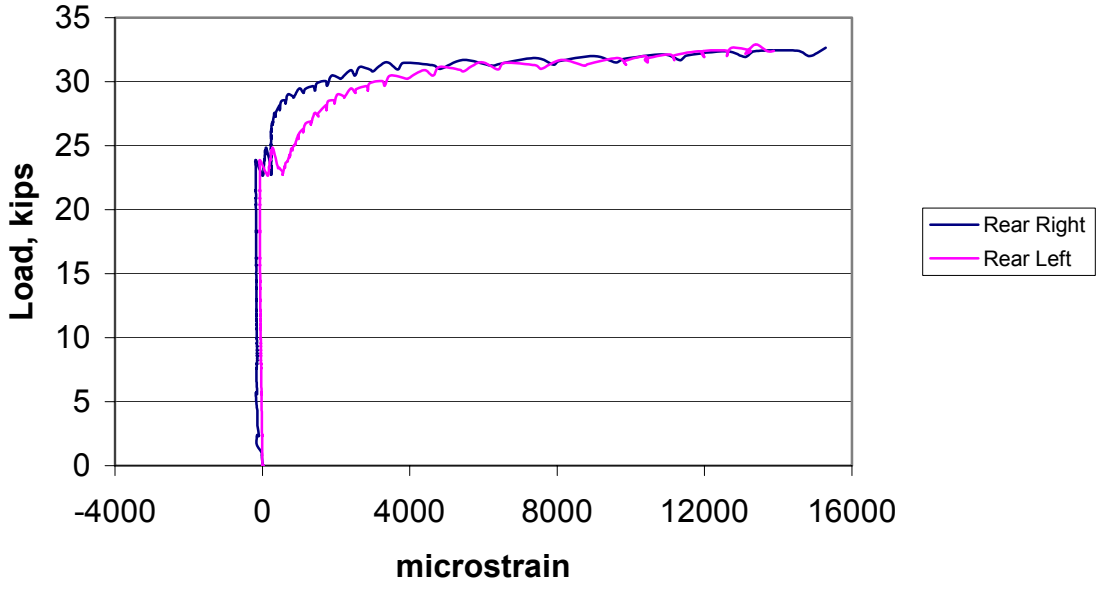

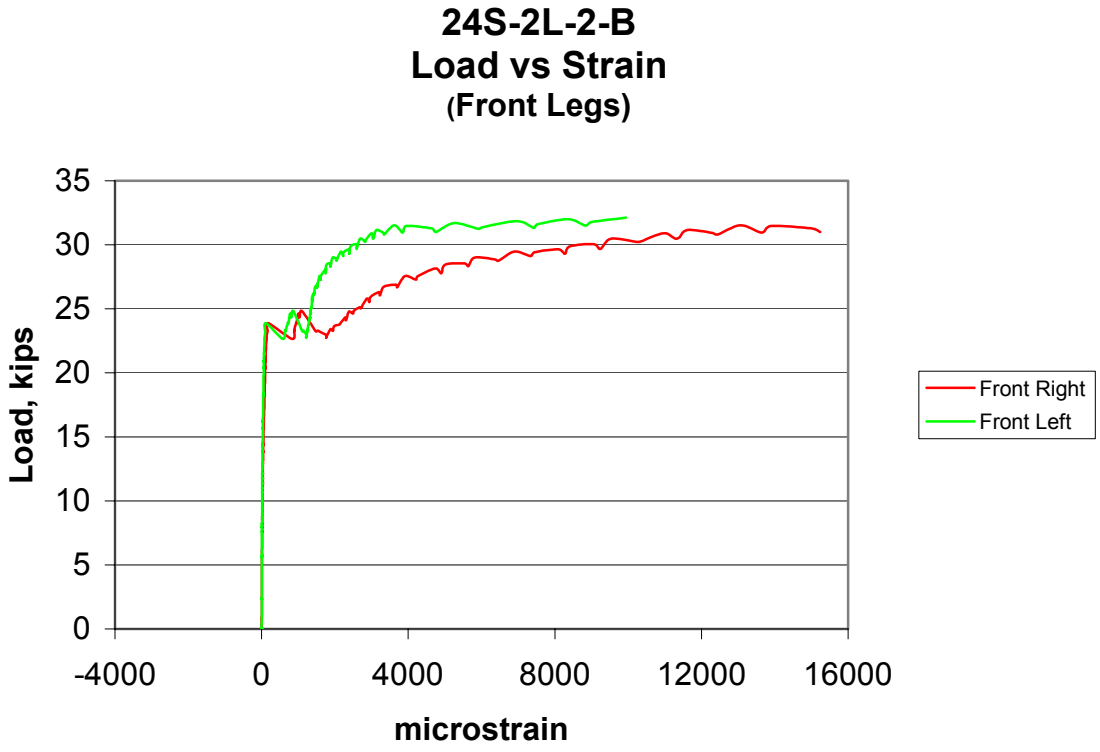
24S-2L-2-B
Load vs Strain
(Front Legs)
Load, kips
35
30
25
20
15
10
5
0
-4000
0
4000
8000
12000
16000
microstrain
Front Right
Front Left

VITA

Timothy Banta was born on October 15, 1979 in Columbia, South Carolina. At the age of six, he relocated to Cherry Hill, New Jersey where he spent the next eleven years of his life. Upon graduating from Cherry Hill High School West in 1997, he began his undergraduate degree at Virginia Polytechnic Institute and State University. While at Virginia Tech, this avid outdoorsman found himself in a setting where he could both obtain an excellent education and fully enjoy the wonders of the Appalachian Mountains. During his undergraduate tenure at Virginia Tech, he made many lifelong friends, watched the Hokies gain national prominence in football, and discovered his calling as an engineer. After graduating from Virginia Tech in 2002 with a Bachelors Degree in Civil Engineering, Mr. Banta decided to continue his education. He returned to Virginia Tech in 2002, and has been working on obtaining his Masters of Science in Structural Engineering. In July 2004, Mr. Banta relocated to Raleigh, North Carolina and presently is working as an engineer.